

ADA 038682

AFAPL-TR-76-68

(12)
NW

SUPERSONIC JET EXHAUST NOISE INVESTIGATION

Volume I SUMMARY REPORT

GENERAL ELECTRIC COMPANY
AIRCRAFT ENGINE GROUP
ADVANCED ENGRG. AND TECH. PROGRAMS DEPT.
CINCINNATI, OHIO 45215

JULY 1976

TECHNICAL REPORT AFAPL-TR-76-68
FINAL REPORT FOR THE PERIOD 1 DECEMBER 1972 - 23 SEPTEMBER 1975

Approved for public release; distribution unlimited

AU NO. _____
DDC FILE COPY

AIR FORCE AERO PROPULSION LABORATORY
AIR FORCE SYSTEMS COMMAND
WRIGHT-PATTERSON AIR FORCE BASE, OHIO 45433
and
DEPARTMENT OF TRANSPORTATION
OFFICE OF NOISE ABATEMENT
WASHINGTON, D.C.

DDC
APR 27 1976
B

NOTICE

When Government drawings, specifications, or other data are used for any purpose other than in connection with a definitely related Government procurement operation, the United States Government thereby incurs no responsibility nor any obligation whatsoever; and the fact that the Government may have formulated, furnished, or in any way supplied the said drawings, specifications, or other data, is not to be regarded by implication or otherwise as in any manner licensing the holder or any other person or corporation, or conveying any rights or permission to manufacture, use, or sell any patented invention that may in any way be related thereto.

This report has been reviewed by the Information Office, ASD/OIP, and is releasable to the National Technical Information Service (NTIS). At NTIS, it will be available to the general public, including foreign nations.

This technical report has been reviewed and is approved for publication.

Paul A. Shahady
PAUL A. SHAHADY
Project Engineer
USAF

G. Banerian
DR. GORDON BANERIAN
Project Manager
Department of Transportation

FOR THE COMMANDER

Robert E. Henderson
ROBERT E. HENDERSON
Manager, Combustion Technical Area

Copies of this report should not be returned unless return is required by security considerations, contractual obligations, or notice on a specific document.

UNCLASSIFIED

SECURITY CLASSIFICATION OF THIS PAGE (When Data Entered)

REPORT DOCUMENTATION PAGE		READ INSTRUCTIONS BEFORE COMPLETING FORM
1. REPORT NUMBER 18 AFAPL-TR-76-68, Vol I	2. GOVT ACCESSION NO.	3. RECIPIENT'S CATALOG NUMBER 9
4. TITLE (and Subtitle) 6 Supersonic Jet Exhaust Noise Investigation Volume I Summary Report		5. TYPE OF REPORT & PERIOD COVERED Technical Report (Final) 1 Dec 1972 - 23 Sept 1975
7. AUTHOR(s) 10 Paul R. Knott		8. PERFORMING ORG. REPORT NUMBER R74AEG452 - Vol-1 9. CONTRACT OR GRANT NUMBER(s)
9. PERFORMING ORGANIZATION NAME AND ADDRESS General Electric Company Aircraft Engine Group (AE&TPD) ✓ Cincinnati, Ohio 45215	10. PROGRAM ELEMENT, PROJECT, TASK AREA & WORK UNIT NUMBERS 15 P.E. 62203F, Project 3066, Task 306614, W.U. 30661407	
11. CONTROLLING OFFICE NAME AND ADDRESS Air Force Aero Propulsion Lab (TBC) ✓ Wright-Patterson Air Force Base, Ohio 45433	12. REPORT DATE 11 JUL 1976	13. NUMBER OF PAGES 105
14. MONITORING AGENCY NAME & ADDRESS (if different from Controlling Office)	15. SECURITY CLASS. (of this Report) Unclassified	15a. DECLASSIFICATION/DOWNGRADING SCHEDULE
16. DISTRIBUTION STATEMENT (of this Report) Approved for Public Release; Distribution Unlimited. V2 A038 613		
17. DISTRIBUTION STATEMENT (of the abstract entered in Block 20, if different from Report) 403 468		
18. SUPPLEMENTARY NOTES: This report is Volume I of a four-volume Final Technical Report prepared by the Advanced Engineering and Technology Programs Department, Aircraft Engine Group of the General Electric Company, under the joint sponsorship of the Air Force Aero Propulsion Laboratory, Wright-Patterson Air Force Base, Ohio, and the Department of Transportation, Washington, D.C.		
19. KEY WORDS (Continue on reverse side if necessary and identify by block number) Supersonic Jet Exhaust Noise, Turbulent Mixing Noise, Aerodynamic Shock Flow, Orderly Structure, Combustion Noise, Jet Refraction, Swirl Jet Noise, Shock Noise, Turbulence, Laser Velocimeter, Turbulence Spectra, In-Jet/Far-Field Acoustic Cross-Correlation, Aeroacoustics.		
20. ABSTRACT (Continue on reverse side if necessary and identify by block number) This report summarizes major theoretical aerodynamic and acoustic developments and experimental findings aimed at providing a better understanding and a detailed mathematical specification of the noise-producing sources of simple exhaust jets. A review is given of calculation procedures for shock wave structure and flow field (continued on reverse side) over		

Copy

Unclassified

SECURITY CLASSIFICATION OF THIS PAGE(When Data Entered)

20.

properties of simple circular jets. Results of new theoretical acoustic developments illustrating the influence of a jet's mean flow shrouding on jet acoustic radiation for unheated and heated jets are outlined. Additional discussions of interesting insights regarding the classical turbulent mixing theory of jet noise and the aeroacoustic formulations for a jet's orderly structure are given. Summaries of a series of high velocity, high temperature velocity field measurements using a General Electric developed laser velocimeter are discussed, and the application of the laser velocimeter for performing turbulence spectra and in-jet to far-field cross-correlation type measurements is reviewed. Key experiments illustrating the influence of swirl and combustion roughness on jet noise generation/reduction are presented. Results of high velocity and high temperature refraction experiments are also discussed, as well as discussions concerning jet flow amplifying effects of injected low frequency noise. Additionally, suggestions concerning shock-related noise as related to full-size engines are given. And finally, recommendations for future investigations are given.

Unclassified

SECURITY CLASSIFICATION OF THIS PAGE(When Data Entered)

FOREWORD

This is Volume I, Summary Report, of a four-volume final Technical Report prepared by the Advanced Engineering and Technology Programs Department, Aircraft Engine Group of the General Electric Company, Evendale, Ohio under the joint sponsorship of the Air Force Aero-Propulsion Laboratory, Wright-Patterson Air Force Base, Ohio and the Department of Transportation, Washington, D.C., under Contract F33615-73-C-2031. The inclusive dates for this work were December 1972 through August 1975. The work was accomplished under Project 3066, Task 14, W.U. 07 with Mr. Paul A. Shahady (AFAPL/TBC) as Project Engineer. Dr. Paul R. Knott of the General Electric Company was technically responsible for the work.

TABLE OF CONTENTS

VOLUME I

<u>Section</u>		<u>Page</u>
1.0	BACKGROUND	1
2.0	REVIEW OF THE THEORETICAL DEVELOPMENTS OF THE AERODYNAMICS OF SUPERSONIC JETS	6
3.0	REVIEW OF RECENT THEORETICAL ACOUSTIC MODEL DEVELOPMENTS	14
4.0	LASER VELOCIMETER DEVELOPMENTS FOR NOISE SOURCE LOCATION	52
	4.1 Basic Idea for LV RMS Measurements	52
	4.2 LV-Measured Turbulence Spectra	54
	4.3 LV Measurements for Noise Source Location	62
5.0	SOME INTERESTING INSIGHTS FROM ACOUSTIC EXPERIMENTS	68
	5.1 Upstream Swirl	68
	5.2 Shock Noise	73
	5.3 Jet Refraction	76
	5.4 Combustion Roughness Experiments	83
6.0	RECOMMENDATIONS FOR FUTURE WORK	89
	REFERENCES	92

ACCESSION for	
NTIS	Write Section <input checked="" type="checkbox"/>
DDC	Full Section <input type="checkbox"/>
UNANNOUNCED	<input type="checkbox"/>
JUSTIFICATION.....	
BY.....	
DISTRIBUTION/AVAILABILITY CODES	
Dist.	AVAIL. and/or SPECIAL
A	

v

TABLE OF CONTENTS

VOLUME II

<u>Section</u>	<u>Page</u>
INTRODUCTION	107
CHAPTER I - Theoretical Acoustic Developments for Turbulent Jets	109
1.0 THE INFLUENCE OF JET FLOW ON JET NOISE	110
1.1 The Noise of Unheated Jets	110
1.1.1 Background	110
1.1.2 Formulation and Method of Solution	113
1.1.3 Application of Theory to Experimental Results	130
1.1.4 Concluding Remarks	139
1.2 The Noise of Heated Jets	141
1.2.1 Interpretation of Lilley's Equation for Heated Jets	141
1.2.2 Method of Solution	147
1.2.3 Physical Interpretation of the Solutions and Applications to Jet Noise Experiments	151
1.2.4 Concluding Remarks	155
2.0 TESTS OF A THEORETICAL MODEL OF JET NOISE	165
2.1 Background	165
2.2 Basic Theoretical Analysis for Model Development	166
2.3 Formalism for Tests of the Model	167
2.4 Tests I: Invariance of β ; Similarity of Self- and Shear-Noise Spectra	170
2.5 Tests II: Model as a Framework for Jet Noise Prediction	176
2.6 Discussion	185
2.7 Conclusions	187
APPENDIX 1 - Theoretical Considerations for Ribner's Self-Noise Model	189
3.0 ANALYTICAL MODELING FOR A JET'S ORDERLY STRUCTURE	193
3.1 Background	193
3.2 The Stability of Turbulent Axisymmetric Compressible Jets	193
3.2.1 The Equations for the Mean Flow and the Wave	194
3.2.2 The Eigenvalue Equation	197

TABLE OF CONTENTS (Continued)

<u>Section</u>	<u>Page</u>
3.3 Determination of the Spectral Characteristics of the "Orderly Structure"	200
3.3.1 Tam's Single-Frequency Analysis	200
3.3.2 Multiple Frequency approaches	206
3.3.3 Effects of Finite Amplitude Waves	207
3.4 Experimental Evidence of Orderly Structure in Jets	208
3.5 Sound Radiation from the Orderly Structure in a Jet	209
3.6 Orderly Structure Flow Field Calculations	212
3.6.1 Integral Form of the Equations of Motion	212
3.6.2 Fluid Dynamic Calculations	214
3.6.3 Equations for the Acoustic Radiation	214
3.7 Summary and Conclusions	220
APPENDIX 2 - Solution of the Eigenvalue Equation in the Region Near the Singularity	
	223
CHAPTER II - Aeroacoustic Investigations for High-Velocity, High-Temperature Jets	
	227
1.0 UPSTREAM DISTURBANCE INFLUENCES ON JET EXHAUST NOISE	228
1.1 Background	228
1.2 Influence of Upstream Swirl on Jet Noise Generation	229
1.2.1 Analytical Aerodynamic Swirl Model	230
1.2.1.1 Description of the Model	233
1.2.1.2 Aeroacoustic Predictions	239
1.2.2 Swirling Jet Aeroacoustic Experiment	241
1.2.2.1 Experiment Apparatus, Test Setup and Conditions	246
1.2.2.2 Aerodynamic Results	258
1.2.2.3 Acoustic Results	277
1.3 Influence of Upstream Turbulence on Jet Noise Generation	291
1.3.1 Analytical Aerodynamic Model for Turbulent Production	291
1.3.2 Combustion Roughness Aeroacoustic Experiment	292
1.3.2.1 Experimental Apparatus, Test Setup, and Conditions	299
1.3.2.2 Aerodynamic Results	301
1.3.2.3 Acoustic Results	305
1.3.3 Afterburner Flameholder/Spraybar Aeroacoustic Experiment	309
1.3.3.1 Experimental Apparatus, Test Setup, and Conditions	309
1.3.3.2 Aerodynamic Results	316
1.3.3.3 Acoustic Results	316
1.4 Summary and Conclusions	327

TABLE OF CONTENTS (Continued)

<u>Section</u>		<u>Page</u>
2.0	JET REFRACTION EXPERIMENTS	340
2.1	Background	340
2.2	Ribner's Refraction Concepts	340
2.2.1	Method of Approach	341
2.3	Test Facility and Apparatus	350
2.3.1	Test Facility	350
2.3.2	Description of Tone Source	351
2.3.3	Instrumentation	356
2.4	Test Matrix and Procedure	356
2.5	Discussion of Results	359
2.5.1	Influence of Tone Source Hardware on Jet Noise	359
2.5.2	Methods of Data Reduction	362
2.5.3	Influence of Velocity Variations on Jet Refraction	362
2.5.4	Influence of Temperature Variations on Refraction	373
2.6	Further Analysis of the Data	373
	 CHAPTER III - Laser Velocimeter Investigations	 389
1.0	PARAMETRIC LASER VELOCIMETER STUDIES OF HIGH-VELOCITY, HIGH-TEMPERATURE, TURBULENT JETS	390
1.1	Background	390
1.2	The Laser Velocimeter Arrangement	390
1.2.1	Actuator and Seeding	394
1.2.2	Signal Processing and Recording	397
1.3	Laser Velocimeter Jet Plume Survey	397
1.3.1	Cold Jet Laser Velocity Measurements	397
1.3.2	Hot Supersonic Jet Laser Velocimeter Measurements	397
1.3.2.1	Shock-Free Jet	397
1.3.2.2	Conical Nozzle Shock Flow Profiles	401
1.3.2.3	Exit Plane Parametric Studies	404
1.4	Summary and Conclusions	414
2.0	IN-JET/FAR-FIELD CROSS-CORRELATION EXPERIMENTS	417
2.1	Background	417
2.2	Acoustic Theory and General Approach	417
2.3	The Random Sample Correlation Estimator	419
2.4	Simulation Experiments	426

TABLE OF CONTENTS (Concluded)

<u>Section</u>	<u>Page</u>
2.5 Cross-Correlation Experiments with General Electric's Laser Velocimeter	429
2.5.1 Experimental Arrangement and Test Conditions	429
2.5.2 Discussion of Results	433
2.6 Conclusions	441
APPENDIX 3 - Tabular Listing of Hot-Film/LV Measurements on 4.3-inch Conic Nozzle	442
APPENDIX 4 - Contour Plots of Mean Velocity, Turbulent Velocity for C/D Shock-Free Flow, $M_j=1.55$, $T_T \cong 1500^\circ, 2500^\circ R$.	447
- Contour Plots of Mean Velocity and Turbulent Velocity for a Conic Nozzle (Shocked-Flow) $M_j \sim 1.55, T_T \sim 1500^\circ R$	447
APPENDIX 5 - Ground Reflection Correction for Cross-Correlation Measurements	455
REFERENCES	458
<u>VOLUME III</u>	
INTRODUCTION	473
1.0 PROGRAM DESCRIPTION	474
1.1 General Description	474
1.2 JETMIX	474
1.3 SSFD	476
1.4 MERGE	478
1.5 NOISE	478
1.6 SSNOISE Calculation Steps and Flow Chart	479
1.7 SSNOISE overlay Description	482
1.7.1 Overlay (0,0) - Entry MAIN	482
1.7.2 Overlay (1,0) - Entry JETMIX	482
1.7.3 Overlay (1,1) - Entry JETMIX 1	482
1.7.4 Overlay (1,2) - Entry JETMIX 2	484
1.7.5 Overlay (2,0) - Entry SSFD	484
1.7.6 Overlay (2,1) - Entry SSFDIN	484
1.7.7 Overlay (2,2) - Entry SSFDCA	484
1.7.8 Overlay (3,0) - Entry MERGE	484
1.7.9 Overlay (4,0) - Entry MAINNS	485

TABLE OF CONTENTS (Continued)

<u>Section</u>		<u>Page</u>
2.0	PROGRAM INPUT	486
2.1	General Description	486
2.2	JETMIX Input	486
2.2.1	Problem Specification	487
2.2.2	Description of Primary and Secondary Jets	487
2.2.3	External Boundary Conditions	488
2.2.4	Fluid Properties	489
2.2.5	Step-Size Controls/Restart	489
2.2.6	Turbulence Scale Calculations	490
2.2.7	Coannular/Coplanar Jet	491
2.2.8	Transverse Mesh Control	495
2.2.9	Species Diffusion Input	495
2.2.10	Station Input	496
2.3	SSFD Input	498
2.3.1	Problem Description	498
2.3.2	Program Controls	499
2.3.3	Total-Pressure Input Stations	499
2.4	MERGE	501
2.5	NOISE Input	501
2.5.1	General Input	502
2.5.2	Acoustic Model Selection	503
2.5.3	Microphone Selection	504
2.5.4	Output Control Cards	504
3.0	PROGRAM OUTPUT	505
3.1	General Description	505
3.2	JETMIX Program Output	505
3.3	SSFD Program Output	508
3.4	MERGE Program Output	509
3.5	NOISE Program Output	509
3.5.1	One-Third Octave Band Analysis	509
3.5.2	Summary Acoustic Analysis	510
3.5.3	Summary Acoustic Power Analysis	511
3.6	Sample Case	511
4.0	OPERATING PROCEDURES	569
4.1	General Description	569
4.2	Maintenance and Modification	569
4.3	Input and Output Files	569
	APPENDIX 6 - Analysis Incorporated in JETMIX	573
	APPENDIX 7 - Analysis Incorporated in SSFD/MERGE	603

TABLE OF CONTENTS (Concluded)

<u>Section</u>	<u>Page</u>
APPENDIX 8 - Analysis Incorporated in Noise	636
APPENDIX 9 - Input Sheets	711
APPENDIX 10 - Sample Cases	723
APPENDIX 11 - Program Listings	902
REFERENCES	1149
<u>VOLUME IV</u>	
1.0 INTRODUCTION	
2.0 NOZZLES TESTED	
3.0 EXPERIMENTAL APPARATUS, TEST SETUP, AND DATA ACQUISITION	
4.0 TEST CONDITIONS	
5.0 CORRECTIONS FOR GROUND REFLECTIONS	
6.0 DESCRIPTION OF ACOUSTIC DATA SHEETS	
6.1 Description of Far-Field Acoustic Data Sheets	
6.2 Description of Near-Field Acoustic Data Sheets	
7.0 ACOUSTIC FAR-FIELD DATA SECTION	
7.1 C/D Nozzle Parametric Far-Field Acoustic Test Points	
7.2 Conical Thin-Lip Parametric Far-Field Acoustic Test Points + Shock-Free Design Line	
7.3 Conical, 1/2-inch, Thick-Lip, Far-Field Nozzle Acoustic Test Points + Shock-Free Design Line	
7.4 C/D Far-Field Acoustic Test Points for Shock-Free Parallel-Flow Conditions	
8.0 ACOUSTIC NEAR-FIELD DATA SECTION	
8.1 C/D Nozzle Parametric Near-Field Acoustic Test Points	
8.2 Conical Thin-Lip Parametric Near-Field Acoustic Test Points + Shock-Free Design Line of C/D Nozzle	
8.3 Conical 1/2-Inch, Thick-Lip, Near-Field Acoustic Test Points + Shock-Free Design Line	
8.4 C/D Near-Field Acoustic Test Points for Shock-Free, Parallel-Flow Conditions.	

LIST OF ILLUSTRATIONS

VOLUME I

<u>Figure</u>		<u>Page</u>
1.	General Electric Aeroacoustic Approach.	4
2.	The Flowfield of an Ideally Expanded Viscous Jet.	7
3.	The Flowfield of an Inviscid Two-Dimensional Supersonic Jet.	7
4.	Subdivision of the Jet into Inner and Outer Regions (Outer Region Shown Shaded).	9
5.	Cross-Stream Variation of Predicted Total Pressure and Static Pressure for a Jet from a Convergent Nozzle, Showing Total-Pressure Loss Due to Both Shocks and Mixing.	11
6.	Predicted Shock Shape and Mean Velocity Decay Versus Measurements, $M_j \sim 1.5$, $T_T \sim 1500^\circ \text{ R}$.	12
7.	Influence of Jet Velocity and Temperature on Jet Density Exponent and Jet Spectra.	16
8.	Effects of Increased Exhaust Turbulence Intensity on Jet Noise.	17
9.	Convective Amplification as a Function of M and $k_0 a$.	22
10.	Implications for Strouhal Scaling.	22
11.	Peak Strouhal Number as a Function of Jet Mach Number.	23
12.	η as a Function of $(St)_0$ for $M_0 = 0.9$.	23
13.	Jet Density Exponent (Figure 17 of Reference 15).	25
14.	Comparison with Data of Lush at $M_j = 0.878$ and 0.57 .	32
15.	Jet Density Exponent for Total Power as a Function of (V_j/c_0) .	36
16.	Jet Density Exponent as a Function of Angle from Jet Axis.	37
17.	Density Index at 90° to Jet Axis as a Function of (V_j/c_0) .	38
18.	Comparison of Normalized Self-Noise and Shear-Noise Spectra.	40

LIST OF ILLUSTRATIONS (Continued)

<u>Figure</u>		<u>Page</u>
19.	Self-Noise, Shear-Noise Comparisons.	41
20.	Directivity of 1/3-Octave Intensity: Comparison with Experimental Data of Ahuja.	44
21.	Theory Vs. Data Comparison for Slug-Flow Shielding Model.	47
22.	Schematic of Laser Velocity Measurements.	53
23.	Comparisons of LV Measurements with Hot-Film/Hot-Wire Measurements for an Ambient Subsonic Jet.	55
24.	LV Measurements of Mean Velocity and Turbulent Velocity Decay for a Shock-Free, High-Velocity, High-Temperature Jet.	56
25.	LV-Measured Normalized Radial Mean Velocity Profiles for Shock-Free and Shock-Flow, High-Velocity, High-Temperature Jet.	57
26.	LV-Measured Normalized Radial Turbulence Velocity Profiles.	58
27.	LV-Measured Influence of Jet Velocity on Exit Plane Turbulence.	59
28.	LV-Measured Mean Velocity and Turbulence Intensity on Centerline for a High-Velocity, High-Temperature Jet.	60
29.	LV-Measured Axial Turbulent Velocity Spectra for Ambient and Heated Jets.	63
30.	Final Cross-Correlation Estimate Without Ground-Reflection Correction.	65
31.	Final Cross-Correlation Estimate with Ground-Reflection Correction.	66
32.	Photograph of Jet Swirl Test Rig.	69
33.	The Influence of Jet Swirl on OASPL Directivity.	70
34.	Influence of Jet Swirl on SPL Spectra.	71
35.	Influence of Swirl on PNL Directivity.	72

LIST OF ILLUSTRATIONS (Continued)

<u>Figure</u>		<u>Page</u>
36.	Estimated Influence of Shock Screech for Full-Size, Heated-Exhaust Jets.	74
37.	Estimated Influence of Shock Screech for Full-Size, Heated-Exhaust Jets.	75
38.	Refraction Experimental Setup.	77
39.	Influence of Refraction on Jet and Siren Tone.	79
40.	SPL Reduction of Tone Due to Jet Flow.	80
41.	The Influence of Jet Flow on Tone.	81
42.	The Influence of Heated Jet Flow on Tone Amplification, $M_o = 1.3$, $V_j = 1450$ fps.	82
43.	Combustion Roughness Parameter Measurements for Acoustic Experiments.	86
44.	Influence of Upstream Combustion Roughness on Supersonic Exhaust Jet Noise.	87
45.	Influence of Upstream Combustion Roughness on Supersonic Exhaust Jet Noise.	88

VOLUME II

46.	Cylindrical Coordinate System for Plug Flow Acoustic Model.	117
47.	Notation for a Moving Source.	121
48.	Schematic of Source Models.	125
49.	Phase Speed or Wave Number Differences Between Incident and Refracted Waves.	128
50.	Comparison with Data of Lush at $M_j = 0.366$ ($V_j = 125$ m/s).	133
51.	Comparison with Data of Lush at $M_j = 0.57$ ($V_j = 195$ m/s).	134
52.	Comparison with Data of Lush at $M_j = 0.878$ ($V_j = 300$ m/s).	135
53.	Comparison with Data of Ahuja and Bushell at $M_j = 0.363$ ($V_j = 400$ ft/s).	136

LIST OF ILLUSTRATIONS (Continued)

<u>Figure</u>		<u>Page</u>
54.	Comparison with Data of Ahuja and Bushell at $M_j = 0.546$ ($V_j = 600$ ft/s).	137
55.	Comparison with Data of Ahuja and Bushell at $M_j = 0.909$ ($V_j = 1000$ ft/s).	138
56.	Coordinate System for the Heated Jet.	143
57.	Schematic for a Transverse Dipole Proportional to $\rho(y)$.	145
58.	Coordinate System for the Plug-Flow Acoustic Model for a Heated Jet.	148
59.	Jet Density Exponent for Total Power as a Function of (V_j/c_0).	154
60.	Jet Density Exponent for $V_j/c_0 = 0.447$ as a Function of Angle from the Jet Axis.	156
61.	Jet Density Exponent for $V_j/c_0 = 0.589$ as a Function of Angle from the Jet Axis.	157
62.	Jet Density Exponent for $V_j/c_0 = 0.741$ as a Function of Angle from the Jet Axis.	158
63.	Jet Density Exponent for $V_j/c_0 = 0.891$ as a Function of Angle from the Jet Axis.	159
64.	Jet Density Exponent for $V_j/c_0 = 1.023$ as a Function of Angle from the Jet Axis.	160
65.	Jet Density Exponent for $V_j/c_0 = 1.175$ as a Function of Angle from the Jet Axis.	161
66.	Index at 90° to the Jet Axis as a Function of V_j/c_0 .	162
67.	Jet Density Exponent at 90° for Various Frequencies for Three Jet Mach Numbers.	163
68.	Convection and Refraction Modify "Basic" Noise Pattern.	168
69.	Tests of the Predicted Invariance of β with Frequency.	171
70.	Basic Self-Noise Spectrum a (CS) with Spectrum Measurements at $\theta = 45^\circ$ and the Extracted Basic Shear-Noise Spectrum b (CS).	172

LIST OF ILLUSTRATIONS (Continued)

<u>Figure</u>		<u>Page</u>
71.	Shear- and Self-Noise Spectra Derived from Cross Correlations Between Hot-Wire and Microphone Signals.	173
72.	Comparison of Normalized Self-Noise and Shear-Noise Spectra (the Self-Noise Has Been Downshifted One Octave).	175
73.	Variation of the Convective Amplification Exponent with (CS) and M.	177
74.	Variation of β with Jet Diameter D (from the Measurements of Reference 35).	178
75.	Empirical Universal Self-Noise Spectrum a_e / a_{\max} .	180
76.	Variation of Source Strouhal Number of Self-Noise Spectrum Peak (CS) _p with Mach Number M.	181
77.	Directivity of 1/3-Octave Intensity; Comparison of Experimental Data of Lush, D=25 mm.	182
78.	Directivity of 1/3-Octave Intensity; Comparison with Experimental Data of Chu.	183
79.	Directivity of 1/3-Octave Intensity; Comparison with Experimental Data of Ahuja.	184
80.	Directivity of 1/3-Octave Intensity; Experimental Data from Ahuja. Theory Based on Empirical β (2.82), on "Theoretical" β (2.0), and on Vanishing β (Complete Neglect of Shear Noise).	186
81.	Deformed Path for Integration Around Logarithmic Singularity in Eigenvalue Equation for Self-Excited and Damped Cases.	201
82.	"Preferred" Waves in Supersonic Jet, Based on Periodic Shock Cell Structure in Nearly Ideally Expanded Jet (from Tam, 1972).	204
83.	Schematic Diagram Showing Broad Band Amplification Which is Available in a Jet (According to Parallel Flow Stability Theory), as Compared with the Energy Distribution in the Orderly Structure Wave (According to Tam, 1972).	205
84.	Variation of Half-Thickness of Mixing Layer with Distance from Nozzle Exit Plane.	215
85.	Variation of Core Radius as a Function of Axial Distance from Nozzle Exit Plane.	216

LIST OF ILLUSTRATIONS (Continued)

<u>Figure</u>		<u>Page</u>
86.	Wave Number of Large-Scale Oscillation as a Function of Half-Width of Shear Layer.	217
87.	Amplification Rate of Large-Scale Oscillation as a Function of Half-Width of Shear Layer.	218
88.	Real and Imaginary Parts of Eigenfunction in Region of Numerical Integration.	219
89.	Directional Distribution of Acoustic Power.	221
90.	Axisymmetric Turbulent Jet Flow Field.	240
91.	Comparison of Predicted and Measured Centerline Decay of Mean Axial Velocity for Swirling Isothermal Subsonic Jets.	241
92.	Predicted Centerline Decay of Mean Axial Velocity for Swirling and Nonswirling Isothermal Subsonic Jets.	242
93.	Predicted Variation of Turbulence Intensity Along the Centerline of Swirling and Nonswirling Isothermal Subsonic Jets.	243
94.	Predicted Variation of Overall Sound Pressure Level Around a 40-foot Arc for Swirling and Nonswirling Isothermal Subsonic Jets.	244
95.	Predicted 1/3-Octave-Band Sound Pressure Level Spectra at 30° from the Jet Axis on a 40-foot Arc for Swirling and Nonswirling Subsonic Isothermal Jets.	245
96.	Single-Flow Facility Burner System.	247
97.	JENOTS Single-Flow Facility.	248
98.	Swirl Test Setup with View of Swirl Vanes.	249
99.	Swirl Vane Section.	250
100.	Swirl Test Setup Schematic.	252
101.	Acoustic Far-Field Measuring Stations.	253
102.	Laser Velocimeter Optics Package.	254
103.	Laser Doppler Velocimeter Setup at JENOTS.	255

LIST OF ILLUSTRATIONS (Continued)

<u>Figure</u>		<u>Page</u>
104.	Cobra Probe Sensing Head.	256
105.	Swirl Test Setup with Cobra Probe.	257
106.	Cobra Probe Measurements 0.5" Downstream of Nozzle Exit, Test Point 1.	259
107.	Cobra Probe Measurements 0.5" Downstream of Nozzle Exit, Test Point 2.	260
108.	Cobra Probe Measurements 0.5" Downstream of Nozzle Exit, Test Point 3.	261
109.	LDV Measurements 0.5" Downstream of Nozzle Exit, Test Point 1.	263
110.	LDV Measurements 0.5" Downstream of Nozzle Exit, Test Point 2.	264
111.	LDV Measurements 0.5" Downstream of Nozzle Exit, Test Point 3.	265
112.	LDV Measurements on the Jet Centerline, Test Point 1.	266
113.	LDV Measurements on the Jet Centerline, Test Point 2.	267
114.	LDV Measurements on the Jet Centerline, Test Point 3.	268
115.	LDV Measurements of Radial Velocity Profiles, Baseline Test Point 1.	269
116.	LDV Measurements of Radial Velocity Profiles, Baseline Test Point 2.	270
117.	LDV Measurements of Radial Velocity Profiles, Baseline Test Point 3.	271
118.	LDV Measurements of Radial Velocity Profiles, Swirl Test Point 1.	272
119.	LDV Measurements of Radial Velocity Profiles, Swirl Test Point 2.	273
120.	LDV Measurements of Radial Velocity Profiles, Swirl Test Point 3.	274

LIST OF ILLUSTRATIONS (Continued)

<u>Figure</u>		<u>Page</u>
121.	Calculated Profiles 0.5" Downstream of Nozzle Exit.	276
122.	Measured Overall Sound Pressure Levels, Test Point 1.	278
123.	Measured Overall Sound Pressure Levels, Test Point 2.	279
124.	Measured Overall Sound Pressure Levels, Test Point 3.	280
125.	Measured 1/3-Octave-Band Sound Pressure Level Spectra, Test Point 1, Microphone at 30° to Jet Axis.	282
126.	Measured 1/3-Octave-Band Sound Pressure Level Spectra, Test Point 2, Microphone at 30° to Jet Axis.	283
127.	Measured 1/3-Octave-Band Sound Pressure Level Spectra, Test Point 3, Microphone at 30° to Jet Axis.	284
128.	Measured 1/3-Octave-Band Sound Pressure Level, Test Point 1, Microphone at 90° to Jet Axis.	285
129.	Measured 1/3-Octave-Band Sound Pressure Level, Test Point 2, Microphone at 90° to Jet Axis.	286
130.	Measured 1/3-Octave-Band Sound Pressure Level, Test Point 3, Microphone at 90° to Jet Axis.	287
131.	Perceived Noise Level Measurements, Test Point 1.	288
132.	Perceived Noise Level Measurements, Test Point 2.	289
133.	Perceived Noise Level Measurements, Test Point 3.	290
134.	Physical Configuration for Analytical Model.	293
135.	Turbulence Intensity at End of Mixing Chamber Versus Air Mach Number at Mixing Station (Plane 1).	294
136.	Turbulence Intensity at End of Mixing Chamber Versus Fuel/Air Ratio.	295
137.	Turbulence Intensity at End of Mixing Chamber Versus Fuel Jet Swirl Number at Mixing Station (Plane 1).	296
138.	Turbulence Intensity at End of Mixing Chamber Versus Fuel-to-Air Velocity Ratio at Mixing Station (Plane 1).	297

LIST OF ILLUSTRATIONS (Continued)

<u>Figure</u>		<u>Page</u>
139.	Turbulence Intensity at Nozzle Exit Plane Versus Fuel-to-Air Velocity Ratio at Mixing Station (Plane 1).	298
140.	4.31" Throat Diameter Water-Cooled, Parallel-Flow, Converging/Diverging Nozzle.	300
141.	LV Measurements 0.5" Downstream of Nozzle Exit.	302
142.	LV Measurements at $x/D_8 = 3.98$.	303
143.	LV Measurements at $x/D_8 = 3.98$.	304
144.	Measured 1/3-Octave-Band Pressure Fluctuation Spectra, Preburner Static Pressure.	306
145.	Measured 1/3-Octave-Band Pressure Fluctuation Spectra, Afterburner Static Pressure.	307
146.	Measured 10-Hz-Narrowband Pressure Fluctuation Spectra.	308
147.	Measured Overall Sound Pressure Levels.	310
148.	Measured 1/3-Octave-Band Sound Pressure Level Spectra, $\theta_{jet} = 40^\circ$.	311
149.	Measured 1/3-Octave-Band Sound Pressure Level Spectra, $\theta_{jet} = 90^\circ$.	312
150.	Measured Overall Sound Pressure Levels.	313
151.	Measured 10-Hz-Narrowband Sound Pressure Level Spectra, $\theta_{jet} = 30^\circ$.	314
152.	Measured 10-Hz-Narrowband Sound Pressure Level Spectra, $\theta_{jet} = 90^\circ$.	315
153.	Flameholder and Typical Spraybar from JENOTS Afterburner Section.	317
154.	LV Measurements 0.5" Downstream of Nozzle Exit, Test Point 1.	318
155.	LV Measurements 0.5" Downstream of Nozzle Exit, Test Point 2.	319
156.	LV Measurements 0.5" Downstream of Nozzle Exit, Test Point 3.	320
157.	LV Measurements on the Jet Centerline, Test Point 1.	321

LIST OF ILLUSTRATIONS (Continued)

<u>Figure</u>		<u>Page</u>
158.	LV Measurements on the Jet Centerline, Test Point 2.	322
159.	LV Measurements on the Jet Centerline, Test Point 3.	323
160.	LV Measurements of Radial Velocity Profiles, Test Point 1.	324
161.	LV Measurements of Radial Velocity Profiles, Test Point 2.	325
162.	LV Measurements of Radial Velocity Profiles, Test Point 3.	326
163.	Overall Sound Pressure Levels, Test Point 1.	328
164.	Overall Sound Pressure Levels, Test Point 2.	329
165.	Overall Sound Pressure Levels, Test Point 3.	330
166.	Measured 1/3-Octave-Band Sound Pressure Level Spectra, $\theta_{jet} = 30^\circ$, Test Point 1.	331
167.	Measured 1/3-Octave-Band Sound Pressure Level Spectra, $\theta_{jet} = 30^\circ$, Test Point 2.	332
168.	Measured 1/3-Octave-Band Sound Pressure Level Spectra, $\theta_{jet} = 30^\circ$, Test Point 3.	333
169.	Measured 1/3-Octave-Band Sound Pressure Level Spectra, $\theta_{jet} = 90^\circ$, Test Point 1.	334
170.	Measured 1/3-Octave-Band Sound Pressure Level Spectra, $\theta_{jet} = 90^\circ$, Test Point 2.	335
171.	Measured 1/3-Octave-Band Sound Pressure Level Spectra, $\theta_{jet} = 90^\circ$, Test Point 3.	336
172.	Measured 10-Hz-Narrowband Sound Pressure Level Spectra, Test Point 2.	337
173.	Measured 10-Hz-Narrowband Sound Pressure Level Spectra, Test Point 3.	338
174.	Ribner's Jet Acoustic Refraction Model.	342
175.	Effect of Jet Velocity on Directivity (Reference 13).	343
176.	Jet Noise Directivity for Air Jet (Reference 13).	344

LIST OF ILLUSTRATIONS (Continued)

<u>Figure</u>		<u>Page</u>
177.	Effect of Jet Temperature on Directivity (Reference 15).	345
178.	Effect of Source Frequency on Directivity (Reference 15).	346
179.	Refraction Schematic for a Point Source Injected into a Jet Flow.	348
180.	Refraction Schematic for a Jet Flow.	349
181.	Schematic of Experimental Setup for Acoustic Far-Field Measuring Stations.	352
182.	Siren Used for Point Source.	353
183.	Directivities of Siren Output in the 500-5000-Hz Frequency Range on a 20-foot Arc with a 0.81" ID Output Port.	354
184.	Comparison of Sound Source Output with Measured Jet Noise Data; Jet at 1670 ft/sec and $T_T = 1500^\circ \text{ R}$.	355
185.	Refraction Experimental Setup with Siren Uncovered.	357
186.	Refraction Experimental Setup with Siren Acoustically Isolated.	358
187.	Jet Acoustics with and without the Tone Source Hardware in the Nozzle.	361
188.	Typical 2-Hz and 10-Hz Bandwidth Data $f_{\text{tone}} = 783 \text{ Hz}$, $M_0 = 1.3$, $T_{T_{\text{jet}}} = 1500^\circ \text{ R}$, and $\theta_{\text{jet}} = 20^\circ$.	363
189.	Typical 1-Hz and 5-Hz Bandwidth Analysis of Siren Tone Data Over the Entire Period of Recording ($\sim 120 \text{ secs}$), $f_{\text{tone}} = 783 \text{ Hz}$, No Jet.	364
190.	Typical 2-Hz Bandwidth Analysis of (Tone + Jet) Data Over the Entire Period of Recording ($\sim 120 \text{ Seconds}$), $f_{\text{tone}} = 783 \text{ Hz}$, $M_0 = 0.9$, $T_{T_{\text{jet}}} = 2000^\circ \text{ R}$.	365
191.	Effect of Jet Velocity on Tone Directivity, $f_{\text{tone}} = 783 \text{ Hz}$, $T_0 = \text{Ambient}$, $M_0 = 0.5, 0.7, 0.9$.	367
192.	Effect of Jet Velocity on Tone Directivity, $f_{\text{tone}} = 783 \text{ Hz}$, $T_0 = \text{Ambient}$, $M_0 = 0.9 \text{ and } 1.3$.	368

LIST OF ILLUSTRATIONS (Continued)

<u>Figure</u>		<u>Page</u>
193.	Comparison of 2-Hz Narrowband Jet Noise Directivity with Siren Tone Directivity, $M_0 = 1.3$, $T_{Tjet} = 1000^\circ \text{ F}$.	369
194.	Effect of Jet Velocity on Tone Directivity, $M_0 = 0.9, 1.3, 1.5$, $T_{Tjet} = 1500^\circ \text{ R}$.	370
195.	Comparison of 2-Hz Narrowband Jet Noise Directivity with Siren Tone Directivity, $M_0 = 1.5$, $T_{Tjet} = 1500^\circ \text{ R}$.	371
196.	Effect of Jet Velocity on Tone Directivity, $M_0 = 1.5$, $T_{Tjet} = 2000^\circ \text{ R}$.	372
197.	Effect of Jet Temperature on Directivity.	374
198.	Effect of Jet Temperature on Tone Directivity, $M_0 = 0.9$, $f_{tone} = 783 \text{ Hz}$, $T_{Tjet} = 1000^\circ$ and 1500° R .	375
199.	Effect of Jet Temperature on Tone Directivity, $M_0 = 1.3$, $f_{tone} = 783 \text{ Hz}$, $T_{Tjet} = 1000^\circ, 1500^\circ, \text{ and } 2000^\circ \text{ R}$.	376
200.	Effect of Jet Temperature on Tone Directivity, $M_0 = 1.5$, $f_{tone} = 783 \text{ Hz}$, $T_{Tjet} = 1500^\circ$ and 2000° R .	377
201.	Tone SPL Reduction Due to Flow, Experiment Versus Theory, $M_0 = 0.5$, $T_{Tjet} = \text{Ambient}$, $f_{tone} = 783 \text{ Hz}$.	379
202.	Tone SPL Reduction Due to Flow, Experiment Versus Theory, $M_0 = 0.7$, $T_{Tjet} = \text{Ambient}$, $f_{tone} = 783 \text{ Hz}$.	380
203.	Tone SPL Reduction Due to Flow, Experiment Versus Theory, Including Convection Amplification Factor, $M_0 = 0.9$, $T_T = \text{Ambient}$, $f_{tone} = 783 \text{ Hz}$.	382
204.	Tone SPL Reduction Due to Flow, Experiment Versus Theory, Including Convection Amplification Factor, $M_0 = 1.3$, $f_{tone} = 783 \text{ Hz}$, $T_{Tjet} = 1000^\circ, 1500^\circ, \text{ and } 2000^\circ \text{ R}$.	383
205.	Tone SPL Reduction Due to Flow, Experiment Versus Theory, Including Convective Amplification Factor, $M_0 = 1.5$, $f_{tone} = 783 \text{ Hz}$, $T_{Tjet} = 1500^\circ$ and 2000° R .	384
206.	Influence of Jet Temperature on Tone SPL Reduction Due to Flow, Experiment Versus Theory.	385
207.	Influence of Tone Frequency on Tone SPL Reduction Due to Flow, $M_0 = 1.5$, $T_T = 2000^\circ \text{ R}$, $f_{tone} = 783 \text{ and } 3000 \text{ Hz}$.	386

LIST OF ILLUSTRATIONS (Continued)

<u>Figure</u>		<u>Page</u>
208.	Influence of Tone Frequency on Tone SPL Reduction Due to Flow Theory, $M_0 = 1.5$, $T_T = 2000^\circ \text{ R}$, $f_{\text{tone}} = 783$ and 3000 Hz .	387
209.	LV Hot-Film Mean Velocity Measurements.	391
210.	LV Hot-Film Turbulent Measurements.	391
211.	LV-Measured Mean Velocity and Turbulent Velocity Axial Decays for a Shock-Free, High-Velocity, High-Temperature Jet.	392
212.	LV-Measured Turbulent Spectrum for Ambient and Heated Jets.	393
213.	Laser Velocimeter Optics Package.	395
214.	Laser Velocimeter Setup at JENOTS.	396
215.	Hot-Film Arrangement on Laser Velocimeter Cart.	398
216.	Mean Velocity Profile Comparison of LV with Hot-Film; $X/D = 2.0$, $M_j = 0.5$.	399
217.	LV-Measured Normalized Radial Mean Velocity Profiles for $M_j = 0.5$, $T_T = \text{Ambient}$ (Conical Nozzle Data).	400
218.	LV-Measured Contour Plot of Mean Velocity in fps at $M_j = 0.5$, $T_T = \text{Ambient}$.	401
219.	LV-Measured Contour Plot of Turbulent Velocity in fps at $M_j = 0.5$, $T_T = \text{Ambient}$.	402
220.	LV-Measured Contour Plot of Turbulent Intensity at $M_j = 0.5$, $T_T = \text{Ambient}$.	403
221.	Laser-Velocimeter-Measured Mean Velocity and Turbulent Intensity Radial Profiles; $M_j = 1.55$, $T_T = 1500^\circ \text{ R}$, $X/D = 9.6$ (C/D Shock-Free Data).	405
222.	LV-Measured Normalized Radial Mean Velocity Profiles for $M_j = 1.55$, $T_T = 1500^\circ \text{ R}$ (C/D Shock-Free Data).	406
223.	LV-Measured Normalized Radial Turbulence Velocity Profiles for $M_j = 1.55$, $T_T = 1500^\circ \text{ R}$.	407
224.	LV-Measured Normalized Radial Mean Velocity Profiles for $M_j = 1.55$, $T_T = 1500^\circ \text{ R}$ (Conical Nozzle Shocked Data).	408

LIST OF ILLUSTRATIONS (Continued)

<u>Figure</u>		<u>Page</u>
225.	LV Measuring Positions for Shock Turbulence Study.	409
226.	Mean Velocity and Turbulence Velocity on Centerline.	410
227.	LV-Measured Turbulence Properties for Shocked Nozzle Flow (Series 2).	411
228.	LV-Measured Turbulence Properties for Shocked Nozzle Flow (Series 3).	412
229.	Influence of Jet Velocity on Exit-Plane Turbulence.	413
230.	Influence of Upstream Temperature on Jet Exit-Plane Temperature.	415
231.	Influence of Upstream Temperature on Jet Exit-Plane Turbulence Intensity.	416
232.	Schematic of Sampling Scheme.	420
233.	Bias Error in Derivative Estimate as a Function of Cut-Off Frequency.	424
234.	Influence of Window Function to Improve Stability of Second Derivative.	425
235.	Schematic of System Used to Generate Simulated Data.	427
236.	Simulation Specifications.	428
237.	Analysis of Simulated Data, N = 20,000 Samples.	430
238.	Analysis of Simulated Data, N = 100,000 Samples.	431
239.	Analysis of Simulated Data, N = 500,000 Samples.	432
240.	General Arrangement for LV to Far-Field Acoustic Cross-Correlation Experiments.	434
241.	Test Arrangement Showing Microphone Slightly Out of Plane for LV Far-Field Acoustic Cross-Correlation Experiments.	435
242.	LV-Measured Normalized Cross Correlation of In-Jet Velocity to Far-Field Acoustic (180,000 Samples).	436
243.	LV-Measured Cross-Power Spectrum.	438

LIST OF ILLUSTRATIONS (Continued)

<u>Figure</u>		<u>Page</u>
244.	Expected Shape of Cross Correlation and Cross-Power Spectrum without Ground Reflection.	439
245.	Cross Spectra of Final Correlation Files.	440
<u>VOLUME III</u>		
246.	Schematic of General Electric Jet Aeroacoustic Computational Procedure.	480
247.	SSNOISE Calculation Flow Chart.	481
248.	Overlay Structure, Including All Subroutines.	483
249.	Subsonic Turbulent Jet.	574
250.	Supersonic Turbulent Jet.	575
251.	Jet Plume Predictions, Free Turbulent Mixing Analysis, $X/D = 1.145$.	586
252.	Jet Plume Predictions, Free Turbulent Mixing Analysis, $X/D = 3.8$.	587
253.	Jet Plume Predictions, Free Turbulent Mixing Analysis, $X/D = 6$.	588
254.	Jet Plume Predictions, Free Turbulent Mixing Analysis, $X/D = 3.8$.	589
255.	Free Turbulent Mixing Data Comparisons, Total Temperature Decay Along Jet Axis.	590
256.	Free Turbulent Mixing Data Comparisons, Total Temperature Decay Along Jet Axis.	591
257.	Free Turbulent Mixing Data Comparisons, Velocity Decay Along Jet Axis.	592
258.	Free Turbulent Mixing Data Comparisons, Mach Number Decay Along Jet Axis.	593
259.	4.3" Conical Nozzle Exhaust Plume Total Temperature Versus Radius, JENOTS Wake Rake Data, $L/Dg = 2.79$.	594
260.	4.3" Conical Nozzle Exhaust Plume Total Temperature Versus Radius, JENOTS Wake Rake Data, $L/Dg = 19.53$.	595

LIST OF ILLUSTRATIONS (Continued)

<u>Figure</u>		<u>Page</u>
261.	4.3" Conical Nozzle Exhaust Plume Velocity Versus Radius, JENOTS Wake Rake Data, $L/D_g = 2.79$.	596
262.	4.3" Conical Nozzle Exhaust Plume Velocity Versus Radius, JENOTS Wake Rake Data, $L/D_g = 19.53$.	597
263.	4.3" Conical Nozzle Exhaust Plume Mach Number Versus Radius, JENOTS Wake Rake Data, $L/D_g = 2.79$.	598
264.	4.3" Conical Nozzle Exhaust Plume Mach Number Versus Radius, JENOTS Wake Rake Data, $L/D_g = 19.53$.	599
265.	4.3" Conical Nozzle Exhaust Plume Total Pressure Versus Radius, JENOTS Wake Rake Data, $L/D_g = 2.79$.	600
266.	4.3" Conical Nozzle Exhaust Plume Total Pressure Versus Radius, JENOTS Wake Rake Data, $L/D_g = 19.53$.	601
267.	The Flow Field of an Ideally Expanded Viscous Jet.	604
268.	The Flow Field of an Inviscid Two-Dimensional Supersonic Jet.	604
269.	Subdivision of the Jet into Inner and Outer Regions.	605
270.	Calculation of Boundary Conditions and Shock Strength and Location by Method of Characteristics.	613
271.	Method for Obtaining Fictitious Shock-Corrected Properties for Use in Calculating Field Points Adjacent to Shocks.	615
272.	Mach Disk Model.	617
273.	Passage of Turbulence Through a Shock.	620
274.	Amplification of Turbulence by a Shock Wave as Predicted by Ribner's Shock-Turbulence Theory.	621
275.	Outline of Complete Computational Procedure.	623
276.	Predicted Shock Shape and Outer Boundary Shape --- Inviscid.	625
277.	Intersection of Shock Shape with Axis of Symmetry.	626
278.	Height of Mach Disk.	627
279.	Shock Shape Prediction on Schlieren Photograph.	628

LIST OF ILLUSTRATIONS (Continued)

<u>Figure</u>		<u>Page</u>
280.	Cross-Stream Variation of Predicted Total-Pressure and Static Pressure for Ideally Expanded Jet, $M_{\text{exit}} = 1.60$, $P_{\text{amb}}/P_{T_{\text{ref}}} = 0.242$.	630
281.	Cross-Stream Variation of Predicted Total Pressure and Static Pressure for Slightly Underexpanded Jet, Showing Total-Pressure Loss Due to Both Shocks and Mixing, $M_{\text{exit}} = 1.25$, $P_{\text{amb}}/P_{T_{\text{ref}}} = 0.242$.	630
282.	Cross-Stream Variation of Predicted Total Pressure and Static Pressure for Jet from Convergent Nozzle, Showing Total-Pressure Loss Due to Both Shocks and Mixing, $M_{\text{exit}} = 1.0$, $P_{\text{amb}}/P_{T_{\text{ref}}} = 0.242$.	631
283.	Comparison Between Predicted Shock Shapes Using Inviscid Prediction Technique and Coupled (Inner-Outer Analysis) Viscous Technique, Shaded Region Represents Flow Which is Significantly Affected by Mixing, $M_{\text{exit}} = 1.25$, $P_{\text{amb}}/P_{T_{\text{ref}}} = 0.242$.	631
284.	Shock Structure Theory Data Comparison, ($P_j/P_{\text{amb}} = 2.1$, $M_{\text{exit}} = 1.0$, $P_{\text{amb}}/P_T = 0.24$).	632
285.	Mean Velocity and Turbulent Velocity on Centerline.	633
286.	Prediction of Overall Power Level.	681
287.	Cold Jet Power Spectrum Prediction Measurement Comparisons.	682
288.	Hot Jet Power Spectrum Theory Data Comparisons for a Shock-Free Supersonic Jet.	683
289.	Cold Jet Power Spectrum Prediction Measurement Comparisons, 2.17-Inch Cold Jet.	684
290.	Cold Jet Power Spectrum Prediction Measurement Comparisons, 2-Inch Cold Jet.	685
291.	1/3-Octave-Band Directivity Patterns for a Cold Supersonic Jet.	686
292.	Predicted Power Distribution for a Cold Subsonic Jet.	687
293.	Predicted Power Distribution for a Cold Supersonic Jet.	688
294.	Directivity Patterns of Overall Sound Pressures for Hot Jets at a Distance of 320 Feet from the Jet Axis.	692

LIST OF ILLUSTRATIONS (Continued)

<u>Figure</u>		<u>Page</u>
295.	Hot Jet Sound Pressure Spectra at Various Angular Positions at a Distance of 320 feet from the Jet Axis (D=45.6 inches, $M_0 = 0.83$).	693
296.	Near-Field Microphone Locations for a Full-Scale Jet Engine (D = 43 inches).	695
297.	Near-Field Sound Pressure Spectra at Various Microphone Locations (An Internal Turbulence Level, $u'/U_0 = 0.15$, Was Assumed for the Calculations), Microphones 23 and 24.	696
298.	Near-Field Sound Pressure Spectra at Various Microphone Locations (An Initial Turbulence Level, $u'/U_0 = 0.15$, Was Assumed for the Calculations), Microphones 1-4 and 27).	697
299.	Near-Field Sound Pressure Spectra at Various Microphone Locations (An Initial Turbulence Level, $u'/U_0 = 0.15$, Was Assumed for the Calculations), Microphones 7 and 8.	700
300.	Near-Field Microphone Locations for a Scale Model Jet (D = 4.55 inches).	701
301.	Near-Field Sound Pressure Spectra at Various Microphone Locations.	702
302.	Comparison of Measurements and Predictions by Composite Acoustic Models.	706
 <u>VOLUME IV</u> 		
303.	4.3-Inch Throat Diameter, Water-Cooled, Parallel-Flow, Convergent/Divergent Nozzle.	1165
304.	4.3-Inch Exit Diameter, Water-Cooled, Conical, Convergent Nozzle.	1166
305.	Engineering Drawing for the 4.3-Inch Throat Diameter, Water-Cooled, Parallel-Flow, Convergent/Divergent Nozzle.	1167
306.	Engineering Drawing for the 4.3-Inch Exit Diameter, Water-Cooled, Conical, Convergent Nozzle.	1168
307.	Acoustic Far-Field Measuring Stations.	1170
308.	Acoustic Near-Field Measuring Stations.	1171

LIST OF ILLUSTRATIONS (Concluded)

<u>Figure</u>		<u>Page</u>
309.	JENOTS Microphone Mount.	1172
310.	Schematic of JENOTS Acoustic Data Acquisition System.	1173
311.	Schematic of Instrumentation Data Room Acoustic Data Reduction System.	1175
312.	Description of Far-Field Acoustic Data Sheets.	1184
313.	Description of Near-Field Acoustic Data Sheets.	1185

LIST OF TABLES

VOLUME I

<u>Table</u>		<u>Page</u>
1.	Summary of Results for the Combustion Roughness Experiments.	85

VOLUME II

2.	Experimental Data for Determining the Ratio of Self-Noise to Shear-Noise.	174
3.	Test Matrix.	360
4.	Hot-Film Turbulence Measurements.	443
5.	LV Turbulence Measurements.	444
6.	$M_j = 0.5$ LV Measurements.	445

VOLUME III

7.	Shear- and Self-Noise Table of Experimentally Determined Constants.	645
8.	Fluid Shrouding for Unheated Jets.	647
9.	Fluid Shrouding for Heated Jets - Influence of Velocity.	667
10.	Fluid Shrouding for Heated Jets - Influence of Temperature.	671

VOLUME IV

11.	C/D Nozzle Flow Conditions, Acoustic Test, and T_t/V_j Matrix	1177
12.	Cone, Thin-Lip Flow Conditions, Acoustic Test, T_t/V_j Matrix + Shock-Free Design Line of C/D Nozzle	1178
13.	Cone, Thick-Lip Flow Conditions, Acoustic Test, Shock-Free Design Line	1180
14.	C/D Nozzle Flow Conditions, Acoustic Test, Shock-Free Design Line	1180
15.	JENOTS Ground Reflection Corrections (Δ dB's to be added to SPL's).	1182

SECTION 1.0

BACKGROUND

With the advent of larger and more powerful military and commercial aircraft propulsion systems, it was increasingly apparent to government and industry that major efforts had to be undertaken to improve the general community environment affected by these systems. With the initiation of the American SST Program and its subsequent cancellation, it was evident that major research efforts were necessary to further investigate the mechanisms of jet noise generation and reduction. Over the last three decades a considerable effort has been directed toward enhancing our understanding and technology. Both scientist and engineer have exerted their talents and experience to solve and mitigate the aeroacoustic aspects of high-velocity exhaust jets-noise. The problem of noise reduction is illustrated by the fact that the acoustic power is but one-millionth of the total flow power. The problem of extracting basic understanding is underscored by the fact that theoreticians are still probing for the more exact theoretical acoustic formulations for jet noise generation and acceptable approximations for their solution. In addition to these complications, considerable energy is being spent developing the instrumentation capable of supporting the theoretician and engineer.

The overall objective of this joint Air Force and Department of Transportation Supersonic Jet Exhaust Noise Investigation was to develop a comprehensive mathematical model capable of providing aeroacoustic design data to develop future supersonic jet exhaust noise suppressors. Because of a lack of a clear understanding and a detailed mathematical specification of the noise-producing sources for even the most simple nozzles, the investigations for this program centered on developing techniques which would contribute to a fuller understanding of noise source generation of simple jets.

The Air Force Aero Propulsion Laboratory supported an initial one-year exploratory research program in 1971. Three contracts were awarded: General Electric Company; Lockheed Aircraft Company; and Bolt, Beranek, and Newman Company (see Reference 1 for General Electric's Phase I Final Report).

As a result of this initial exploratory program, two two-year contracts were awarded, one to the General Electric Company, and one to the Lockheed Aircraft Company under the joint sponsorship of the Air Force and the Department of Transportation.

At the time of the initial phase of work, a thorough review of various competing mathematical models used to explain supersonic jet noise generation processes was performed. Additionally, work was begun to develop the type of instrumentation necessary to measure the detailed in-jet flow properties of heated supersonic jets.

One result of General Electric's initial theoretical efforts was the establishment of a comprehensive turbulent mixing aeroacoustic model capable of computing detailed aerodynamic flow properties - velocity (mean and turbulent), pressure, temperature, density, and length scale of turbulence, as well as being capable of computing all the main acoustic properties - overall sound power level, power spectra, overall sound pressure level, sound pressure level spectra, and jet directivity. The method was additionally applied toward predictions of axial power distributions of subsonic and supersonic jets, acoustic peak frequency distribution, and the effects of initial turbulence intensity on jet noise. This computational scheme was so designed as to enable the acoustic predictions to be based on aerodynamic input which could be predicted or measured, thus allowing the scheme to be compatible with exhaust nozzle suppressor investigations where the detailed properties cannot yet be predicted.

To complement the theoretical developments the General Electric Company developed a unique in-jet, noncontact-type probe, capable of velocity measurements in high temperature jets - General Electric's laser velocimeter. The development work performed in this area clearly marked the laser velocimeter as the measurement tool for the future.

It was found during the first phase of effort that the models which yielded the greatest information were indeed the more classical turbulent mixing noise theories of Lighthill, Ribner, and Ffowcs-Williams. In spite of the success demonstrated with these models, limitations were found. Two examples which illustrate the limitations of the classical theories are: 1) jet noise does not obey a density squared (ρ^2) power law except at high acoustic Mach numbers ($Mo \geq 1.50$); 2) the refraction or convection/refraction coupling was not adequately represented in these theories.

In this time period investigators were becoming increasingly concerned with experimental findings which suggested that jets were highly ordered. Essentially, implying that the basic assumption of source compactness of the Lighthill class of turbulent mixing theories was invalid. Advocates for the "orderly structure" of jets claimed that the dominant noise source for jets was the orderly structure models.

With the initiation of the follow-on contract, our approach was to maintain the close relationship of the aerodynamic nature of the supersonic jets, to identify what acoustic characteristics needed better specification and theoretical definition; to continue with the development and application of our laser velocimeter - particularly for flows commensurate with industrial application; and, to examine the feasibility of using the laser velocimeter for direct point source location application.

The method of approach that the GE team elected was to model the problems as simply as possible (conceptually and theoretically), with the aim of clarifying the physics of the problems rather than creating further complications. The goal was to shed "new light", and to give direction by which suppressor technology could be influenced and improved.

An illustration of the General Electric aeroacoustic approach is schematically shown in Figure 1. The idea that is portrayed is to develop a "coupled aeroacoustic approach for predicting the essential features of jet noise. The aerodynamic input is to be computed or measured. The acoustic model is linked to the aerodynamics to predict the acoustic spectral characteristics at all observation stations. The aerodynamic input should

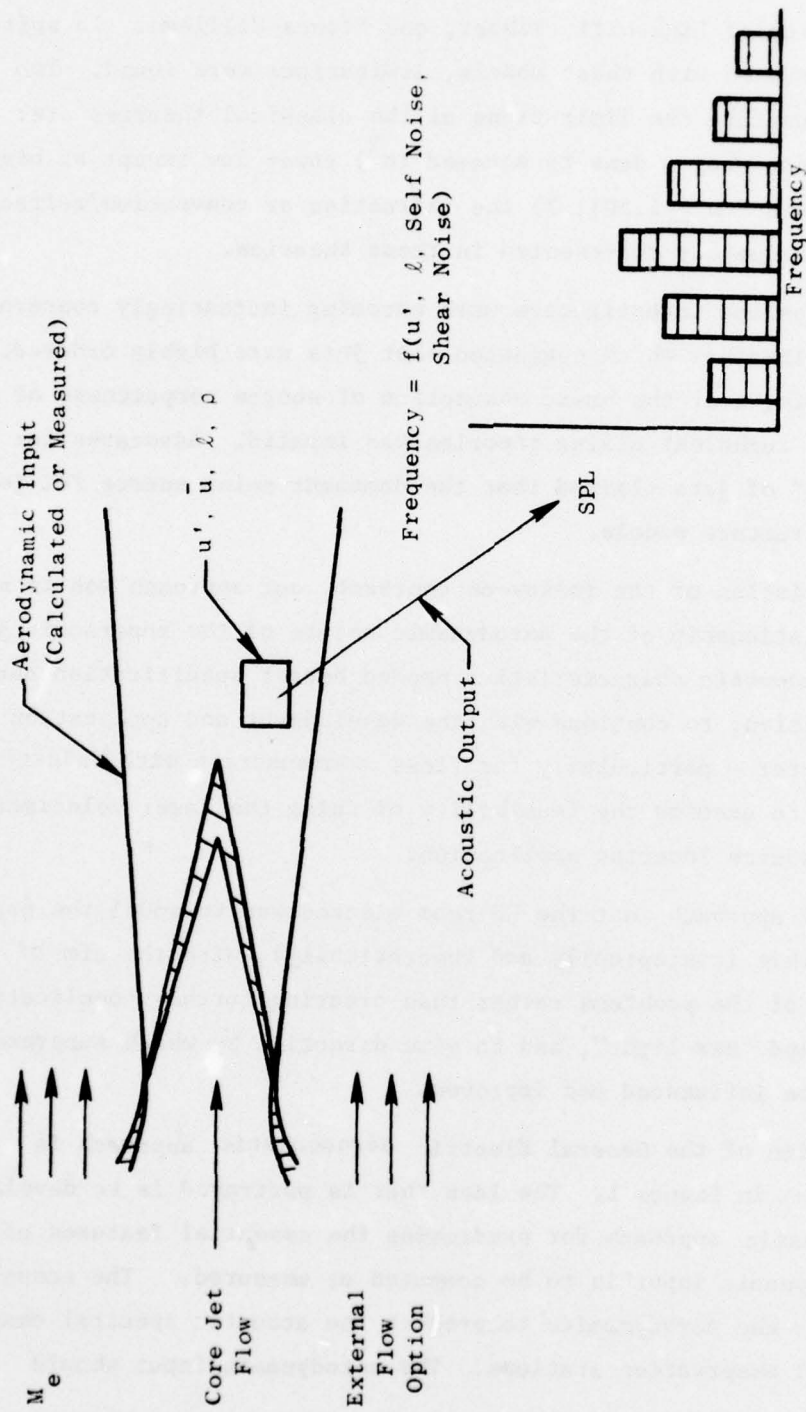


Figure 1. General Electric Aeroacoustic Approach.

provide mean flow and turbulent flow characteristics and should be capable of computing subsonic as well as supersonic jet exhaust information.

As is true with any investigation, certain ventures were successful, and others were less successful. The following discussion represents summaries of the major accomplishments of the contract effort. This volume (which is the summary volume) is complemented by three additional volumes which represent the final report. Volume II contains detailed discussions of the theoretical and experimental work efforts performed during the second year of the contract. It extends the work reported in Reference 2 which was an interim technical report. Volume III is a computer user's manual which describes the aeroacoustic computational methods developed. Volume IV is a data volume of far-field and near-field acoustic measurements.

SECTION 2.0

REVIEW OF THE THEORETICAL DEVELOPMENTS OF THE AERODYNAMICS OF SUPERSONIC JETS

There are two distinct techniques which have been used to analyze the aerodynamic flow field in a supersonic jet. In the first approach, the jet is treated as a viscous, boundary-layer flow. The resulting flow field is of the type depicted in Figure 2. According to the usual boundary layer approximations, the radial velocity components are assumed small in comparison to their axial counterparts, and, in addition, the pressure is taken to be constant throughout the whole flow field. These approximations implicitly assume that the static pressure at the jet exit plane is identical to the ambient pressure and that Prandtl-Meyer expansions and/or shock waves are not present in the flow field. Consequently, this viscous boundary layer analysis can only be applied to subsonic jets, or to supersonic jets which are ideally (or nearly ideally) expanded.

In contrast to this viscous analysis, the second traditional technique for analyzing supersonic jets completely ignores the effects of turbulent mixing. In this second (inviscid) analysis, the full two-dimensional equations of motion are used, and strong radial and axial pressure gradients can occur. These pressure gradients have their origin at the nozzle exit plane where the static pressure is generally significantly different from the ambient pressure. In adjusting to the ambient pressure, the flow field generally develops a series of shock waves and Prandtl-Meyer expansions in a nearly periodic, cell-like fashion. A schematic description of the qualitative features of a jet described by this two-dimensional analysis is shown on Figure 3.

As indicated above, both of these approximate models are applicable to the analysis of a certain class of supersonic jet. However, as might be expected, neither model applies to all supersonic jets. Thus, for example, the effects of friction can never be entirely removed from the jet. Further,

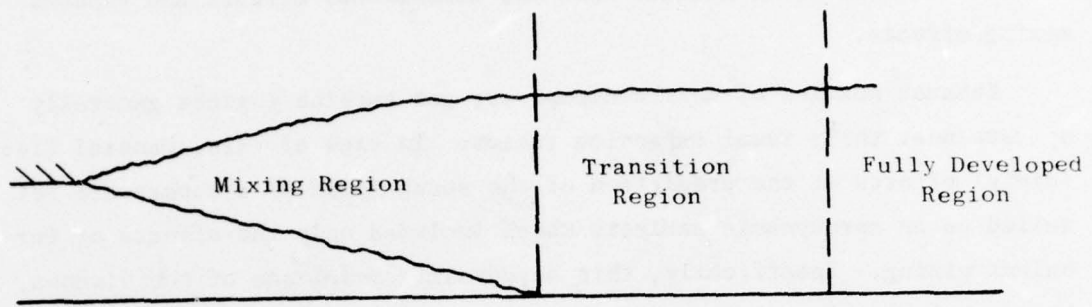


Figure 2. The Flowfield of an Ideally Expanded Viscous Jet.

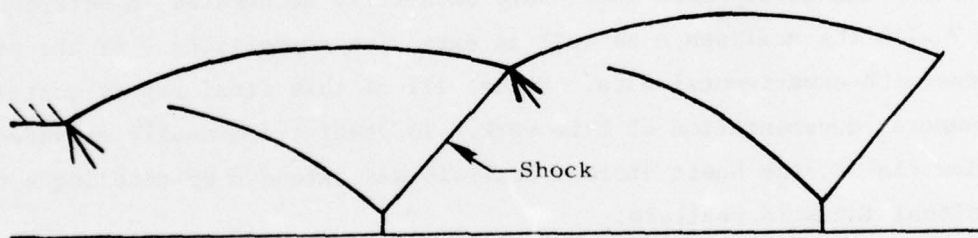


Figure 3. The Flowfield of an Inviscid Two-Dimensional Supersonic Jet.

supersonic jets are seldom uniform, parallel ideally expanded jets. Consequently, in order to obtain an acoustic prediction technique which is applicable to both ideally expanded and non-ideally expanded jets, the aerodynamic model must include both two-dimensional effects and viscous mixing effects.

Exhaust nozzles of most contemporary gas turbine engines generally operate near their ideal expansion ratios. In view of this, General Electric's initial efforts at the prediction of the sound field of a supersonic jet relied on an aerodynamic analysis which included only the effects of turbulent mixing. Specifically, this aerodynamic model was of the viscous, boundary layer type described above. The computerized version of this analysis is referred to as the JETMIX computer program. This computer program solves the time-averaged turbulent boundary layer equations using boundary conditions which are appropriate for free jets. The turbulent Reynold's stresses are included by means of a turbulence model which is based on turbulent kinetic energy concept. This turbulence model is based on those developed by Rotta⁽³⁾, Glushko⁽⁴⁾ and Spalding⁽⁵⁾. The details of this turbulence aerodynamic model have been fully documented in References 6 and 7 with the analyses - as well as extensive comparisons - of the predictions with experimental data. Volume III of this final report contains the computer documentation of this work. To predict nonideally expanded jet flow fields, the basic viscous analysis was extended by coupling a two-dimensional inviscid analysis.

The method used was to include the two-dimensional effects which occur in nonideally expanded jets by dividing the jet into an inner region and an outer region as shown in Figure 4. The outer region of the jet contains that part of the jet in which the effects of turbulent mixing are significant. Near the nozzle exit, the outer region is composed of a narrow annular portion of the flow field on the outer edge of the jet; downstream of the exit plane, the thickness of the outer region increases until it eventually includes the entire jet. In the analysis, the outer region is computed by the original viscous, boundary layer computer program. Now, whereas the outer region of the jet is dominated by the effects of viscous mixing, the inner region of

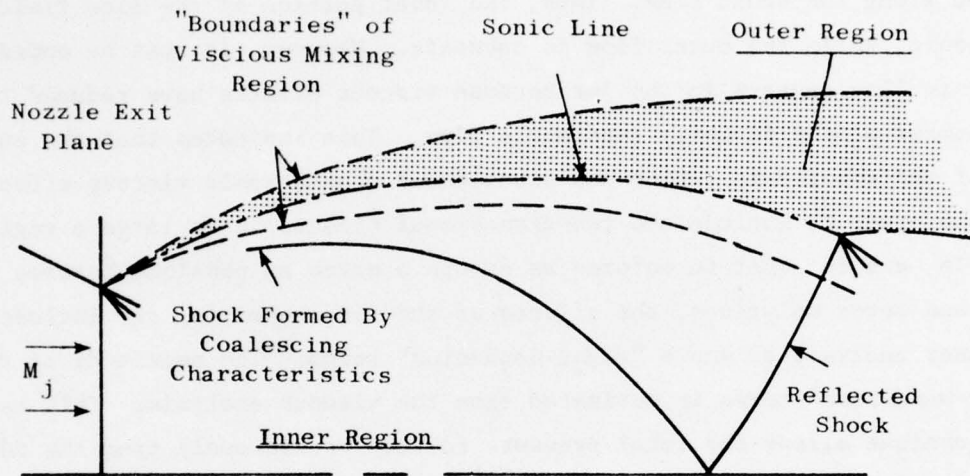


Figure 4. Subdivision of the Jet into Inner and Outer Regions (Outer Region Shown Shaded).

the jet is dominated by the familiar Prantl-Meyer expansions and shock waves which characterize two-dimensional supersonic flow fields. Complete descriptions of this shock flow analysis are given in References 8 and 9.

As indicated in Figure 4, the two separate parts of the flow field are matched along the sonic line. Thus, the inner portion of the flow field is supersonic, while the outer flow is subsonic. However, it must be noted that the sonic line appears in the jet because viscous effects have reduced the Mach number of the formerly supersonic flow. This indicates that the outer edge of the supersonic region has experienced considerable viscous effects. Thus, in order to include the two-dimensional effects in as large a region as possible, and in order to enforce as smooth a match as possible between the inner and outer solutions, the effects of the viscous mixing are included in the inner analysis as known "right-hand-side" terms. The magnitude of the "right-hand-side" terms is estimated from the viscous analysis. This matching technique allows the total pressure to vary continuously from the outer edge of the jet (where the flow is essentially stagnated) through the sonic line and all the way to the jet centerline (where the flow is supersonic). Then, by matching the static pressure at the sonic line, it is ensured that all flow properties are continuous at the matching line. The equations expressing this model, as well as the methods for matching the inner and outer solutions and shock reflections, are well described in the mentioned references.

To illustrate the capability of the techniques described, Figures 5 and 6 are shown. Figure 5 corresponds to flow from a convergent nozzle with sonic velocity at the exit. The pressure ratio is $P_j/P_{amb} = 2.1$. This figure shows radial variations of both total and static pressures at each of two axial locations ($X/R = 1.9$ and $X/R = 2.65$). The rate at which the mixing region spreads with distance from the nozzle exit can be seen, as can the increasing total-pressure loss due to shocks. Relatively large levels of static pressure variation also are observed, even though the underexpansion is still mild.

Figure 6 represents predictions of the coupled analysis (for a jet of pressure ratio $P_j/P_{amb} = 2.1$). The top portion of the figure shows a super-

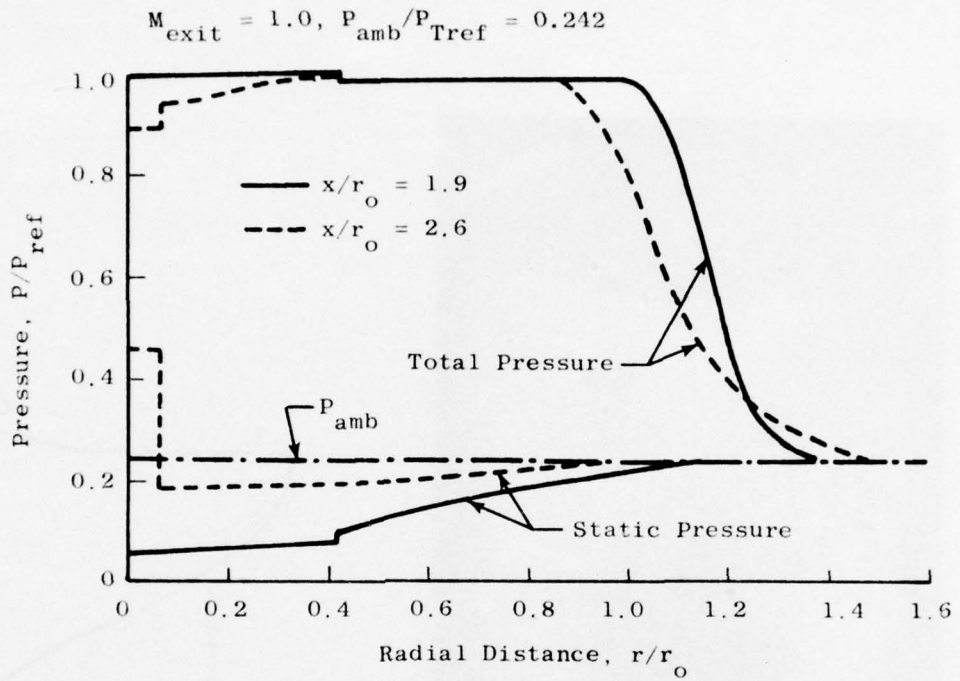


Figure 5. Cross-Stream Variation of Predicted Total Pressure and Static Pressure for a Jet from a Convergent Nozzle, Showing Total Pressure Loss Due to Both Shocks and Mixing.

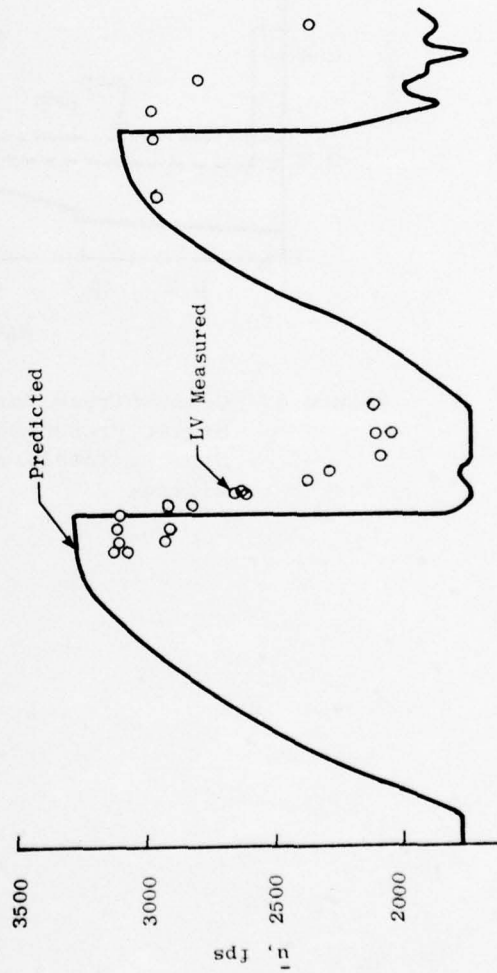
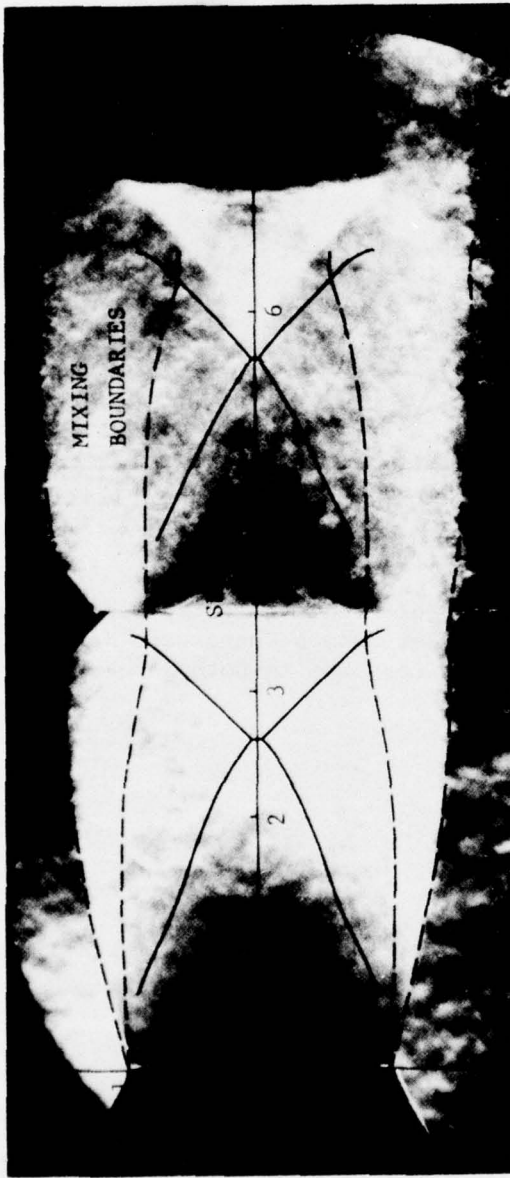


Figure 6. Predicted Shock Shape and Mean Velocity Decay Versus Measurements, $M_j \sim 1.5$, $T_T \sim 1500^\circ R$.

position of the predicted shock structure on a Schlieren photograph of a jet at the same conditions. The agreement for the first shock cell is seen to be excellent; however, at the second location, the predicted solutions do deviate from the observed locations. The bottom portion of Figure 6 shows the predicted axial distribution of mean velocity and turbulent velocity on the jet's outer line. The open symbols were from data measurements using General Electric's laser velocimeter. As can be seen, the theory data comparisons are certainly reasonable.

The discussion given above described the most recent improvements obtained in General Electric's development of predictive procedures for supersonic jet exhaust plumes. We have found that the techniques developed are very tractable and can be used with reasonable confidence for studying the aerodynamic flow field of high velocity and high temperature jets. The computer programs developed for the flow field predictions can be found fully described in Volume III of this final report.

A key aspect of all the aerodynamic programs is that the turbulent kinetic energy is computed. As was indicated by Figure 1, any of the turbulent mixing noise models depend on this input. Thus, the acoustic radiation from an off-design jet can be computed directly as was done for ideally expanded jets (see references 1, 10). This type of calculation automatically takes into account the indirect effect of shock structure on jet noise. That is, the local turbulence level is increased by the shock and so the local acoustic source term is similarly affected. Nevertheless, the presence of shock waves in nonideally expanded jets will not necessarily lead to a higher predicted level of noise (as compared to the corresponding ideally expanded jet). The reason is that with the increase in turbulence there exists a corresponding change in the mean velocity which could tend to off-set the generation of turbulence by the shocks.

SECTION 3.0

REVIEW OF RECENT THEORETICAL ACOUSTIC MODEL DEVELOPMENTS

In the Background section it was indicated that, although the classical turbulent mixing theories were quite successful, they also had limitations. A list of constraints, which was drawn up as the criterion for jet noise theories, follows:

1. Directivity
2. Density and temperature characteristics
3. Source distribution information
4. Influence of initial turbulence
5. Shock effects
6. Calculations must be based on an aerodynamic input, either calculated or measured profiles

Classical Lighthill/Ffowcs-Williams/Ribner turbulent mixing theories will predict (for subsonic jets) peak noise along the jet axis for all frequency bands. Acoustic experiments clearly show that the zero angle peak noise prediction for all frequencies is incorrect and overpredicts the noise, and that the jet noise directivity is a function of frequency. The acoustic engineer has recognized this fact for many years. In most instances the jet noise "dip" was associated with the refractive properties of the jet. Ribner⁽¹¹⁻¹⁷⁾ and his team at the University of Toronto have investigated this problem extensively and have shed a great deal of light on this problem and on methods of jet noise modeling to incorporate refractive phenomena. Much of the concern, however, centered on the higher frequencies. An enlightening presentation of experimental jet noise tests by Lush⁽¹⁸⁾ pointed to the low frequencies. There it was shown that, in contrast to the high frequency jet noise, jet noise convection amplification was greater than classical theory at the low frequency.

Hock, Puponchel, Crocking, and Bryce⁽¹⁹⁾ illustrated characteristics of jet noise, namely the influence of jet density and temperature. Classical

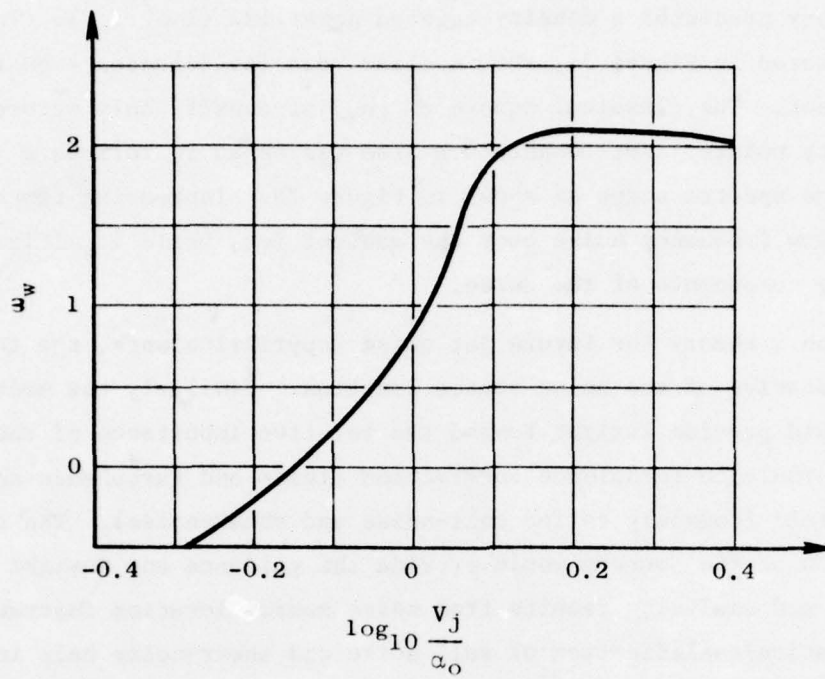
jet noise theory predicted a density-squared power law ($I \propto \rho^2 \dots$). The results, illustrated in Figure 7a, show a clear velocity dependence on the density exponent. The classical square of the jet density only occurs at the higher velocity points. Jet temperature also was shown to influence jet noise by shifting the spectra shape as shown in Figure 7b. Increasing temperature enhanced the low frequency noise over the ambient jet, while it mitigated the high frequency components of the noise.

To draw on a theory for future jet noise suppression work, the theory should be indicative of the noise source location. Similarly the models developed should provide insight toward the relative importance of the roles between the turbulence-turbulence interaction fields and turbulence-shear interaction field (commonly called self-noise and shear-noise). The aspect of the location of the sources would provide the guidance and insight relative to developing and analyzing results from noise source location instruments. The identification/qualification of self-noise and shear-noise help in selecting the proper aerodynamic parameters of interest.

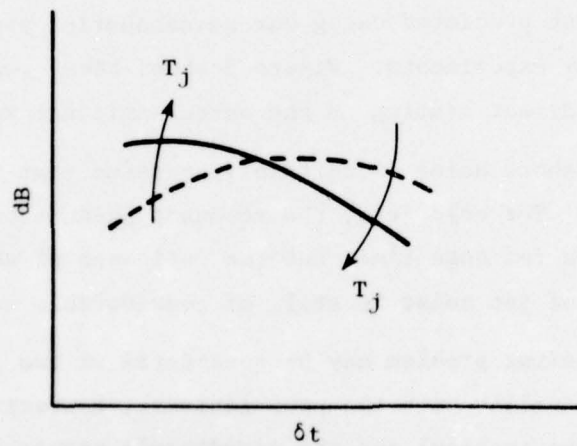
It has been found that, by significantly increasing the exit plan turbulence levels of the jet, the noise level would correspondingly be increased. These results were first predicted using our aeroacoustic prediction methods and further verified by experiments. Figure 8 shows these results. Information such as this has direct bearing on the aerodynamic nature of jet noise.

The influence of shock noise is certainly an issue that far too few people have addressed. For cold jets, the resonant phenomenon, or shock screech, has been known for some time, but the influence of shock noise on the broadband content of jet noise is still of considerable concern.

The jet noise modeling problem may be considered in two parts: the purely acoustic part (dealing with the propagational, convective, and refractive portions of the problem) and the aerodynamic nature of the problem. Both parts of the problem are important for understanding the full aspects of the problem. The approach taken has been to make reasonably sure that the aerodynamics of the problem are intimately connected to the acoustics of the problem. The name of the jet noise problem is aerodynamic or turbulent mixing noise, and we should have assurance that we understand the aerodynamic/acoustic coupling.



(a) Experimental Jet Density Exponent.



(b) Influence of Jet Temperature on Jet Noise Spectra

Figure 7. Influence of Jet Velocity and Temperature on Jet Density Exponent and Jet Spectra.

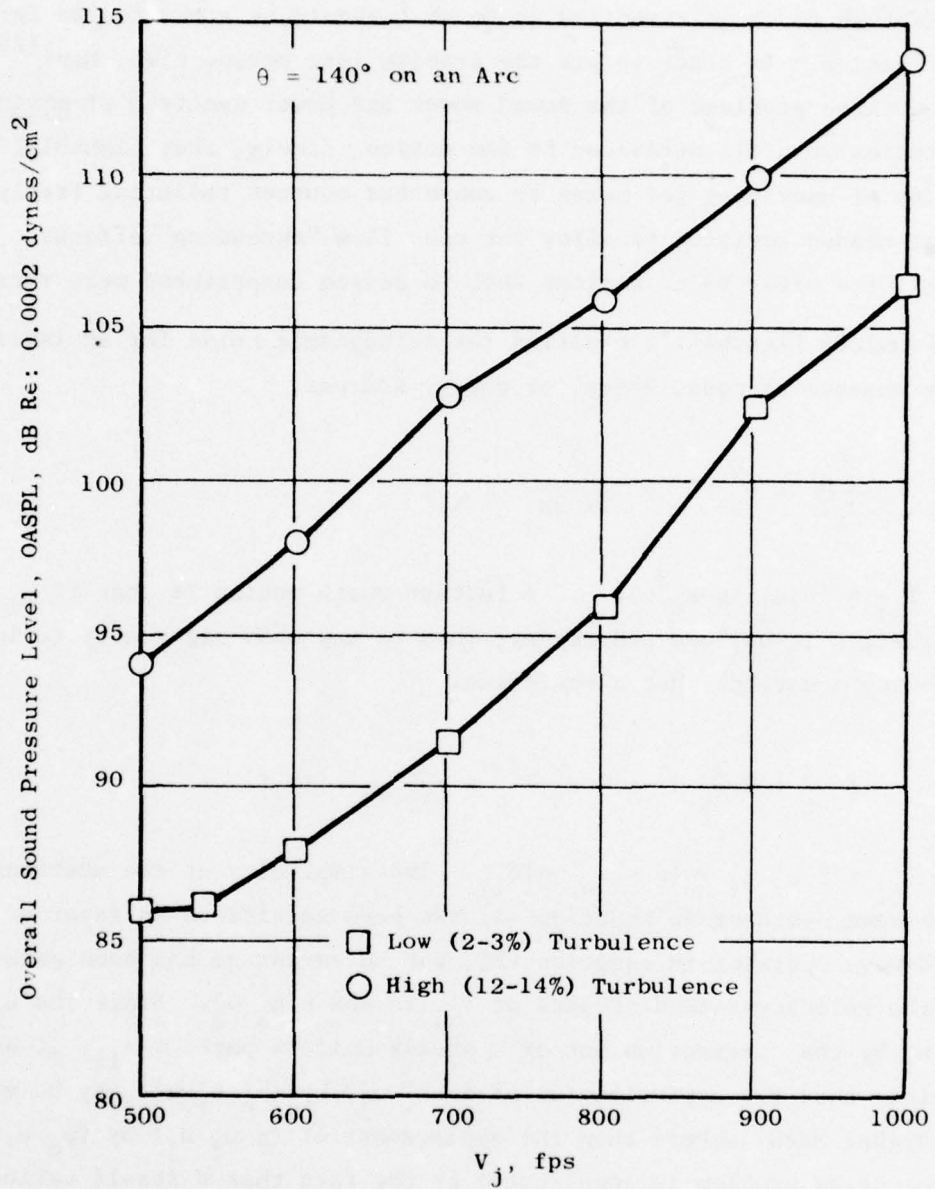


Figure 8. Effects of Increased Exhaust Turbulence Intensity on Jet Noise.

To improve our modeling and understanding of jet noise, the list given above served to focus attention as to what should be attempted as further clarification. In order to put the problem into perspective, Mani⁽²⁰⁾ considered three problems of the sound power and power spectrum of moving sources. The studies were all motivated by one notion, namely, that Lighthill's original idea of ascribing jet noise to convected sources radiating freely to the ambient needed revision to allow for mean flow "shrouding" effects. In his work all the other basic notions such as source compactness were retained.

Consider Lighthill's equation for aerodynamic noise for an inviscid gas in the absence of mass, force, or energy sources:

$$\frac{\partial^2 \rho}{\partial t^2} - a_o^2 \nabla^2 \rho = \frac{\partial^2}{\partial x_i \partial x_j} [T_{ij}] \quad (1)$$

where $T_{ij} = \rho u_i u_j + (p - a_o^2 \rho) \delta_{ij}$. A feature worth noting is that if $u_i = u_i' + U \delta_{ij}$ where U is uniform and steady, then we may show rigorously (using the continuity equation) that ρ satisfies:

$$\left[\frac{\partial}{\partial t} + U \frac{\partial}{\partial x} \right]^2 \rho - a_o^2 \nabla^2 \rho = \frac{\partial^2}{\partial x_i \partial x_j} [T'_{ij}] \quad (2)$$

where $T'_{ij} = \rho u_i' u_j' + [p - a_o^2 \rho] \delta_{ij}$. The simplicity of the stationary medium-wave operator in equation (1) has been sacrificed in favor of the convected-wave operator in equation (2), but an advantage has been gained in that the velocity-dependent part of T'_{ij} is now $\rho u_i' u_j'$. Since the u_i' differ from u_i by the subtraction out of a steady uniform part, $U \delta_{ij}$, it becomes plausible that the approximation of $(\rho u_i' u_j')$ by $(\rho_o u_i' u_j')$ may be valid for much higher Mach numbers than the replacement of $(\rho u_i u_j)$ by $(\rho_o u_i u_j)$. The jet noise problem is complicated by the fact that U itself varies (particularly in the transverse direction), but the transformation of equation (1) into equation (2) does serve to illustrate one of the motivations that has led investigators [most notably O.M. Phillips⁽²¹⁾] to describe the aerodynamic sound generation problem in terms of a convected-wave equation rather than a stationary medium-wave equation. For example, the starting point of Reference (21) is equation (2.8) of Reference (21), wherein a convected-wave

equation is obtained for $\log(p/p_0)$ with a source term on the right-hand side involving only velocity fluctuations.

The difficulty with the convected-wave equation of the general type as developed by Phillips is that it is very difficult to obtain general solutions to it. Studies with the Phillips' equation as a starting point generally employ an asymptotic, high frequency analysis thus rendering the analysis most suitable for high velocity jets. Mani's study was motivated by the need to develop solutions pertinent to lower frequencies (and, hence, lower jet velocities). For such lower frequencies, it seems permissible to approximate the true jet velocity profile by a slug flow or top-hat-type velocity profile jet.

There are two aspects of the presence of a mean flow that do receive explicit recognition in Lighthill's work. One is the recognition that transverse gradients of the mean flow couple with gradients of the fluctuating flow to produce "shear noise." The other, more subtle effect of the flow (in view of the largely solenoidal nature of the u_j'), is that the noise generation process is best ascribed to moving sources. It may be said that as important as Lighthill's recognition of the quadrupole order of jet noise was, his recognition that the sources must be viewed in a convected frame of reference in order to preserve source compactness and in order not to artificially inflate the time rate of change of the turbulence was even more important (a frozen, subsonically convected pattern of turbulence radiates no sound). Peculiarly, however, this very insistence on use of convected sources led to a major difficulty of the theory, because the effect of motion on the acoustic output of a source is to enhance its output, an effect described as "convective amplification." This led to a prediction that jet noise power could exhibit a higher-than-eighth-power dependence on jet exhaust velocity, a result never observed experimentally. Jet noise data show a very good eighth-power dependence over a wide velocity range up to jet exit Mach numbers of 2.

Three good explanations have been given for the tenacity of the observed eighth-power dependence. First (as proposed by Lighthill himself), it is experimentally observed that turbulence intensity (RMS turbulence level

jet mean velocity) drops off somewhat as jet exit Mach numbers are raised. Second, the finite eddy life time correction to Lighthill's moving source solutions of Ffowcs-Williams⁽²²⁾ and Ribner⁽²³⁾ tends to reduce the radiative efficiency of the quadrupoles at higher jet velocities (and associated higher frequencies). Finally, as pointed out by Ribner⁽²⁴⁾, Powell⁽²⁵⁾, and Csanady⁽²⁶⁾, the fact that the moving quadrupoles are embedded in fast moving fluid (with respect to which they are not moving at all) indicates that only limited convective amplification will occur (in fact, at very high frequencies, no convective amplification will occur).

The last explanation is probably the most pertinent one. The reduction of turbulence intensity with increasing jet speed is experimentally found to be too small to effectively counterbalance the theoretically predicted convective amplification. Measurements by Davies, Fisher, and Barratt⁽²⁷⁾ have shown that the finite eddy life time correction of Ribner and Ffowcs-Williams cannot be significant for subsonic jet Mach numbers. Most importantly, recent careful jet noise experiments by Lush⁽¹⁸⁾ lend strong support to the third explanation. Lush analyzed jet noise spectra at various angular positions in terms of a source frequency parameter (which corrects out the Doppler shift effect). He found that for off-axis locations and for low enough values of the source frequency parameter, the predicted convective amplification does indeed occur. It is at shallow angles to the jet axis and for high values of the source frequency parameter that the convective amplification fails to occur. Such a detailed picture of jet noise can be shown to be fully compatible with the idea that the shrouding of a moving source by a fast-moving fluid inhibits convective amplification.

Mani initially considered jets to be characterized by a slug flow mean velocity profile. The sources were simple harmonic in their own frame of reference and were assumed to convect with the same velocity as the jet. Three problems were considered in Reference 20. The first problem was the case of a simple *monopole* convecting along the axis of a round jet. The second problem considered the need to understand off-axis lines of convection. The third problem considered the jet density issues.

From the first model problem, Mani analytically showed a couple of key features: (1) the incorporation of fluid shrouding confirmed the frequency-dependent nature of convection amplification, (2) at low frequencies there exists greater-than-classical convection amplification, while at high frequencies, there is less convection amplification, and (3) the intrinsic source strengths follow Strouhal scaling with respect to velocity. Figures 9, 10, 11, and 12 illustrate these results.

Figure 9 expresses the total power emitted by a source nondimensionalized by the classical convective amplification power. Corrections of > 0 dB are indicative of underestimates of classical convection amplification. The figure clearly shows that the moving source model includes the frequency-dependent nature of convective amplification.

Figure 10 is a starting point to consider the implications with regard to Strouhal scaling of the results shown in Figure 9. Shown under the curve labelled $M = 0.3$, one-third octave intensities obtained by Lush⁽¹⁸⁾ for a jet Mach number of 0.37 at 90° are shown. This curve is chosen as a baseline because, at that low Mach number of 0.37 and location (90° to jet axis), we expect little convective amplification effects. The abscissae are shown in Strouhal numbers, $St = (2fa/M_c)$, and the ordinates are only relative decibel levels.

An intensity spectrum at 90° was chosen because, in addition to lack of convective amplification effects, the 90° location also provides a very good and clean measure of the intrinsic strength of the sources (their frequency distribution). This is because that location is largely characterized by "self noise." A basic assumption of the process used in deriving Figure 11 is that the frequency distribution of the "intrinsic source strengths" does follow Strouhal scaling with respect to velocity. The basic argument of what follows is to point out that the radiative efficiency of the sources is frequency-dependent and, being higher for the low frequencies than for the high frequencies, causes peak frequencies of the sound power spectrum to scale with velocity much slower than a first power (as is assumed in conventional Strouhal scaling). The particular low Mach number datum used to establish this result (taken in this case as the 90° intensity spectrum of

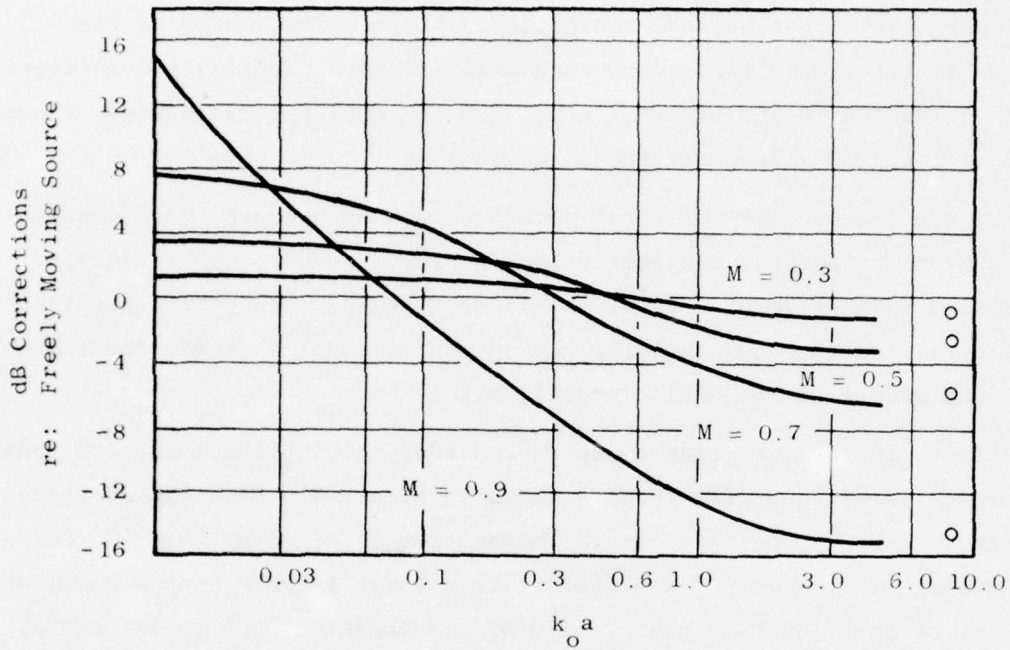


Figure 9. Convective Amplification as a Function of M and ka .

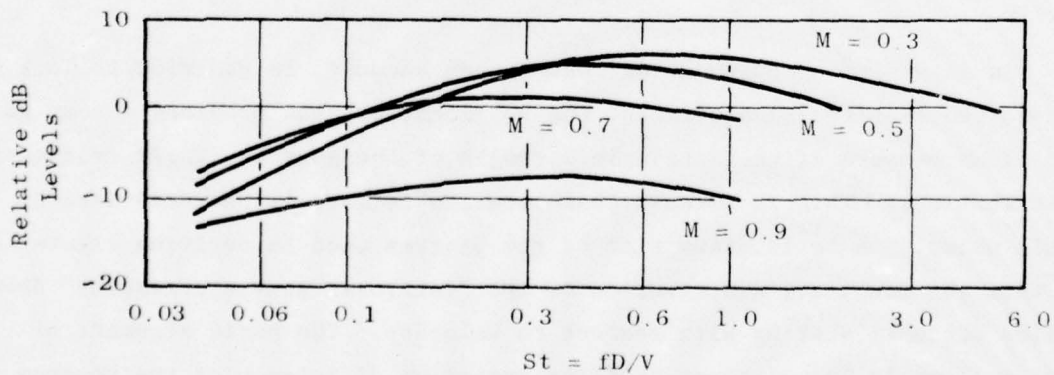


Figure 10. Implications for Strouhal Scaling.

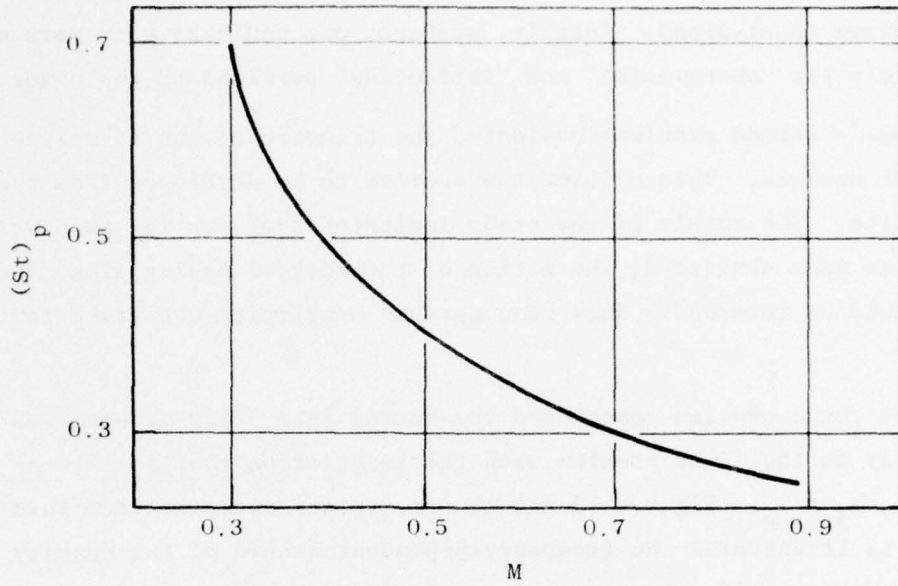


Figure 11. Peak Strouhal Number as a Function of Jet Mach Number.

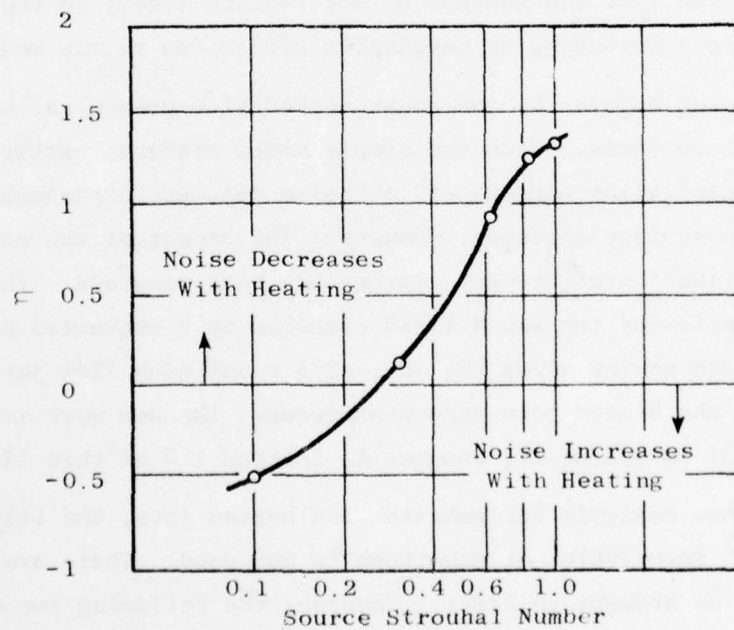


Figure 12. η as a Function of $(St)_o$ for $M_o = 0.9$.

Lush⁽¹⁸⁾) is not the main issue - a different datum would lead to the same qualitative conclusions. Ideally, perhaps, one would have to work out separately the "shear-noise" and "self-noise" portions of the power spectra.

Mani's second problem considered the acoustic output of a line of acoustic sources. This allowed the sources to be developed from the jet centerline. The result of the study indicated that, as far as power estimates were concerned, the notion of the sources moving along the centerline could be retained. Thus considerable simplicity was saved for future work.

The third problem considered the heated jet. This problem was treated similarly to the first problem with the restriction that $\rho_j a_j^2 = \rho_o a_c^2$ but $\rho_j \neq \rho_o$, $a_j \neq a_o$. Figures 12 and 13 are typical examples from this exercise. Figure 12 illustrates the frequency-dependent nature of the density experiment, and Figure 13 illustrates its velocity dependence.

In summary, all three models were pursued with a notion that there may be purely acoustical explanations for several features of jet noise, provided it is recognized that the sources do not radiate freely to the ambient but are subject to a shrouding or developing effect due to the mean jet flow.

The success enjoyed by the above method of approach encouraged further work along these lines. With the simple model studies, particular success was achieved in explaining aspects of jet noise data not explainable by the Lighthill acoustic analogy approach. However, the aspect of the noise sources being a distribution of compact sources has been retained. The new work in this area considered the sound field produced by a convected point quadrupole embedded in and moving along the axis of a round slug flow jet. Both the unheated and the heated jets were considered. The new work is described in detail by Mani in Volume II, Chapter 1, Section 1.0 of this final report.

In the new analysis for unheated and heated jets, the Lilley⁽²⁸⁾ and Goldstein⁽²⁹⁾ formulation of equations is now used. There are several points which should be brought to light. Consider the following two equations:

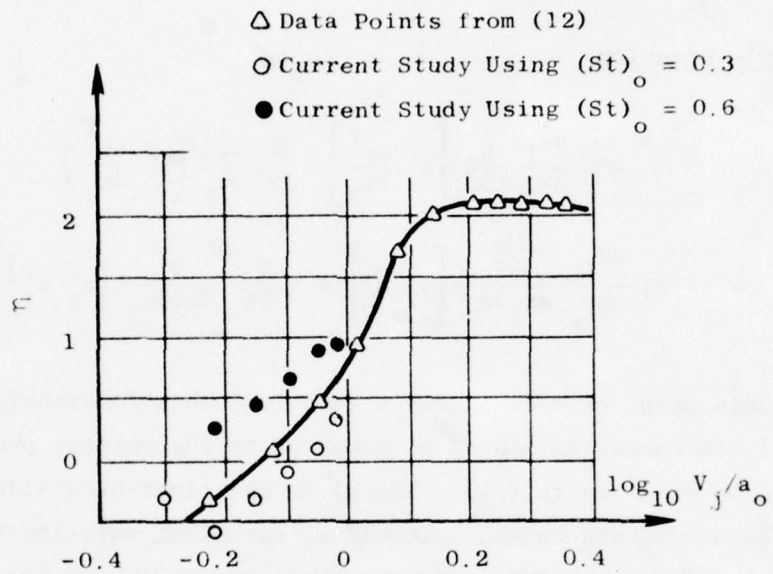


Figure 13. Jet Density Exponent (Figure 17 of Reference 15).

Lighthill's Equation

$$\frac{\partial^2 \rho}{\partial t^2} - a_o^2 \nabla^2 \rho = \frac{\partial^2 (\rho u_i u_j)}{\partial x_i \partial x_j} \quad (3)$$

Lilley's Equation

$$\begin{aligned} & \frac{D^3 r^1}{Dt^3} + 2 \frac{dV_1}{dx_2} \frac{\partial}{\partial x_1} \left[a^2 \frac{\partial r^1}{\partial x_2} \right] - \bar{D} \frac{\partial}{\partial x_i} \left(a^2 \frac{\partial r^1}{\partial x_i} \right) \\ & = - 2\gamma \frac{dV_1}{dx_2} \frac{\partial^2}{\partial x_1 \partial x_k} \left[u'_2 u'_k \right] + \gamma \frac{D}{Dt} \frac{\partial^2}{\partial x_i \partial x_j} \left[u'_i u'_j \right] \end{aligned} \quad (4)$$

From this point of view Lilley's equation needs interpretation. The quantity r^1 , for small values of p^1 compared to the ambient pressure p_A , may be shown to be equal to (p^1/p_A) . The u'_i on the right-hand side of equation (4) are regarded as the known, solenoidal, turbulent velocity fluctuations and equation (4) then provides the required correct inhomogeneous wave equation for (p^1/p_A) driven by the turbulent velocity field. The improvement of equation (4) over equation (3) or even Phillips' equation (1960) is that the source term is clearly in the form of a quadratic function of the fluctuating velocities. The operator $\frac{D}{Dt}$ in equation (4) stands for $\left[\frac{\partial}{\partial t} + V_1 \frac{\partial}{\partial x_1} \right]$. Mani's study dealt primarily with the noise produced by the source term:

$$\gamma \frac{\bar{D}}{Dt} \frac{\partial^2}{\partial x_i \partial x_j} \left[u'_i u'_j \right]$$

Both Lilley's equation (4) and Lighthill's equation (3) exhibit "self-noise" and "shear-noise" source terms. However, the relationship of the self-noise term in Lilley's equation namely $\frac{D}{Dt} \frac{\partial^2}{\partial x_i \partial x_j} \left[u'_i u'_j \right]$ to the shear-noise term in Lilley's equation, i.e.:

$$\frac{dV_1}{dx_2} \frac{\partial^2}{\partial x_1 \partial x_k} \left[u'_2 u'_k \right]$$

is quite different from that for Lighthill's equation where the analogous terms would be as $\frac{\partial^2}{\partial x_1 \partial x_j} (u'_i u'_j)$ and $\frac{d v_1}{dx_2} \frac{\partial u'_2}{\partial x_1}$. Lighthill's equation (3) suggests the following three notions concerning "shear-" and "self-" noise. First of all, it appears that shear noise might be much more important than self noise since shear noise is only linear in the turbulent velocities while self noise is quadratic in the turbulent velocities. This is what Lighthill (1952, 1954) had in mind when he referred to the "amplifying" effect of mean flow gradients on jet noise. Secondly, it appears that the shear noise may be responsible for the low frequency sound with the self noise accounting for the high frequency sound. Related to this is the observation by Jones⁽³⁰⁾ that shear noise should have a convection factor of $(1 - M_c \cos\theta)^{-3}$ as opposed to the $(1 - M_c \cos\theta)^{-5}$ factor for self noise. Finally, unlike self noise which has an isotropic or omnidirectional character, the shear-noise term appears to have a preferred axial directionality. In Lilley's formulation, neither of the first two notions is true, while the third notion still carries over (in a somewhat weaker form). Since the shear-noise term of Lilley's equation is quadratic in the fluctuating velocities, as is the self-noise term, it is neither more important than the self-noise term nor is it responsible for lower frequency radiation as compared to the self-noise term. In fact, the two terms in Lilley's equation are qualitatively very similar, since the operator $\frac{\bar{D}}{\bar{D}t}$ operating on the self-noise term $\frac{\partial^2}{\partial x_i \partial x_j} [u'_i u'_j]$ essentially effects a multiplication of it by ω_0 , where ω_0 is a frequency of the self-noise eddy in its own (convected) frame of reference. The experimental study of Davies, Fisher, and Barrat⁽²⁷⁾ has shown that $\omega_0 \sim \left(\frac{d v_1}{dx_2}\right)$ and, thus, there exists a considerable qualitative similarity between the self-noise and shear-noise terms of Lilley's equation. It is true, of course, that the scalar function $\frac{\partial^2}{\partial x_1 \partial x_k} [u'_2 u'_k]$ associated with the shear-noise term in Lilley's equation has a mildly preferred axial orientation as compared to the isotropic function $\frac{\partial^2}{\partial x_1 \partial x_j} [u'_i u'_j]$ associated with the self-noise term. This aspect is ignored in Mani's study. Only with solutions to equation (4) with a source term of

type $\bar{D} \frac{\partial^2}{\partial x_i \partial x_j} [u'_i u'_j]$ were considered. One further point worth noting with regard to equation (4) is that, since the jet flow is at constant static pressure, \bar{a}^2 can be written as $\gamma P_A / \bar{\rho}(x_2)$. Then for r' depending on x_1 , t as $\exp[j(\alpha x_1 - \omega t)]$ and for small r' , the homogeneous portion of equation (4) [i.e., equation (4) with the right-hand side set equal to zero] yields that across a thin shear layer the quantity:

$$\frac{1}{\bar{\rho}(x_2) \left[\omega - \alpha V_1(x_2) \right]^2} \cdot \frac{\partial p'}{\partial x_2}$$

must be continuous. This is of course equivalent to the usual kinematic condition that the transverse acoustic particle displacement across the shear layer be continuous. The reason for pointing out this feature of the homogeneous form of Lilley's equation (4) is that the homogeneous form of Phillips' (21) equation fails to yield the correct kinematic condition when examined in the limit for a vanishingly thin shear layer.

As a first case which serves to illustrate the differences in solution, the case of the x-x quadrupole is given. Mani's solution for the far-field pressure due to an x-x quadrupole can be written as:

$$p' = \frac{-j \rho_o Q_{xx}^o \omega_o \cos^2 \theta e^{j(\omega_o t - k_o R)}}{2\pi^2 R a_o^2 (1 - M_c \cos \theta)^3 \left[(\alpha^+ a) J_o'(\alpha^+ a) H_o^{(2)}(\alpha^+ a) - (\alpha^+ a) (1 - M \cos \theta)^2 H_o^{(2)}(\alpha^+ a) J_o(\alpha^+ a) \right]} \quad (5)$$

The corresponding Lighthill expression (with $V_1 \rightarrow 0$, but $V_c = C_o M_c$) is:

$$p' \sim \frac{\rho_o Q_{xx}^o \omega_o^2 \cos^2 \theta e^{j(\omega_o t - k_o R)}}{4\pi R a_o^2 (1 - M_c \cos \theta)^3} \quad (6)$$

The major difference between equations (5) and (6) is that, in the case of equation (5), the far-field directivity is completely frequency-dependent.

The relevant nondimensional parameters governing the directivity are now M and $(k_0 a)$. For $0 \leq \theta \leq \cos^{-1} (1/1 + M)$ (the so-called "zone of silence") and high $(k_0 a)$, the exponential nature of the I functions is a manifestation of refraction of the sound by the jet. Also for nonzero $(k_0 a)$, $p' \rightarrow 0$ logarithmically as $\theta \rightarrow 0$ or $\rightarrow \pi$. [Gottlieb⁽³¹⁾ refers to this as the "Lloyd's mirror" effect.] A most interesting result is obtained by examining equation (3) as $(k_0 a) \rightarrow 0$ (low frequency result) we find that p' tends to:

$$p' \sim \frac{\rho_0 Q_{xx}^0 \omega_0^2 \cos^2 \theta e^{j(\omega_0 t - k_0 R)}}{4\pi a_0^2 R (1 - M \cos \theta)^5} \quad (7)$$

(If the problem had been worked with $V_1 \neq V_c$, the expression $(1 - M \cos \theta)^5$ in the denominator of equation (7) would be modified to $(1 - M_c \cos \theta)^3 (1 - M_1 \cos \theta)^2$ where $M_c = V_c/c_0$ and $M_1 = V_1/c_0$). In other words, equation (6) is not a valid low frequency limit. Such a feature of low frequency noise emission was first noticed experimentally by Molloy-Christenson and Narasimha⁽³²⁾ and qualitatively ascribed by them to the influence of jet flow. Berman⁽³³⁾ has also drawn attention to it, pointing out that it is not an instability effect but rather that "the noise generation process is enhanced by a fully stable resonance phenomenon."

Equations (7) and (5), to some extent, explain why an expression of the type found in equation (6) by Lighthill has seemingly worked well in the past at least for the noise of cold jets. It turns out, roughly speaking, that equation (6) underestimates the variation of p' with respect to θ at low frequencies [when compared to equation (5)] as indicated by equation (7), while overestimating it at high frequencies. The overestimation arises essentially because [as pointed by Ribner^(33,34), Powell⁽³⁵⁾, and Csanady⁽³⁶⁾] at high frequencies, the radiation of the eddy is primarily governed by its own immediate environment (namely the jet flow) with respect to which it is not convecting at all. Regardless of how high $(k_0 a)$ may be, both $(\alpha^+ a)$ and $(\alpha^- a)$ or $(\underline{\alpha}^+ a)$ approach zero as $\theta \rightarrow 0$ or π and $\theta \rightarrow \cos^{-1} (1/1 + M)$. Because of this, it was not possible to extract a high frequency limit of equation (5). Besides, a plug flow model of the jet flow is obviously a poor model at high frequencies. In any event, this feature of underestimation of noise

generation at low frequencies by equation (6) and overestimation at high frequencies is apparently the reason why expressions of type found in equation (6) essentially succeeded in explaining jet noise directivity in the past when such directivities were measured for the overall sound pressure (i.e., the integral of the pressure spectrum over all of the frequencies). To conclude this portion of the discussion of equation (5), it is emphasized that it is an expression that exhibits simultaneously the combined convection-refraction effect which is so crucial to the determination of jet noise directivity. It also emphasizes the need to plot all jet noise directivity data at constant source frequencies, as this is the only directivity plot that can be checked directly against an acoustic theory. It is the only manner in which we can bypass our current inability to predict the turbulence source spectrum in detail.

Application of Mani's work proceeded with the aid of Ribner's⁽³⁴⁾ study of how various quadrupoles can be employed to derive the axially symmetric sound field of a round jet. By and large, six basic quadrupoles (x-x, x-y, x-z, y-z, y-y, and z-z) are considered to contribute independently, but with various derived weights. The noise contribution was evaluated by the formula:

$$\begin{aligned}
 & \text{(far-field intensity)} \sim \\
 & \text{(mean square pressure of x-x quadrupole) +} \\
 & \quad 4 \times \text{(circumferential average of mean square pressure of x-y} \\
 & \quad \text{or x-z quadrupoles)} \\
 & \quad + 2 \times \text{(circumferential average of mean square pressure} \\
 & \quad \text{of y-y or z-z quadrupoles) + 2} \times \text{(circumferential} \\
 & \quad \text{average of mean square pressure y-z} \\
 & \quad \text{quadrupole). . .}
 \end{aligned}$$

The only difference from the above formula and that of Ribner is in the neglect of the weak cross quadrupole contributions (i.e., of the xx-yy, xx-zz and yy-zz types). Both the above formula and Ribner's more exact result yield a basic omnidirectional pattern for the self noise for Lighthill's equation excepting for the $(1 - M_c \cos\theta)^{-5}$ convection effect.

Figure 14 illustrates a resultant prediction using this technique. The agreement between theory and experiment appears to be very good.

For the heated jet, the convected-wave equation approach based on Lilley's equation was again used. It was found that excess pure jet noise mechanisms scaled as M^6 and M^4 are found to result from the density gradients of the mean flow. Mani's solution for the far-field pressure fluctuation for the x-x quadrupole for a heated jet becomes:

$$p' \sim \frac{-j \rho_o Q_{xx}^o \omega_o^2 e^{j(\omega_o t - k_o R)} \cos^2 \theta}{2\pi^2 R (1 - M_o \cos \theta)^3 a_o^2 \left[H_o^{(2)}(\alpha^+ a) I_o'(\underline{\alpha}^+ a) (\underline{\alpha}^+ a) \rho_o / \rho_1 \right]}$$

$$= (\alpha^+ a) H_o^{(2)'}(\alpha^+ a) I_o(\underline{\alpha}^+ a) (1 - M \cos \theta)^2 \quad (8)$$

for $0 \leq \theta \leq \cos^{-1} \frac{1}{(c_1/c_o + M_o)}$, where $\alpha^+ = k_o \sin \theta / (1 - M_o \cos \theta)$ and $\underline{\alpha}^+$ is the positive square root $\sqrt{k_1^2 - \alpha^2}$ with $\alpha = k_o \cos \theta / (1 - M_o \cos \theta)$. For $\cos^{-1} [1/(a_1/a_o + M_o)] \leq \theta \leq \pi$, the same expression applies with $\underline{\alpha}^+$ replaced by $\underline{\alpha}^+$, which is the positive square root $\sqrt{\alpha^2 - k_1^2}$, and the I functions are replaced by the J functions.

The additional solutions that need to be worked out correspond to:

- (a) An axial dipole solution, i.e. with a source term of type:

$$\frac{\partial}{\partial x} [\delta(x - Vt) \delta(y) \delta(z)],$$

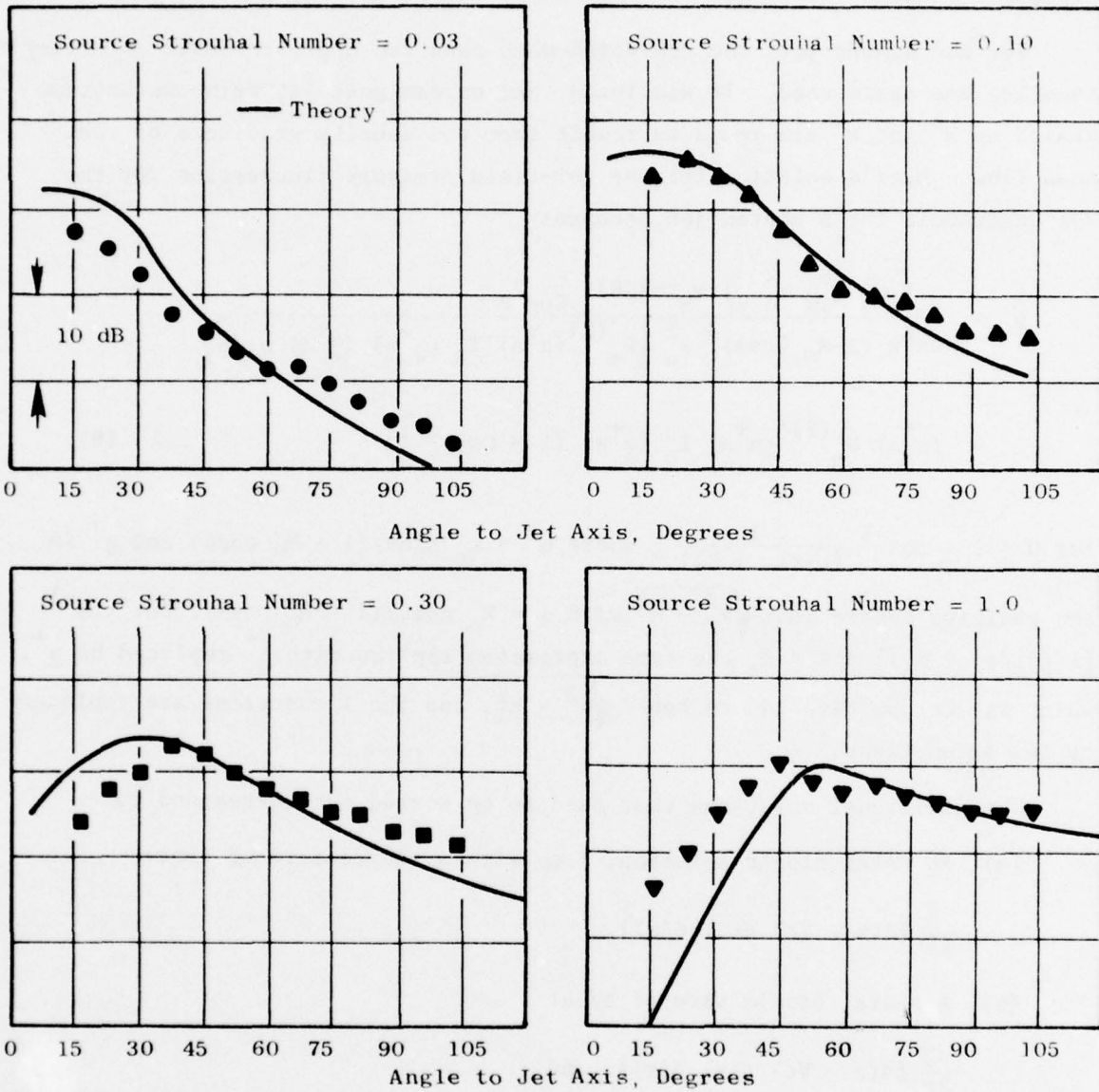
- (b) A radial dipole term of type:

$$\frac{\partial}{\partial r} [\delta(x - Vt) \delta(y) \delta(z)], \text{ and}$$

- (c) A pressure source term of type:

$$\delta(x - Vt) \delta(y) \delta(z).$$

These solutions are just as easy to derive as the quadrupole solution and, hence, only the broad outlines will be sketched. The solution to (a) is very similar to equation (8) with the multiplier $\omega_o^2 / [a_o^2 (1 - M \cos \theta)^2]$ (or α^2)



(a) $M_j = 0.878$ ($V_j = 300$ m/s)

Figure 14. Comparison with Data of Lush at $M_j = 0.878$ and 0.57 .

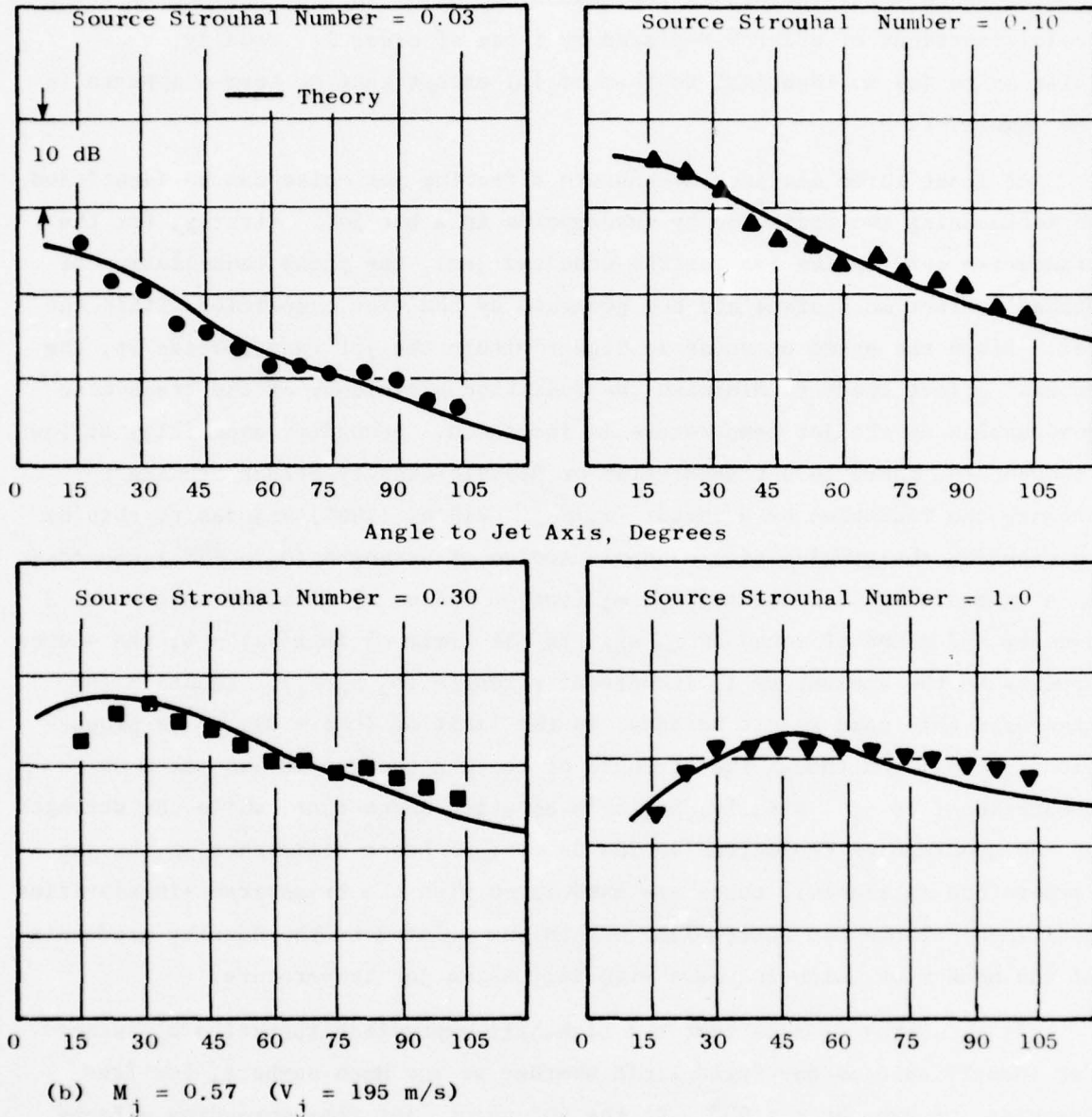


Figure 14. Comparison with Data of Lush at $M_j = 0.878$ and 0.57 (Concluded).

replaced by just $\omega_0 \cos\theta/[a_0(1 - M \cos\theta)]$ (or α). The solution to (b) is similar to that for (a) with α replaced by $\underline{\alpha}^+$ or $\underline{\underline{\alpha}}^+$ in the numerator and the Bessel functions of order 0 replaced by those of order 1. Finally, the solution to (c) is identical to that of (a) except that no term α appears in the numerator.

At least three distinct mechanisms affecting jet noise can be identified as influencing the radiation by quadrupoles in a hot jet. Firstly, for the transverse quadrupoles (as for the unheated jet), the phase cancellation or Stokes'-effect mechanisms are now governed by the flow properties within the jet. Since the speed of sound is higher within the jet than outside it, the Stokes' effect tends to diminish the radiative efficiency of the transverse quadrupoles as the jet temperature is increased. Secondly, especially at low frequencies, there is a transmission or dynamic-density effect tending to enhance the radiation by a factor (ρ_0/ρ_1) . Ribner (1964) alludes to this by considering the problem of a monopole source of strength $(Q_0 e^{j\omega_0 t})$ embedded in a sphere of gas of density ρ_1 , a_1 (and of radius a) with the ambient at a density and speed of sound of ρ_0 , a_0 . In the limit of $(\omega_0 a/a_0) \rightarrow 0$, the source appears to the ambient as if it were of strength $(Q_0 \rho_0/\rho_1)$. Equation (8) manifests this same result because, in the limit of $(k_0 a \rightarrow 0)$, p' is proportional to ρ_0 even though the strength of the x-x quadrupole was taken as proportional to ρ_1 . Finally, Lilley's equation shows that, while the strength of the quadrupoles themselves varies as ρ_1 (and hence diminishes as the jet temperature increases), there are associated with the transverse singularities additional dipole and source-like mechanisms related to the density gradients of the mean flow which increase with increasing jet temperature.

It is worthy of note that the Lighthill expression (Equation 6) is not now identifiable as any valid limit whether at low Mach numbers, low frequencies, or even at $\theta = 90^\circ$. At the 90° point, jet flow shrouding effects are present for hot jets simply because a temperature inhomogeneity is a scalar inhomogeneity unlike a velocity inhomogeneity so that there is no question of there not being a component at $\theta = 90^\circ$. Besides, the 90° radiation is dominated by the transverse singularities which generate the additional source-like and dipole-like terms not accounted for by Lighthill's

expression. Indeed, of the various agencies identified as governing the radiation by quadrupoles in a hot jet, the Lighthill expression picks up only one effect (namely, the variation of the quadrupole strength as ρ_j).

For a full description of the above to jet noise data, the reader is referred to the detailed account in Volume II, Chapter 1, Section 1.2 by Mani. Figures 15, 16, and 17 are given as examples of the resultant predictions.

Taken together, the results of the work for unheated and heated jets have given considerable guidance to the better understanding of jet noise generation. The problem of heated jet noise is one in which Lighthill's analysis of jet noise offers very little guidance. However, the physical picture of jet noise being compact eddies convecting and decaying with the flow still carries over.

One particular aspect of the discussion of the theoretical work described above concerns the characterization of shear noise. As was indicated earlier, the classical approaches for turbulent mixing noise should indicate that there should be an octave shift between shear noise and self noise, and that the shear noise may even dominate the noise spectrum. The logical analysis from the Lilley-type of equations indicates that this octave shift does not occur and that the self-noise and shear-noise source terms are essentially equivalent. Ribner and Nosseir (Section 2.0 of Chapter 1 of Volume II of this final report) have attempted to formulate classical theory in such a way that tests for this hypothesis could be examined.

The model for their analysis is as follows:

For a narrow frequency band Δf centered at f , and for direction θ with the jet axis, the mean sound pressure emitted may be expressed as:

$$p'_\theta (CS) = \left[a(CS) + b(CS) \frac{\cos^4 \theta + \cos^2 \theta}{2} \right] C^4 \quad (9)$$

where,

$$C = \left[(1 - M_c \cos \theta)^2 + \alpha^2 M_c^2 \right]^{1/2}$$

$$S = fD/V_j \text{ observed Strouhal number}$$

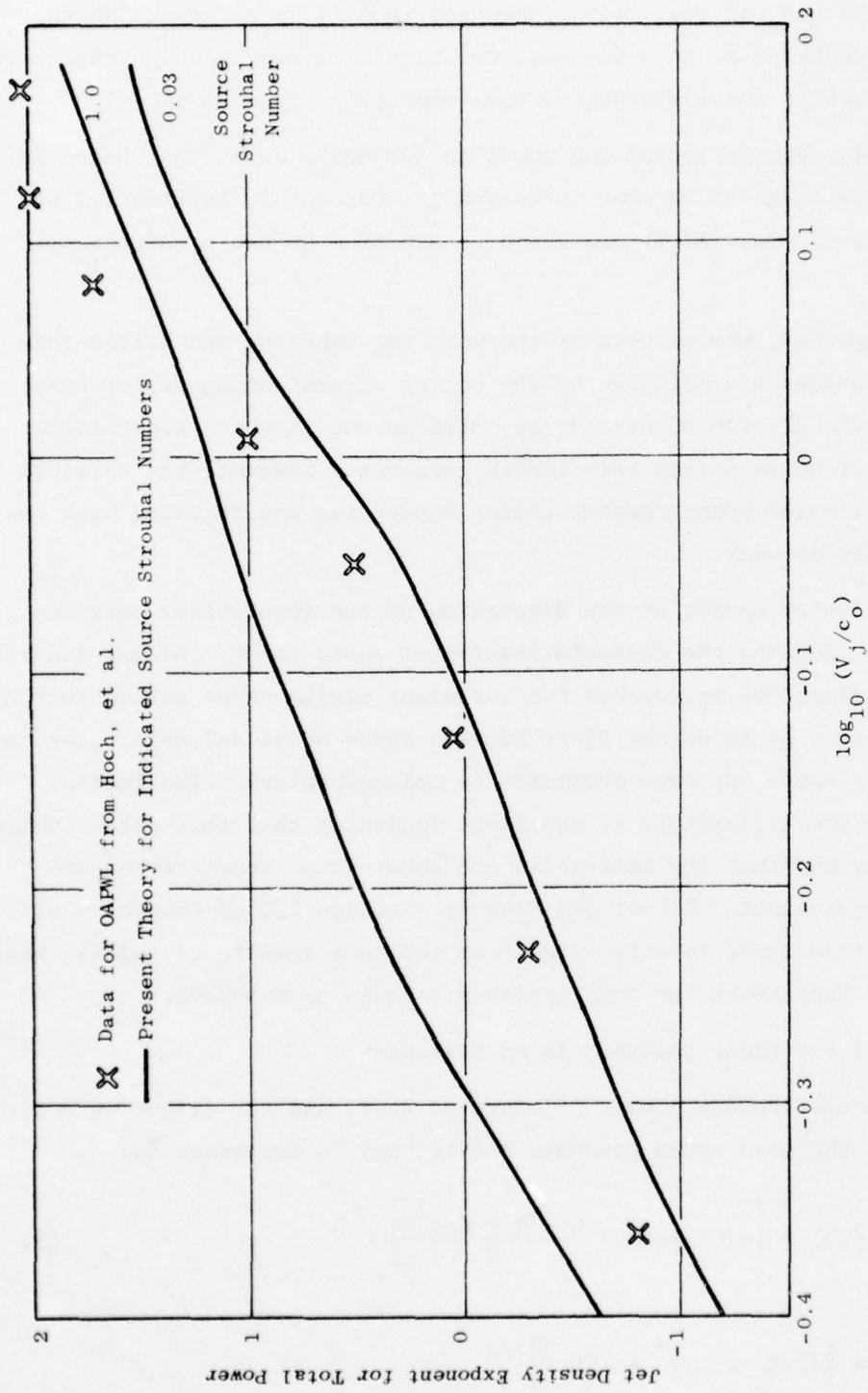


Figure 15. Jet Density Exponent for Total Power as a Function of (V_j/c_0) .

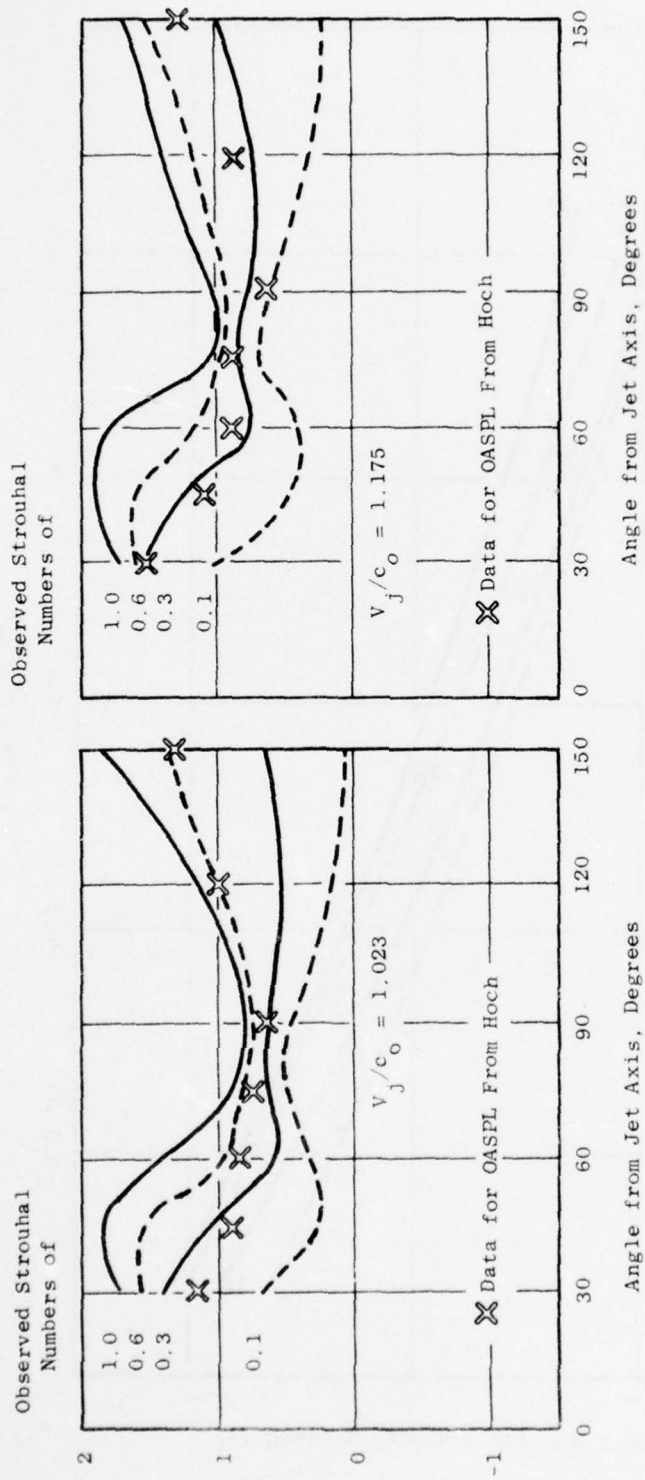


Figure 16. Jet Density Exponent as a Function of Angle from Jet Axis.

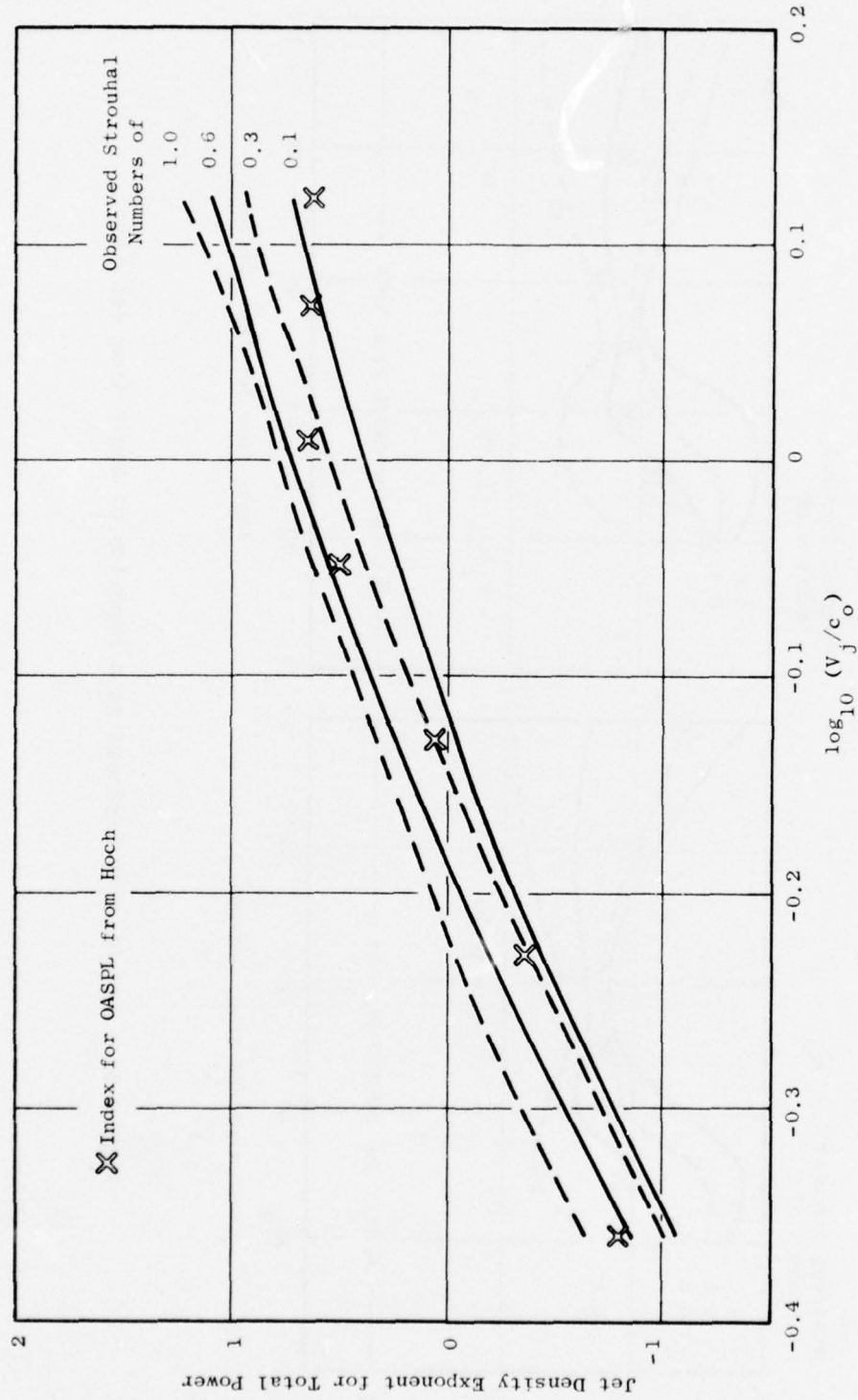


Figure 17. Density Index at 90° to Jet Axis as a Function of (V_j/c_0) .

a(CS) = self-noise source term

b(CS) = shear-noise source term

such that:

$$a(\text{CS}) = \frac{\bar{p}_{90^\circ}^{-2}}{C_{90^\circ}^4} (\text{CS}) \quad (10)$$

$$b(\text{CS}) = \frac{C_\theta^4 \bar{p}_\theta^{-2} (\text{CS}) - C_{90^\circ}^4 \bar{p}_{90^\circ}^{-2} (\text{CS})}{(\text{Cos}^4_\theta + \text{Cos}^2_\theta)/2} \quad (11)$$

Classical theory predicts that shear-noise and self-noise spectra have similar shapes, and that the self-noise spectrum is shifted an octave as compared to shear noise. Therefore:

$$b(\text{CS}) = \beta a(\text{CS}) \quad (12)$$

This states that the b spectrum and the a spectrum have the same shape after the octave shift, but with a vertical scale factor β . Thus, the scale factor β (as well as "a" and "b") can be written explicitly in terms of experimentally measured parameters:

$$\beta = \frac{b(\text{CS})}{a(2\text{CS})} = \frac{C_\theta^4 \bar{p}_\theta^{-2} (\text{CS}) - C_{90^\circ}^4 \bar{p}_{90^\circ}^{-2} (\text{CS})}{C_{90^\circ}^4 \bar{p}_{90^\circ}^{-2} (2\text{CS}) \left[(\text{Cos}^2_\theta + \text{Cos}^4_\theta)/2 \right]} \quad (13)$$

The similarity between self noise and shear noise is illustrated in Figure 18. The data used in these comparisons are from several independent sources. The predicted constancy of β is largely confirmed (over much of the CS range); the variation does not exceed 1 dB in most cases.

The shift in frequency between self noise and shear noise is illustrated in Figures 19a and 19b. Figure 19a shows self- and shear-noise spectra extracted from Ahuja⁽³⁵⁾ data using the approximate theory described above. The self-noise spectrum is seen to be roughly half the amplitude of the shear noise spectrum and peaks approximately an octave higher - these are both features of the classical theory. Figure 19b shows self-noise and shear-noise spectra derived from cross correlations of a far-field microphone signal with hot-wire signals (these results were obtained at the University of Toronto by Dr. Philip Morris). The spectral curves shown in Figure 19b are similar to those found in Figure 19a.

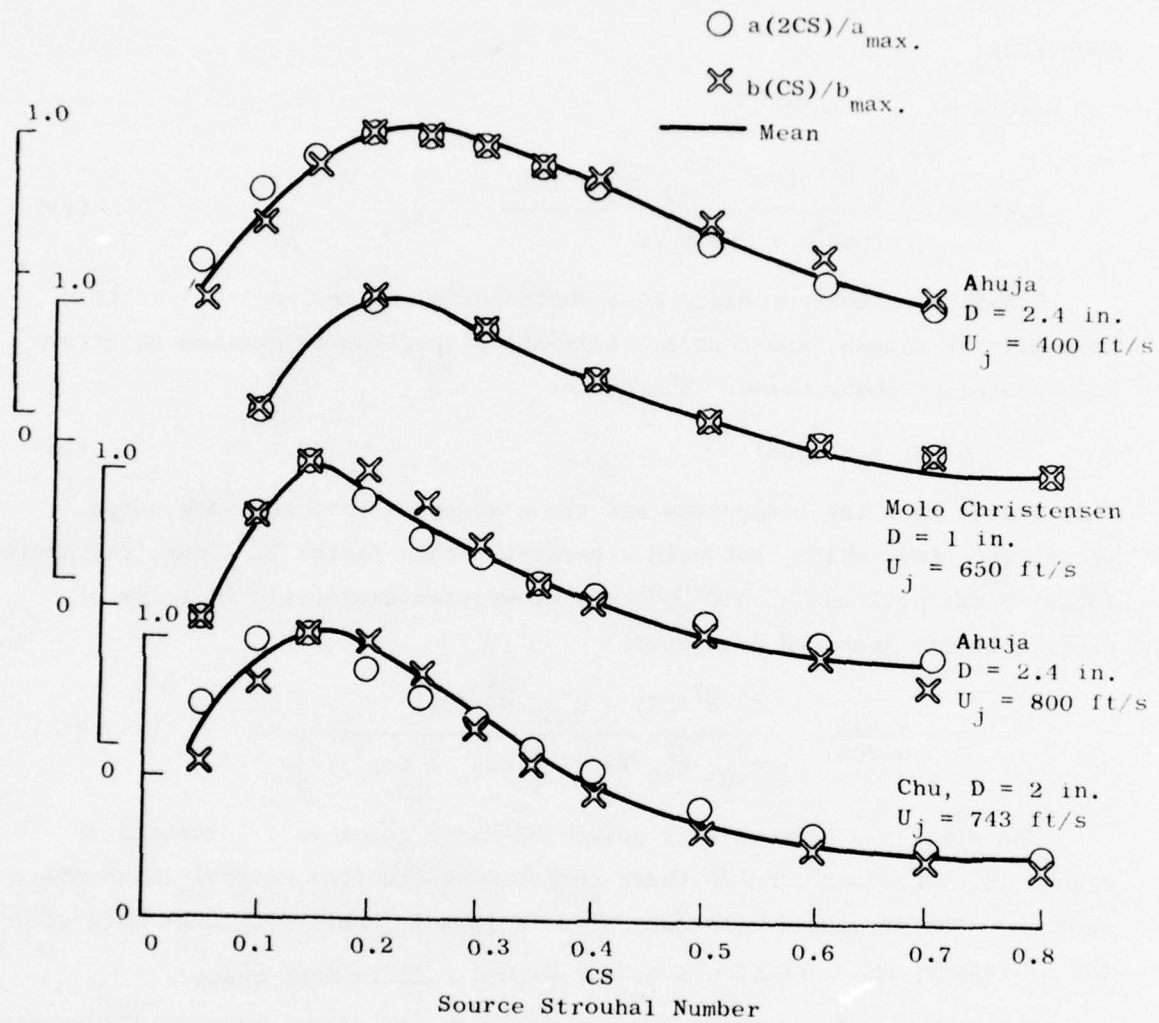
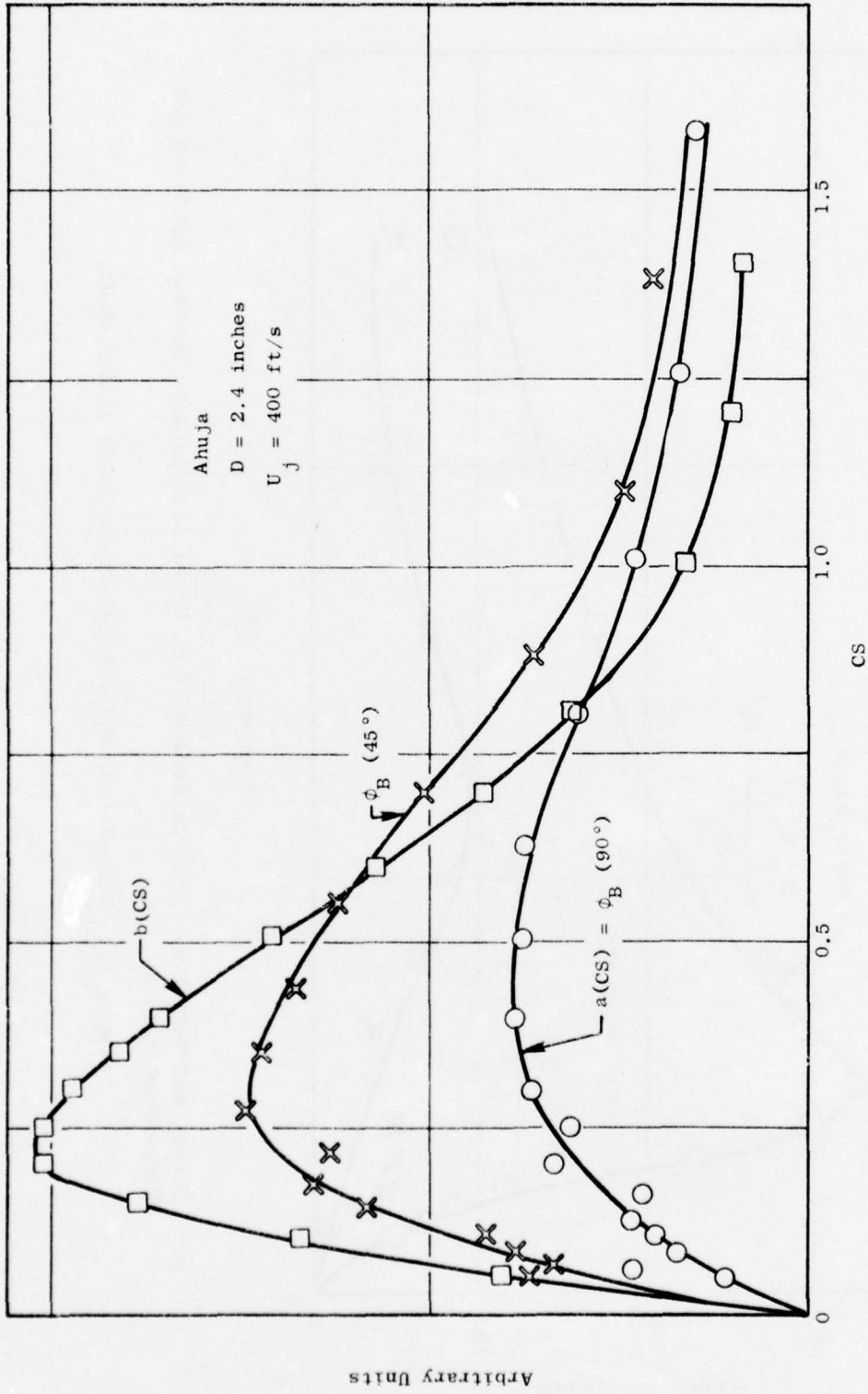
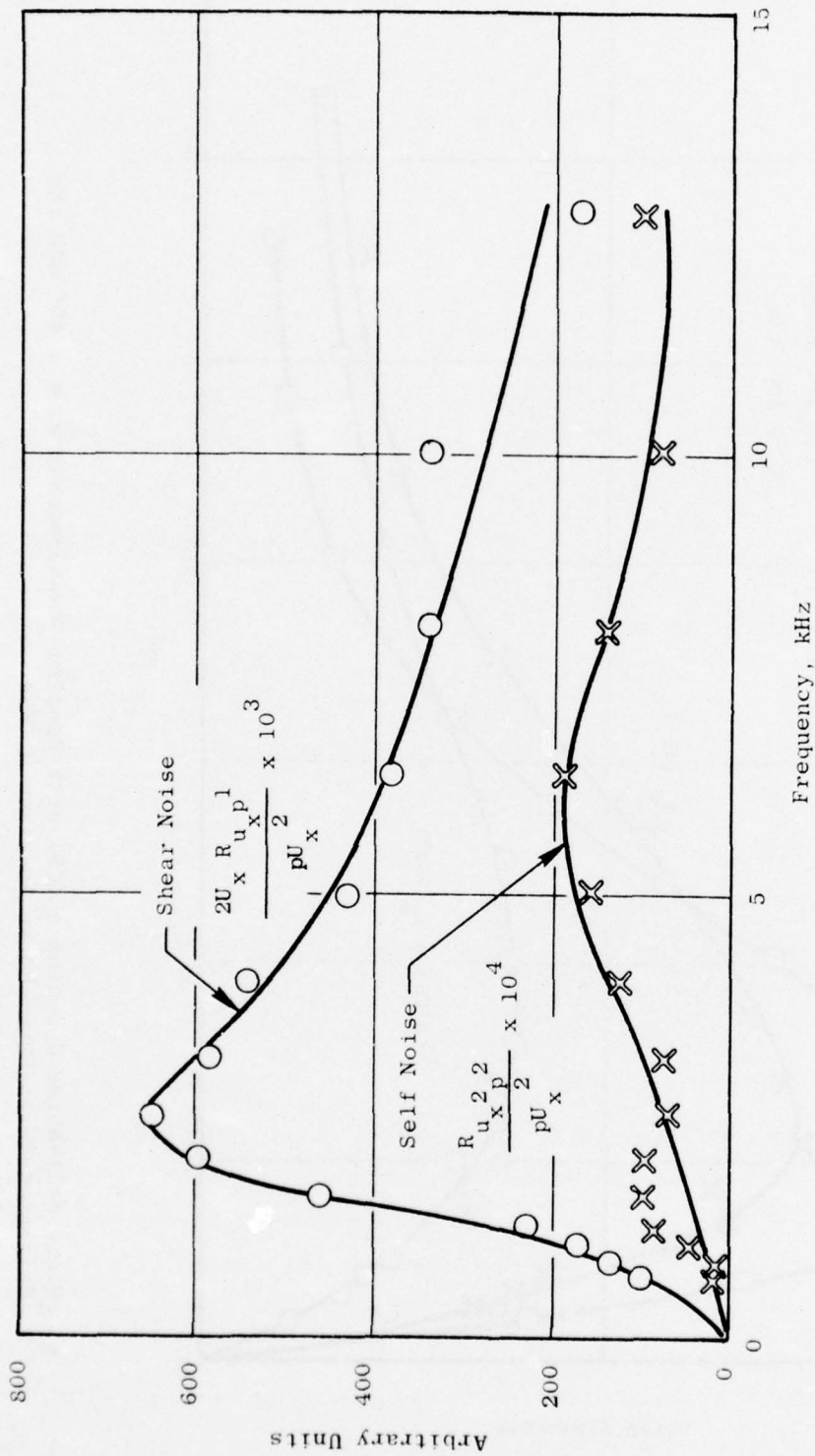


Figure 18. Comparison of Normalized Self-Noise and Shear-Noise Spectra (the Self-Noise Has Been Down Shifted One Octave).



a) Basic Self-Noise Spectrum a (CS) with Spectrum Measurements at $\theta = 45^\circ$ and the Extracted Basic Shear-Noise Spectrum b (CS).

Figure 19. Self-Noise, Shear-Noise Comparisons.



b) Shear- and Self-Noise Spectra Derived from Cross Correlations Between Hot Wire and Microphone Signals.

Figure 19. Self-Noise, Shear Noise Comparisons (Concluded).

Another feature of the approximate theory given above is the predictive capability. From the theory, the prediction of the mean square sound pressure \bar{p}^2 is given by three quantities: the filtered sound pressure in direction 90° at two frequencies (f and $2f$) and the parameter β (can be taken as an empirical constant). The prediction equation becomes:

$$\frac{\bar{p}_\theta^{-2} \text{ (CS)}}{\bar{p}_{90^\circ}^{-2} \text{ (CS)}} = \frac{C_{90^\circ}^4}{C_\theta^4} \left[1 + \beta \frac{\bar{p}_{90^\circ}^{-2} \text{ (2CS)}}{\bar{p}_{90^\circ}^{-2} \text{ (CS)}} \frac{\cos^4 \theta + \cos^2 \theta}{2} \right] \quad (14)$$

Figure 20 illustrates such a prediction. The predicted directional patterns fit the general trend of the experimental data in the middle range of Strouhal numbers.

These results are at some variance with the results given earlier when the fluid shrouding effects of Mani were discussed. It should be recalled that the above predicted directivity results were given for unheated jets. Therefore, as discussed earlier, it is expected that not too great a variance will exist between the classical theory and the newer theory (which includes fluid shrouding). The effects of fluid shrouding in Mani's model would certainly improve the classical turbulent mixing noise model of Ribner, particularly after the refractive dip.

However, the spectral shift between self noise and shear noise observed above is at variance with the basic Lilley equations which insist that the source terms are all quadratic in the turbulent velocity. In terms of noise source location, identification, and quantification, this issue is of importance and warrants further clarification.

In addition to the above studies, a review of analytical modeling for a jet's orderly structure was performed (see Section 3.0 of Chapter 1, Volume II of this final report). The work performed in this area reviewed the aerodynamic and acoustic methods of leading contenders for formulating the jet as an orderly structure. Particular care was directed to the formulation of the problem and its theoretical basis for high velocity jets. Although this work does give credibility toward understanding aerodynamic disturbances

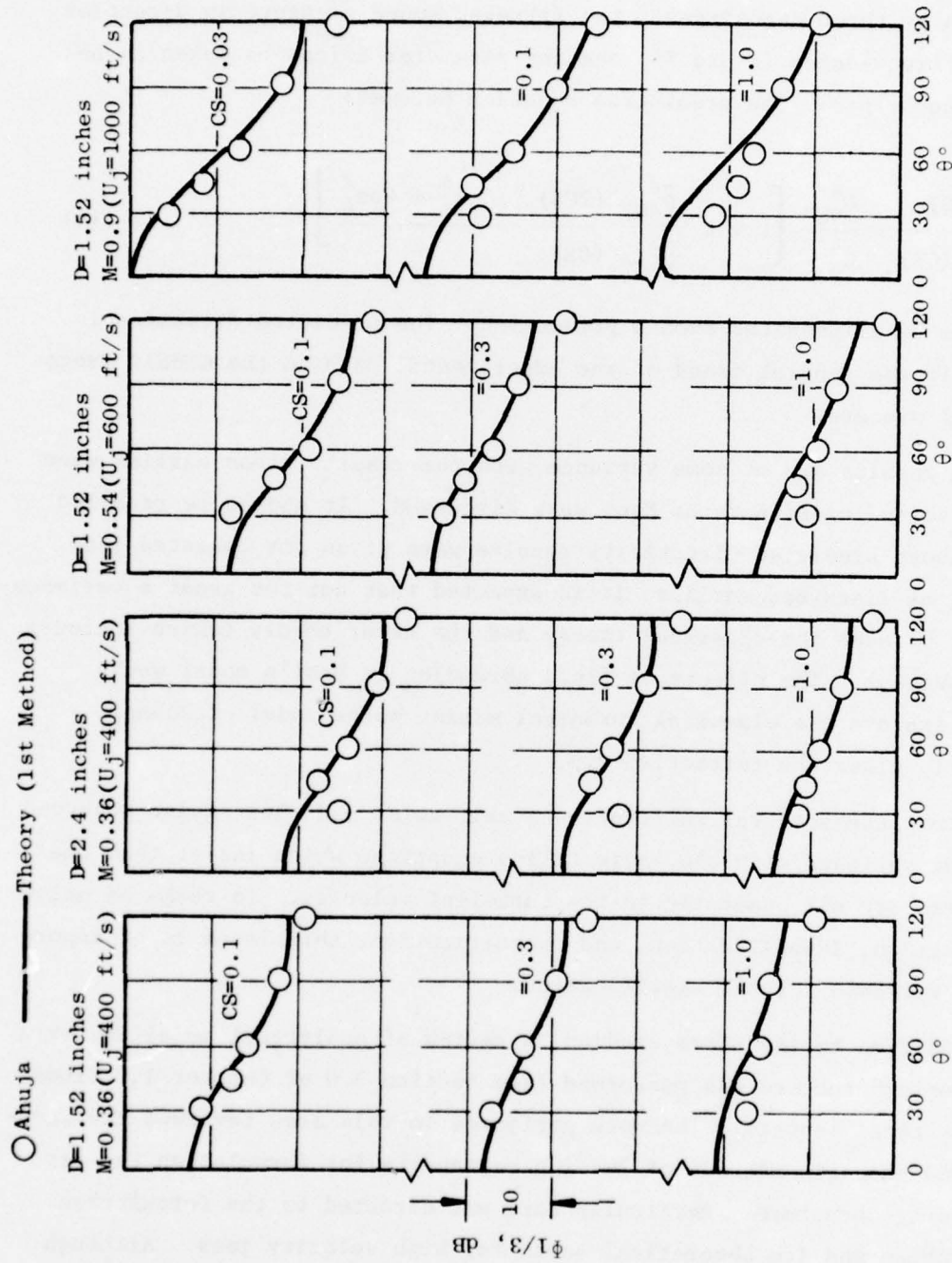


Figure 20. Directivity of 1/3-Octave Intensity: Comparison with Experimental Data of Ahuja.

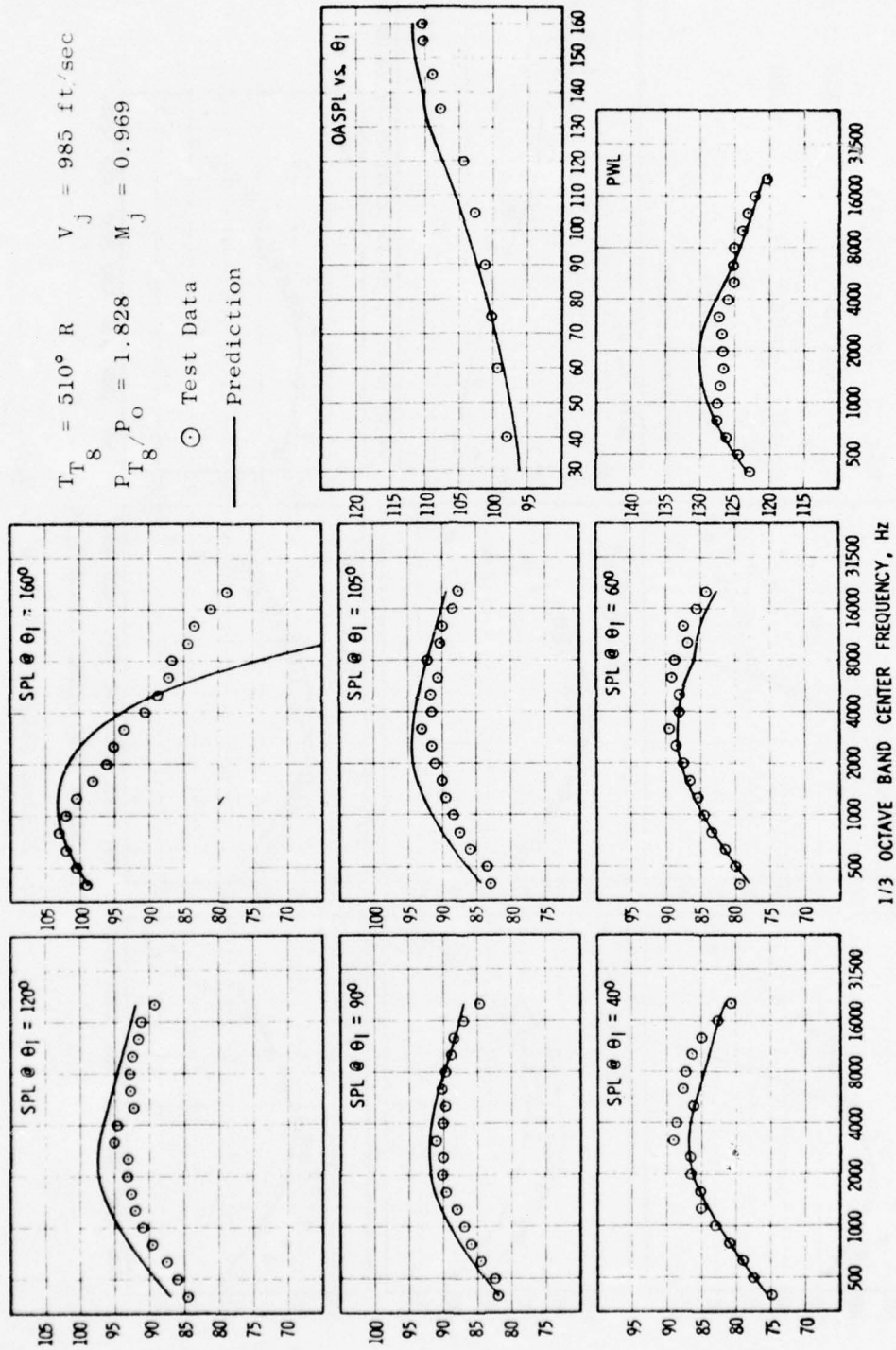
which can be effected by the jet's flow, the results of these studies did not indicate that such an approach could lead to any further insights toward explaining key features of jet noise. The most which can be said is that jets are inherently unstable, the instabilities produce turbulence, and the turbulence produces the noise. All of our experience to date still suggests that compact eddies, radiating through a mean flow, provide a clearer insight to jet noise phenomenon. The review of the instability analysis does suggest in fact that the aerodynamic analysis could be incorporated into an eigensolution for local acoustic sources, analogous to the General Electric turbulent mixing acoustic models.

Of the acoustic models considered during this program the model selected for further development and for preliminary predictive purposes is the slug-flow fluid shielding model by R. Mani, and discussed in detail in Volume II, Section 1 of this final report. This model was chosen because of its sound theoretical basis and because it was found to represent, in a closed non-empirical form, most of the key and heretofore puzzling features of unheated and heated jet noise. Because of time limitations on this contract, the slug-flow fluid shielding model was not computationally lined with computer programs discussed in Volume III of this final report. However, this model is being used and improved upon on a DOT/FAA Contract (DOT OS-30034) for investigating jet noise suppression concepts. To illustrate the predictive capability of the slug-flow model for unheated and heated jets developed on this program, a series of aeroacoustic predictions was performed using the models of the DOT program and compared with available unheated NASA-Lewis data and heated jet noise data obtained under this contract. The aerodynamic source intensity spectrum used with the fluid shielding model is the basic Lighthill/Ribner formulation. The aerodynamic program used to predict the turbulent mixing source noise is an aerodynamic prediction method similar to the JETMIX computer program given in Volume III, but of a much simpler form to enhance computational speed. The source intensity spectrum served as the anchor point for the predictions at $\theta = 90^\circ$. The slug-flow shielding analysis provided the change in spectrum shape and level at all other angles.

As a first illustration of the prediction model, a cold round subsonic jet case was computed corresponding to data supplied by Dr. W.A. Olsen of the NASA-Lewis Research Center. This case, a 3.0-inch-diameter jet run at 985 fps, had a nozzle exit Mach number of $M = 0.969$. The comparison of the aeroacoustic predictions with the experimental measurements is shown in Figure 21a. It can be seen from these results that the slug-flow shielding model quite well predicts the observed spectral characteristics of a cold subsonic jet. The only major discrepancy occurs at $\theta_i = 160^\circ$, where the slug-flow approximation overpredicts the shielding effect at high frequencies. This over-prediction of the SPL at $\theta_i = 160^\circ$ is reflected also in the somewhat higher PWL prediction in the 2000 Hz region.

A similar computation was made for a heated subsonic jet case, and the data/theory comparisons are shown in Figure 21b. This case corresponds to Reading 3, Point 7 of the 4.31-inch-diameter thin-lip conical nozzle test given in Volume IV. The nozzle exit Mach number for this case is $M = 0.9$, while the jet exit stagnation temperature is 2.72 time ambient. The predicted spectral characteristics are seen to agree well with the data for $\theta_i < 130^\circ$. For observer angles close to the jet axis, however, several areas of deficiency can be seen. First, the previously noted overprediction of the shielding (underprediction of SPL) at high frequencies and angles close to the jet axis is even more pronounced for the heated jet case. Secondly, the low-frequency peak noise is underpredicted at shallow angles ($\theta_i > 130^\circ$), and this results in an underprediction of the PWL spectrum peak and the peak OASPL.

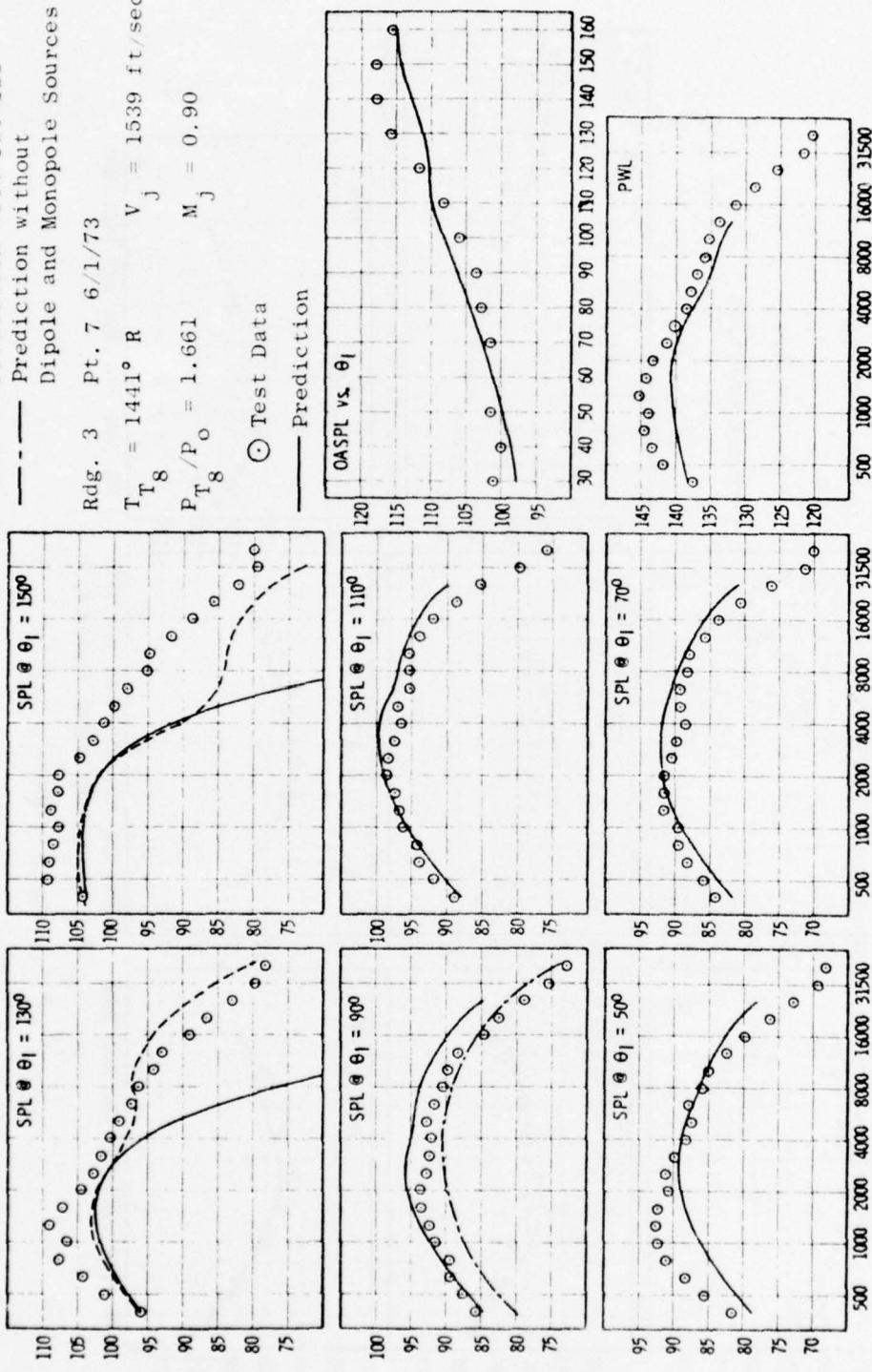
In an attempt to understand the high frequency shallow-angle discrepancy, the measured shallow-angle directivity [$SPL(\theta_i) - SPL(90^\circ)$] was compared with predicted directivity, and the general trend of these comparisons is shown qualitatively in the following sketch.



(a) Cold Subsonic Jet, $M_j = 0.97$

Figure 21. Theory vs. Data Comparison for Slug-Flow Shielding Model

— Prediction with Cut-Off
 - - - Prediction without
 - - - Dipole and Monopole Sources
 Rdg. 3 Pt. 7 6/1/73
 $T_{T_8} = 1441^\circ R$ $V_j = 1539$ ft/sec
 $P_{T_8}/P_o = 1.661$ $M_j = 0.90$
 ○ Test Data
 — Prediction



(b) Heated Subsonic Jet, $M_j = 0.9$
 Figure 21. Theory vs. Data Comparison for Slug-Flow Shielding Model (Continued).

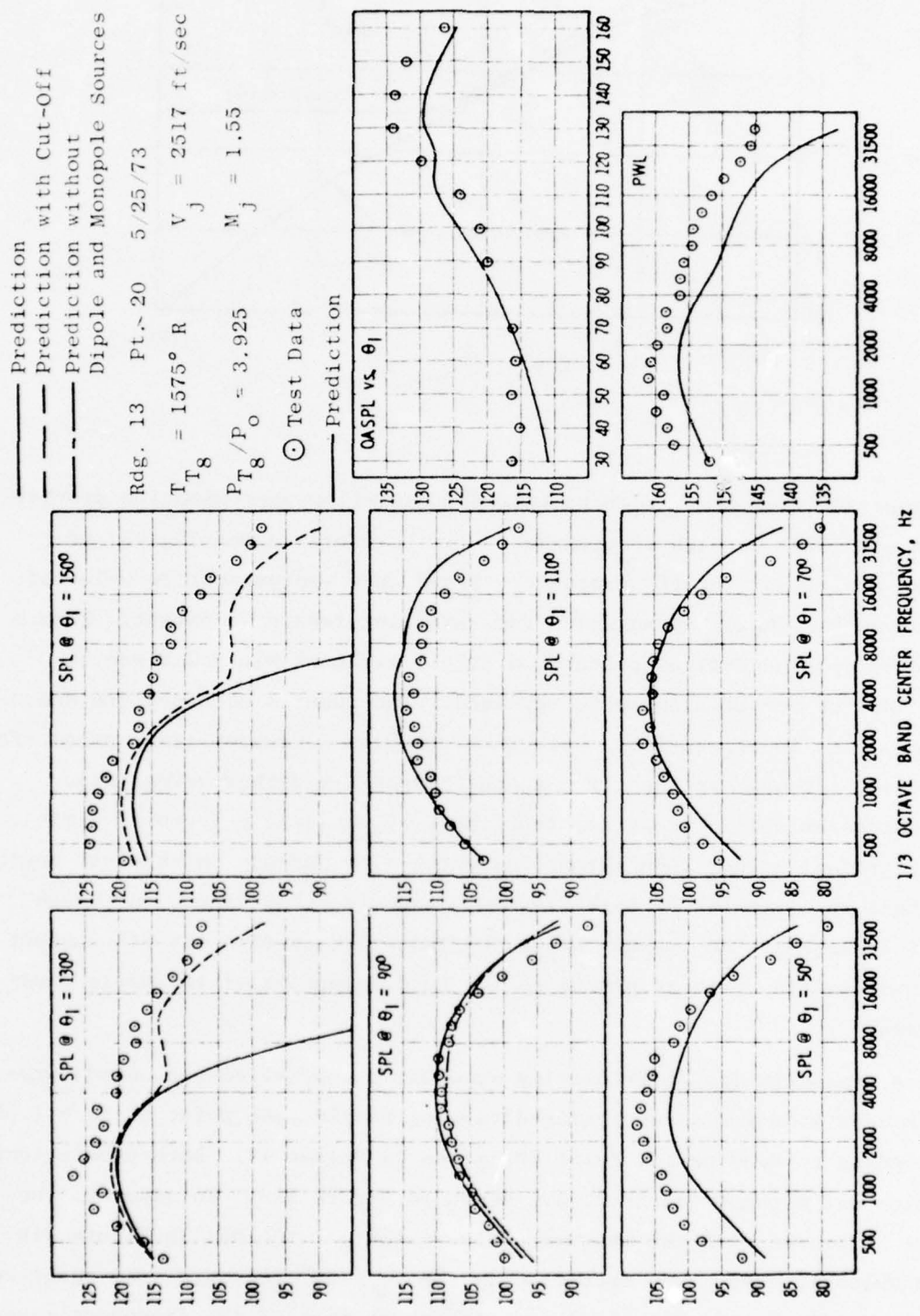
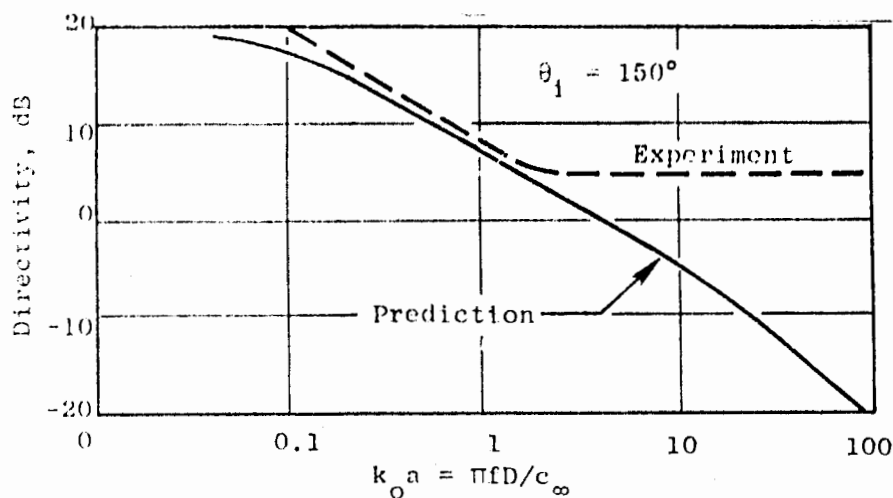


Figure 21. Theory vs. Data Comparison for Slug-Flow Shielding Model (Concluded).



It was apparent from these results that the slug-flow approximation provides too much shielding at high frequencies. It therefore seemed logical to devise an empirical "cutoff" frequency, based on a representative value of Strouhal number ($k_0 a$) beyond which the shielding remains constant. From a preliminary trial-and-error process, a cutoff limit of $k_0 a = 2.0$ was selected, and the computations were repeated. The results obtained are shown as dashed lines in Figure 21b. Note that the high frequency noise prediction is improved, although the spectrum shape possesses a rather unrealistic "wavy" characteristic. It is apparent that, by devising a "cutoff" limit which is gradual rather than abrupt and which also depends on observer angle, a satisfactory agreement at high frequencies could be obtained. Although beyond the scope of the present study, optimization of the "cutoff" concept would be a fruitful path to pursue in future development of the basic slug-flow model.

As a demonstration of predicting supersonic shock-free jet noise, predictions were made for a converging-diverging nozzle test point at $M_j = 1.55$, corresponding to Reading 13, Point 20, given in Volume IV. Both predictions, i.e., with and without "cutoff", are shown in Figure 21c. In general, the relative agreement with the measured data is similar to that in Figure 21b for the subsonic case. One exception is the $\theta_1 = 50^\circ$ (forward-arc) spectrum, where the prediction is 3 to 4 dB low throughout most of the frequency range. The reason for this underprediction at 50° is not known.

A final point to be made is the necessity for including lower-order source terms (dipole and monopole) which depend on the jet mean density gradient and second-derivative used in the slug-flow fluid shielding model. Shown in Figures 21b and 21c are 90° SPL spectra predictions with these additional noise sources removed, shown as dash-dot lines. It is seen that the $M_j = 0.9$ spectrum would be underpredicted by 5-6 dB without these heated-jet additional noise terms. Their effect is much less for the $M_j = 1.55$ case, however, due to their sixth and fourth power velocity dependence, and the high velocity case become dominated by the quadrupole turbulence sources.

The results of these theory data comparisons have indicated some deficiencies which could be corrected. Work in this area currently is being pursued under Contract DOT OS-30034. On that contract, the basic essence of the fluid shielding model is being maintained, but with improvements to account for the influence of off-axis source location, variation in velocity and temperature profiles, and improvements in the theory for the high frequency noise which the current slug-flow fluid model does not include.

SECTION 4.0

LASER VELOCIMETER DEVELOPMENTS FOR NOISE SOURCE LOCATION

During the course of this program a considerable amount of energy was directed toward developing instrumentation capable of examining the detailed characteristics of turbulent jet plumes. In the first phase of study, advanced pressure probe developments (See Reference 36) were pursued as were initial demonstrations using a General-Electric-developed laser velocimeter (LV) on heated supersonic jets. It became clear that the laser velocimeter was the measurement tool for the future. The LV offered a means of measuring the flow properties of high velocity/high temperature jets without disturbing the flow. The LV also offered a conceptually easy and accurate method of measurement not only of rms mean velocity and turbulent velocity distributions, but also of spectral and cross-correlation type of information; for direct noise source location type of information the cross-correlation type is very important.

To be discussed below are the major results obtained in GE's studies. References 37 through 40 contain the background descriptions of General Electric's laser velocimeter system and test results. Section 1.0 of Chapter III in Volume II of this report contains extensive test results of flow measurements for heated high velocity jets and of LV-to-far-field cross-correlation experiments.

4.1 BASIC IDEAL FOR LV RMS MEASUREMENTS

The concept of laser velocimeter measurement for routine mean velocity and turbulent velocity may be described in the following simple fashion. Two beams of monochromatic light intersect at a point in space and set up a fringe pattern of known spacing (See Figure 22). The flow is seeded with small particles which pass through the measuring volume. The light scattered from the particles is collected, and the laser signal processor measures the time it takes for the particles to pass through each fringe. Knowing the fringe space and traverse time for each validated particle enables the con-

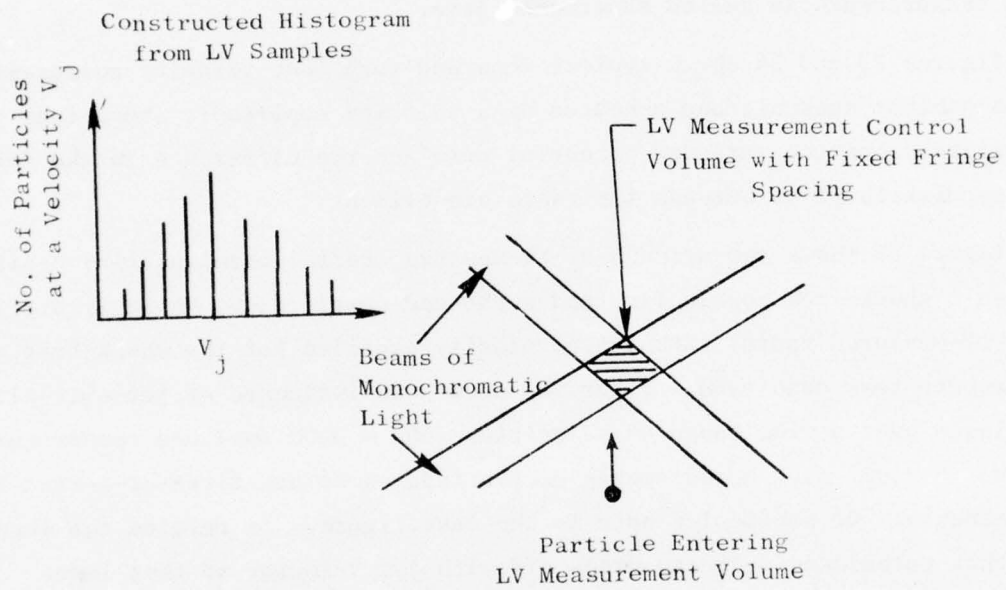


Figure 22. Schematic of Laser Velocity Measurements.

struction of a histogram (See insert on Figure 22). Then, by statistical techniques, the mean values and standard deviations are constructed (the mean velocity and turbulent velocity, respectively). Although the principle of measurement is easy, the practical aspects of designing an electronic processing unit to monitor valid particles is of no small consequence. Investigators have had great difficulty performing measurements in low velocity jets, let alone measurements in heated supersonic jets.

Figures 23 and 24 shown typical mean and turbulent velocity measurements for an ambient subsonic and a heated high velocity supersonic shock-free jet. The existence of the extended potential core and the difference in the turbulence distributions between the cases are evident.

Figure 25 shows comparisons of LV-measured radial mean velocity profiles between a shock-free nozzle flow and a shocked-nozzle flow, while Figure 26 shows LV-measured radial turbulence velocity profiles for the shock-free high temperature test condition. Figure 27 shows the influence of jet-exit-plane turbulence over a wide range of velocities (500 - 3500 fps) and temperatures (ambient - 2500° R). Measurements of the type shown are first-of-a-kind type measurements. Of particular note is the last figure. It refutes the argument that turbulence velocity drops off with jet velocity so that lower velocity power laws occur (an argument proposed by Lighthill). Additionally, Figure 28 shows measured mean and turbulent velocity measurements along the axis of a high-temperature, high-velocity, shocked-flow jet. These results show the capability of the LV for defining the shock structure of high-velocity jets.

4.2 LV-MEASURED TURBULENCE SPECTRA

To construct turbulence spectra from the LV device presents a difficulty not encountered with continuous-type measurement instrumentation. Conventional spectra estimation techniques assume that all values of the input signal are known in the analysis interval. Such knowledge is not available at the LV output. Using the direct time signal in order to construct the turbulence signal results in excessively high sampling noise levels in the estimated spectra. To overcome this problem, it is necessary to reconstruct

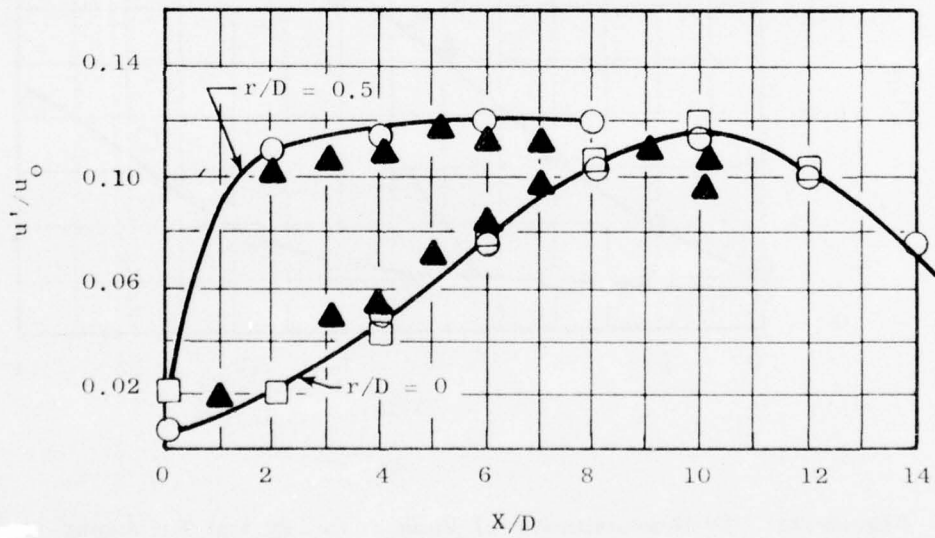
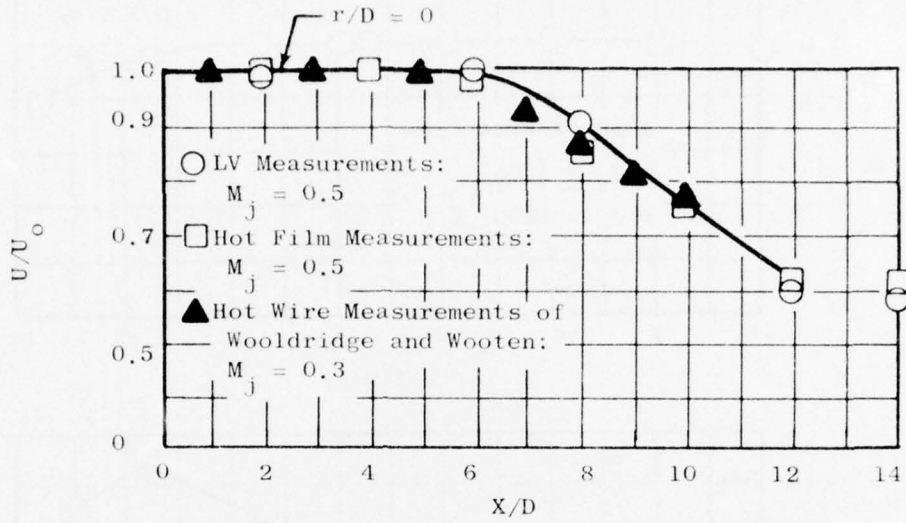


Figure 23. Comparisons of LV Measurements with Hot Film/Hot Wire Measurements for an Ambient Subsonic Jet.

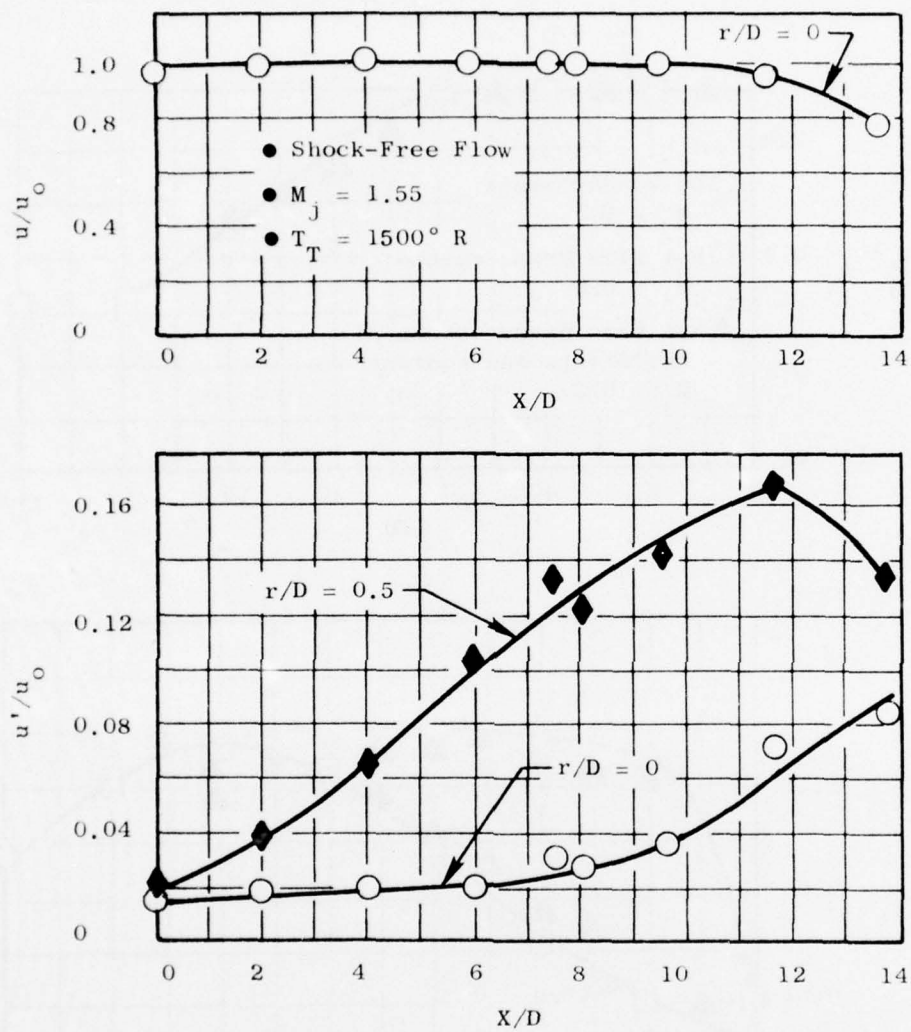


Figure 24. LV Measurements of Mean Velocity and Turbulent Velocity Decay for a Shock-Free, High-Velocity, High-Temperature Jet.

$M_j = 1.55, T_T = 1500^\circ R$

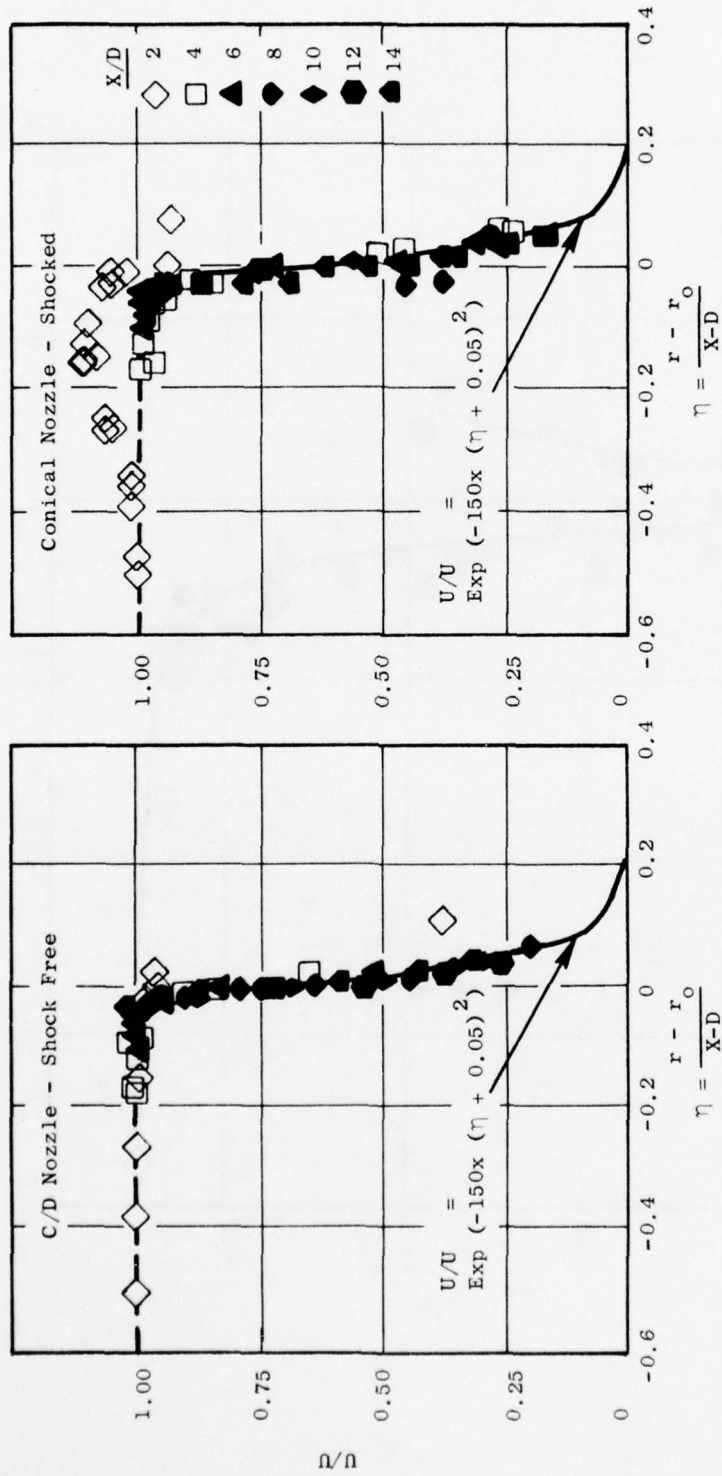


Figure 25. LV-Measured Normalized Radial Mean Velocity Profiles for Shock-Free and Shocked-Flow, High-Velocity, High-Temperature Jet.

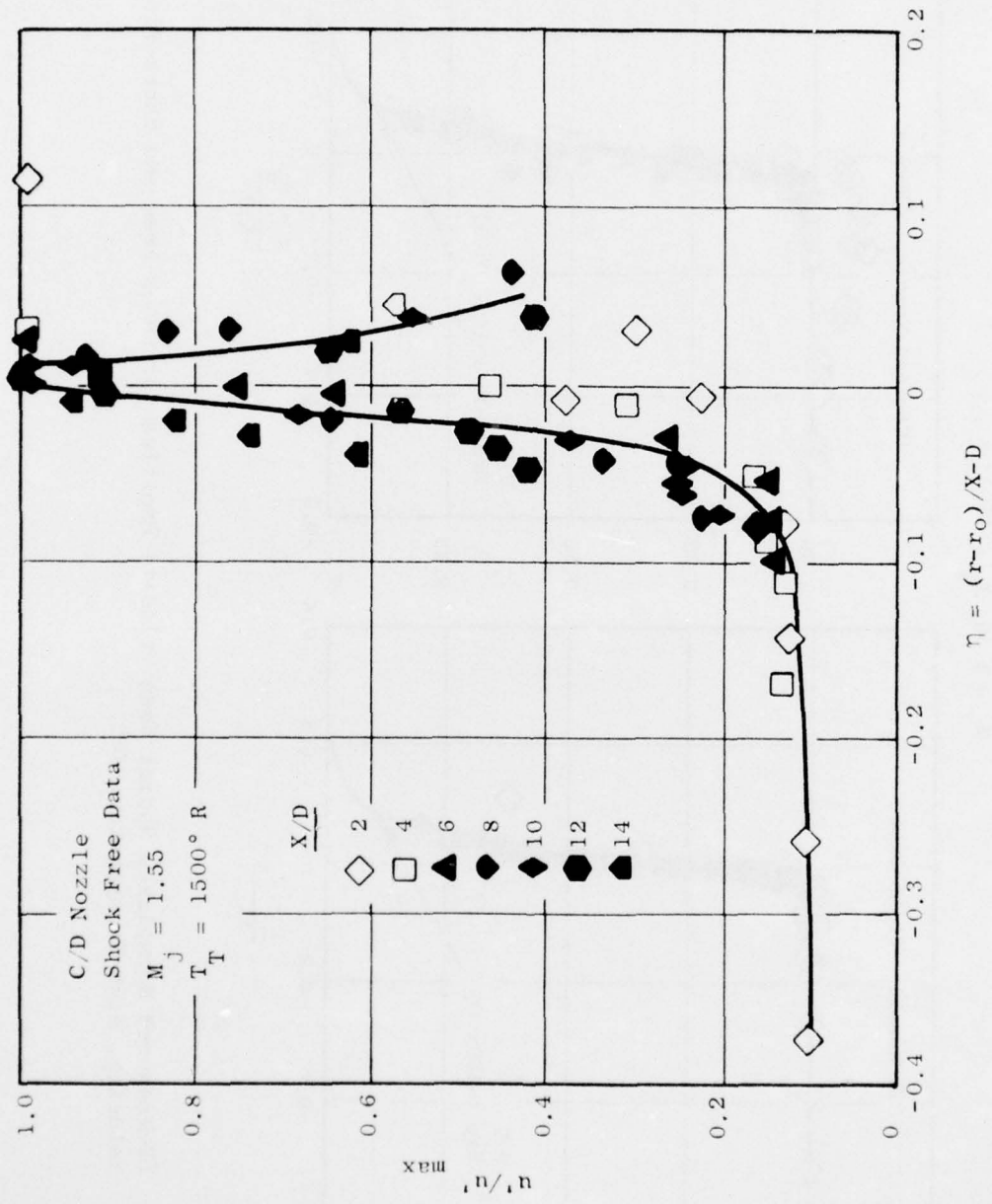


Figure 26. LV-Measured Normalized Radial Turbulence Velocity Profiles.

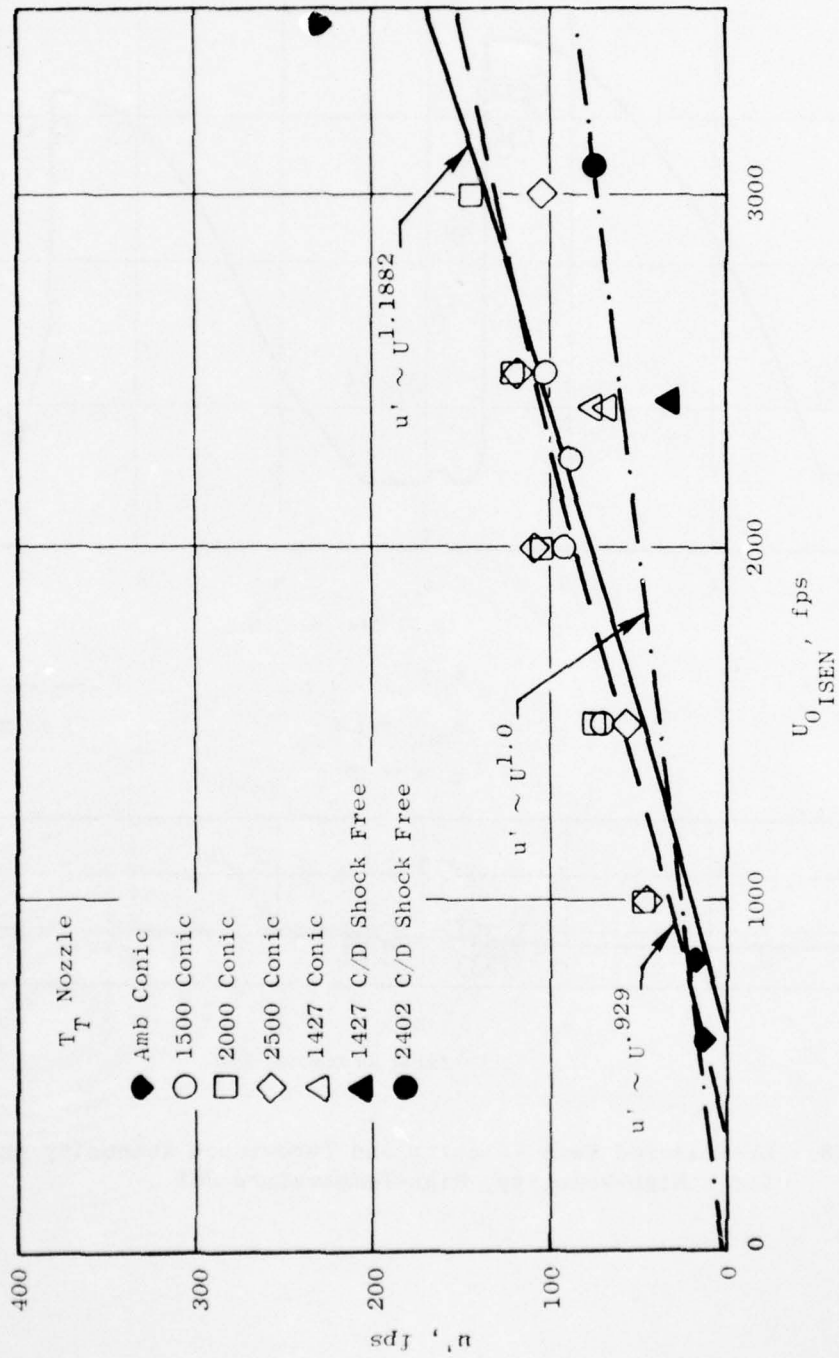


Figure 27. LV-Measured Influence of Jet Velocity on Exit Plan Turbulence.

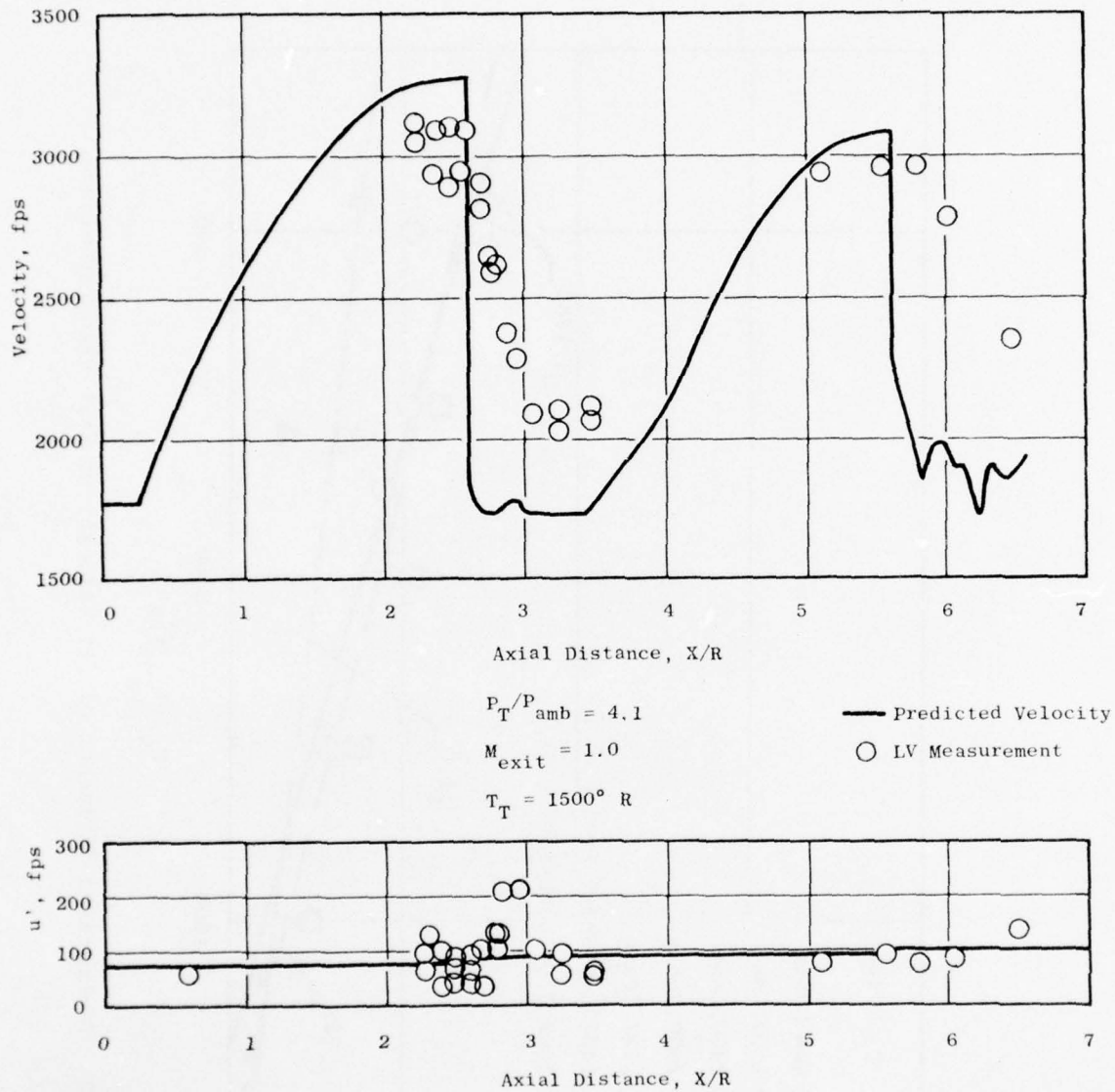


Figure 28. LV-Measured Mean Velocity and Turbulence Intensity on Centerline for a High-Velocity, High-Temperature Jet.

the autocorrelation function of the velocity signal, then obtain the spectrum as its Fourier transform.

To illustrate this process, a model for the output of the LV, $y(t)$, may be constructed as the product of a sampling sequence $s(t)$ (consisting of impulses at the particle-arrival times), and $v(t)$, the actual velocity signal. For $v(t)$ and $s(t)$ statistically independent:

$$Y(t) = S(t) v(t)$$

and:

$$R_{yy}(\tau) = R_{ss}(\tau) R_{vv}(\tau)$$

where $R(\tau)$'s are the appropriate autocorrelation functions.

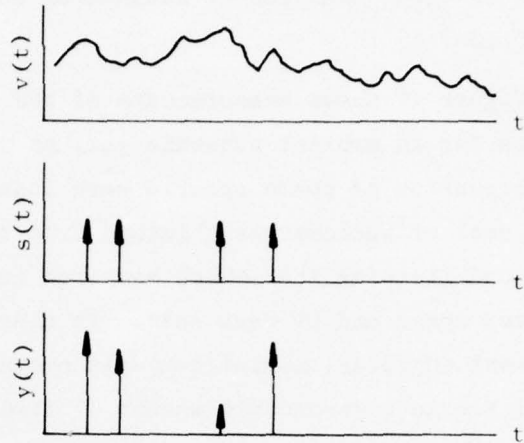
Then, if $R_{ss}(\tau) \neq 0$

$$R_{vv}(\tau) = R_{yy}(\tau) / R_{ss}(\tau)$$

where both of the terms on the right-hand side are measurable. Thus $R_{vv}(\tau)$ may be reconstructed and the velocity spectrum $S_{vv}(\omega)$ obtained by the Weiner relation:

$$S_{vv}(\omega) = \int_{-\infty}^{\infty} R_{vv}(\tau) e^{-i\omega\tau} d\tau$$

As was the case for the measurement of rms velocity, the principle for estimating an LV turbulence spectrum is straightforward. The success one has in reconstructing the velocity spectrum depends a great deal on the accuracy



Model for Sampling Process for LV Spectra.

of the timing of the sampling and output signals, and upon the proper application of error analyses of estimating autocorrelation functions on finite time grids.

Figure 29 shows measurements of the axial component of turbulent velocity spectra for an ambient subsonic jet, as well as a sonic heated jet. The reconstruction of these spectra were indeed quite encouraging. Although a great deal of success was obtained from these demonstration spectral experiments one limiting item which hampered further measurements was the lack of computer speed and LV data rate. In these experiments, the PDP-8 Digital Equipment Corporation mini computer system was used. Performing the necessary arithmetic in a reasonable amount of time with this system was not practical. Any future work in this area should include the use of a much faster system. For future GE work, a PDP 1145 has been selected. Below is a discussion of how the LV/PDP 1145 was used for performing in-jet-to-far-field cross-correlation measurements.

4.3 LV MEASUREMENTS FOR NOISE SOURCE LOCATION

The starting point of the in-jet-to-far-field cross correlation is with Proudman formulation of the Lighthill equation:

$$\frac{dp'(t)}{dV} = \frac{\rho_o}{4\pi Ra_o^2} \frac{\partial^2}{\partial \tau^2} U_R^2(t) \quad (16)$$

Lee-Ribner⁽⁴¹⁾ and Siddon⁽⁴²⁾ further extended this result as:

$$\overline{\frac{dp'_p(\tau)}{dV}} = \frac{-\rho_o}{4\pi Ra_o^2} \frac{\partial^2}{\partial \tau^2} U_R^2 p(\tau + R/a_o) \quad (17)$$

Therefore, the contribution to the farfield pressure autocorrelation function, from a volume element of jet, is proportional to the second derivative with respect to the retarded time of the cross correlation between the in-jet velocity squared and the far-field pressure evaluated at the retarded time. The problem at hand is to measure the right-hand side of equation (17).

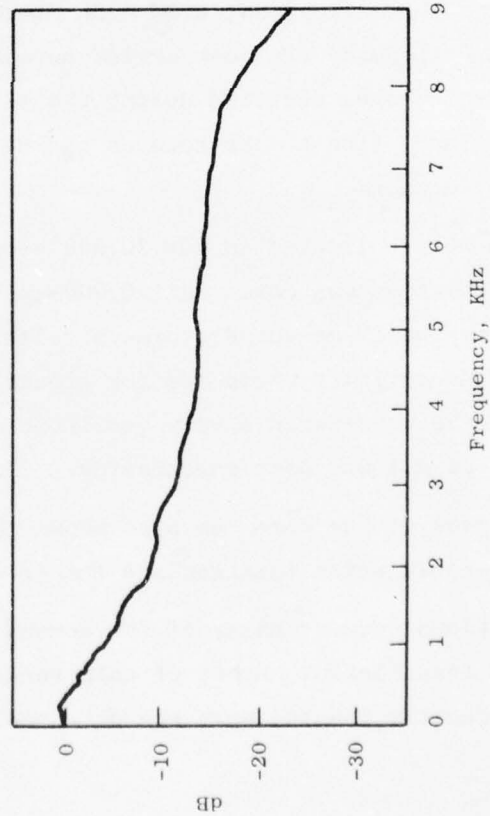
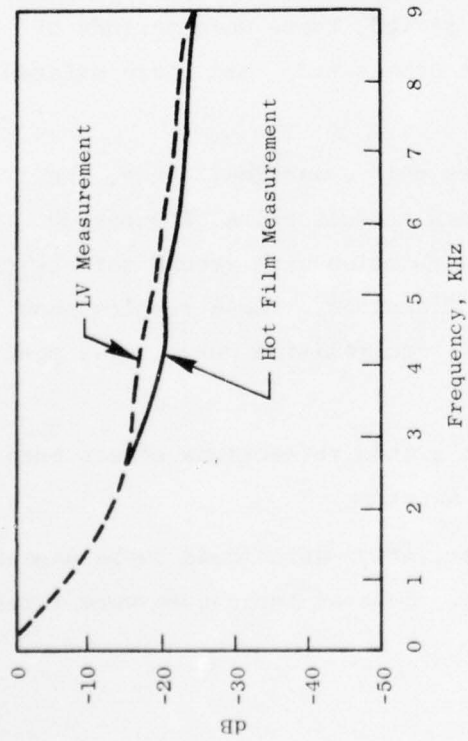


Figure 29. LV-Measured Axial Turbulent Velocity Spectra for Ambient and Heated Jets.

As was the case for the turbulent spectra measurements, the LV output for the cross correlation consists of particles randomly arriving at the probe volume. The velocity information is available as point estimates at random times. Thus, a special estimator is required to construct the cross-correlation function (the detailed description of the cross-correlation function and the variance of the estimator is described in Chapter 3, Section 2.0 of Volume II of this final report). In addition to constructing the cross correlation from LV measurements, methods for constructing its second derivative are also important to performing the total measurement.

As a demonstration experiment, tests were performed at General Electric's outdoor test site. Measurements were taken on a 4-5/8 inch diameter conical nozzle. The LV measuring volume was at $X/D = 4$ and $r/r_0 = 1$. The flow conditions were $T_T \sim 700^\circ R$, $V_j \sim 600$ fps. The LV velocity vector was pointed at a far-field microphone at 30° to the jet axis, 50 diameters away. To avoid phase shift problems, a BK 4136 microphone was used with the end grid removed. Performing the test series outdoors complicated the measurement. Temperature changes occurred during the test period, there were periods of "wind-gusting" (these data records had to be eliminated), and there existed ground reflections.

Data were collected in six 20,000 product pair ensembles. Thus, the cross correlation was based on 120,000 averaged product pairs. Figures 30 and 31 show the LV-measured cross-correlation function with ground reflections and an estimate corrected for ground reflections. These results show what would be considered a very realistic cross-correlation curve. The peak amplitude of 0.1 was most encouraging.

Analysis of the data has also shown that ground reflections effect both the cross-correlation function and the cross spectra.

Additionally, estimates of the second derivative were found to be unusable, due to an insufficient number of data records. Several techniques were tried, but satisfactory results were not obtained.

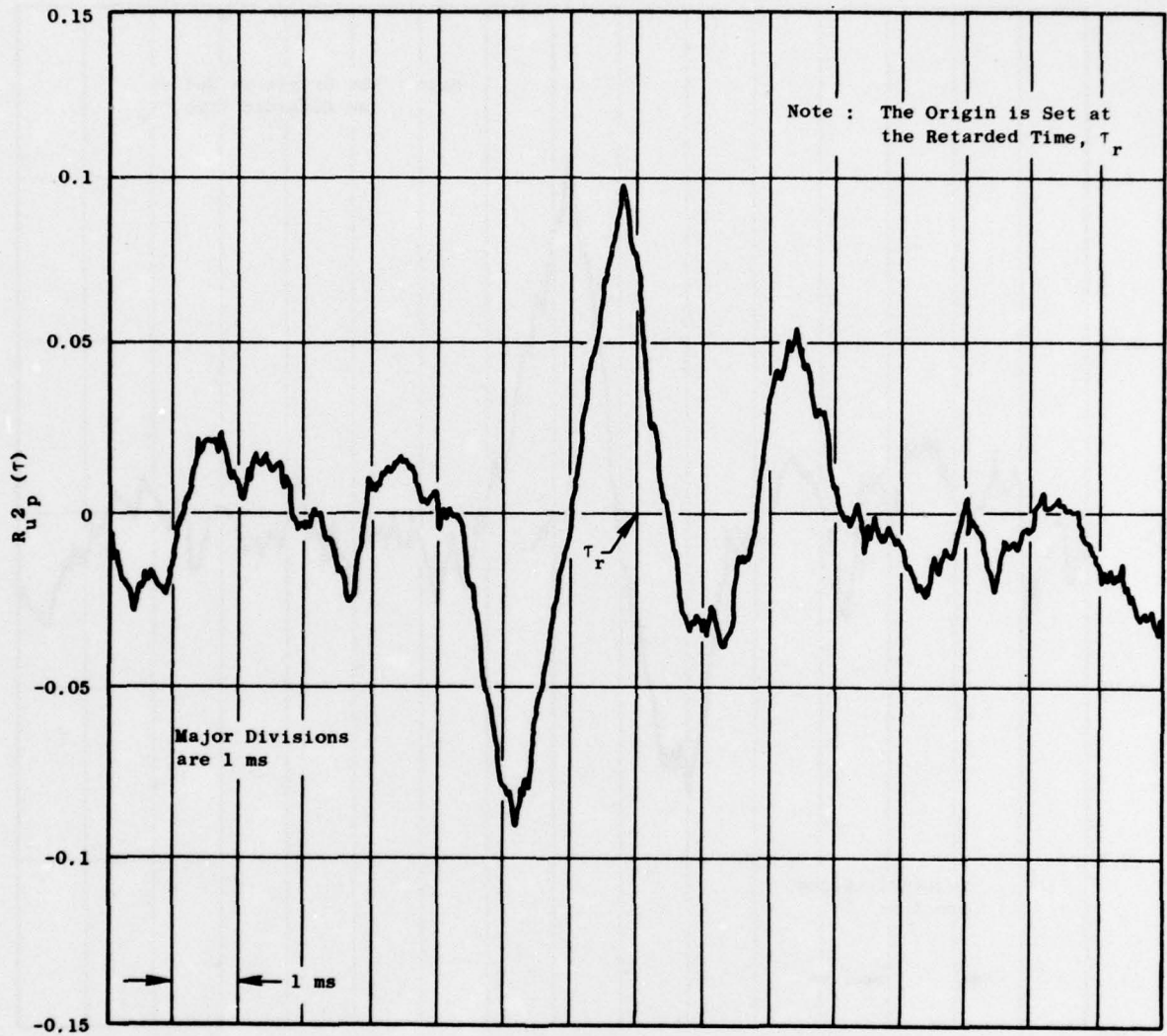


Figure 30. Final Cross-Correlation Estimate Without Ground-Reflection Correlation.

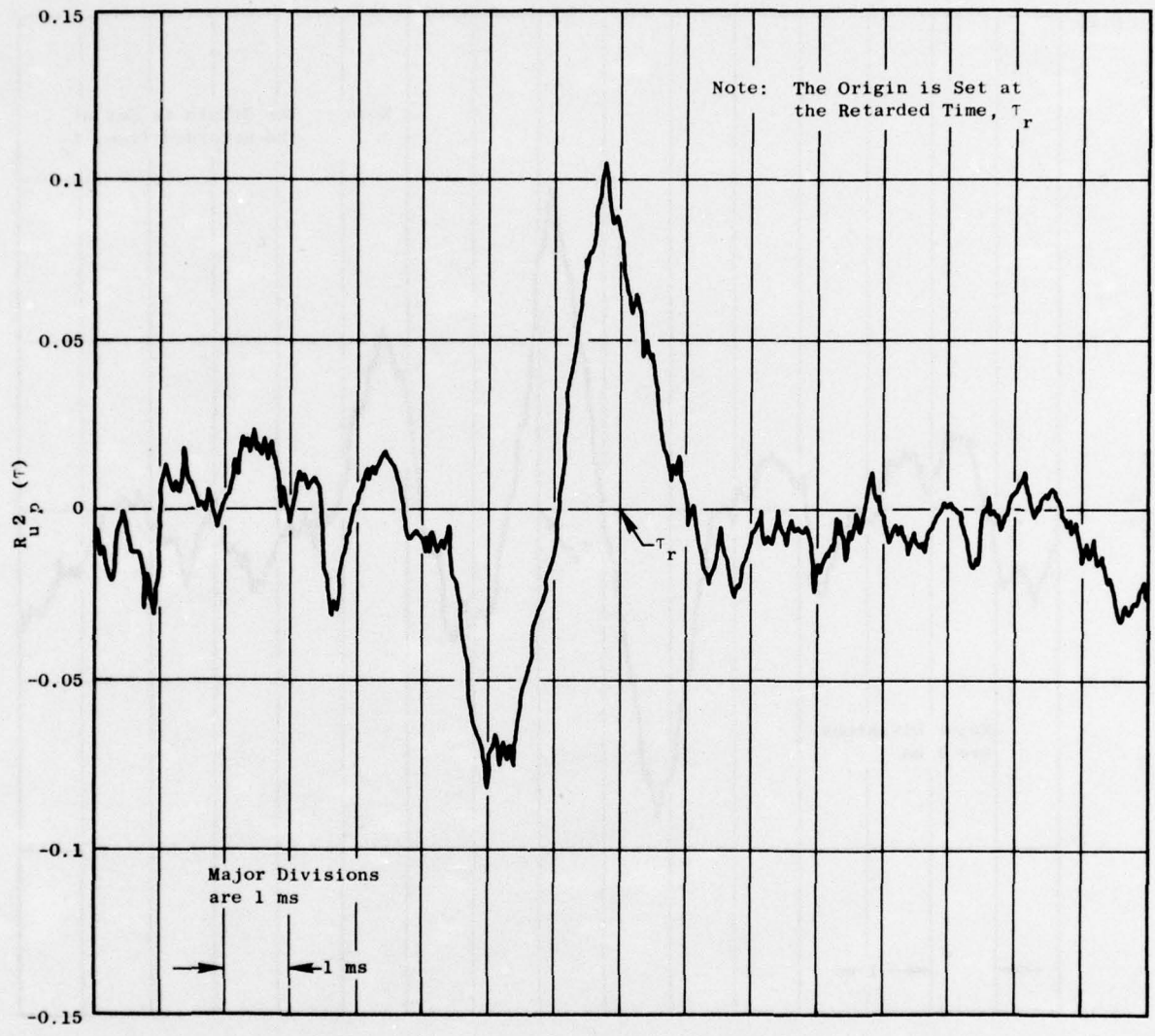


Figure 31. Final Cross-Correlation Estimate with Ground-Reflection Correlation.

The techniques developed for obtaining cross correlation between LV in-jet measured velocity and far-field microphone acoustic pressure measurements have been demonstrated, while estimates for the second derivative were not as successful. To improve on the second derivative estimators, more data are necessary. Improvements toward this end are certainly feasible. Estimates are that more efficient data collection procedure would increase the data taken by a factor of 6-8. Additionally, improved seeding techniques would also increase the amount of data available.

SECTION 5.0

SOME INTERESTING INSIGHTS FROM ACOUSTIC EXPERIMENTS

In addition to the work described in the first four sections, several experiments were performed which have served to stimulate interest and suggest some new insights regarding jet noise. These experiments dealt with the influence of upstream aerodynamic disturbances and the influence on jet noise (upstream swirl, and combustion roughness effects, jet refraction, and snock noise).

5.1 UPSTREAM SWIRL

To study the influence of jet swirl on jet noise generation, a swirl vane system was designed as shown in Figure 32. The system consisted of a set of 16 swirl vanes designed for a 30° swirl angle with 89% mass flow penetration. Three conditions were tested: Mach number of 0.8 at ambient and 1500° R, and $M_j = 1.0$ at 1500° R. It was found that, for the heated jet conditions, power-level reductions did occur. At peak jet noise angles on an arc considerable noise reduction also was observed (see Figures 33 and 34). Although the spectral results show reductions over a rather wide band of frequencies, for small jet angles, on a PNL basis the results were found to be different. Figure 35 shows a PNL directivity of the same swirl data shown in Figures 33 and 34, but now on a 300-foot sideline. Here the subjective noise due to swirl was found to actually increase. This was due to the fact that, on a sideline basis, the peak angle noise shifts to the larger jet angles. As can be observed from Figure 33, at the larger angles, the OASPL is also greater for swirl than without swirl. Thus, although our work indicated that swirl can lead to noise reduction in terms of OAPNL (and even OASPL and SPL at particular angles and frequencies), and results show a general increase in PNdB levels.

Estimates of performance losses for swirl were also performed. It was found that, for the ambient jet case, a 10% specific thrust loss due to the 30° swirl was measured. Such a high level of thrust loss is certainly unacceptable from a practical standpoint.

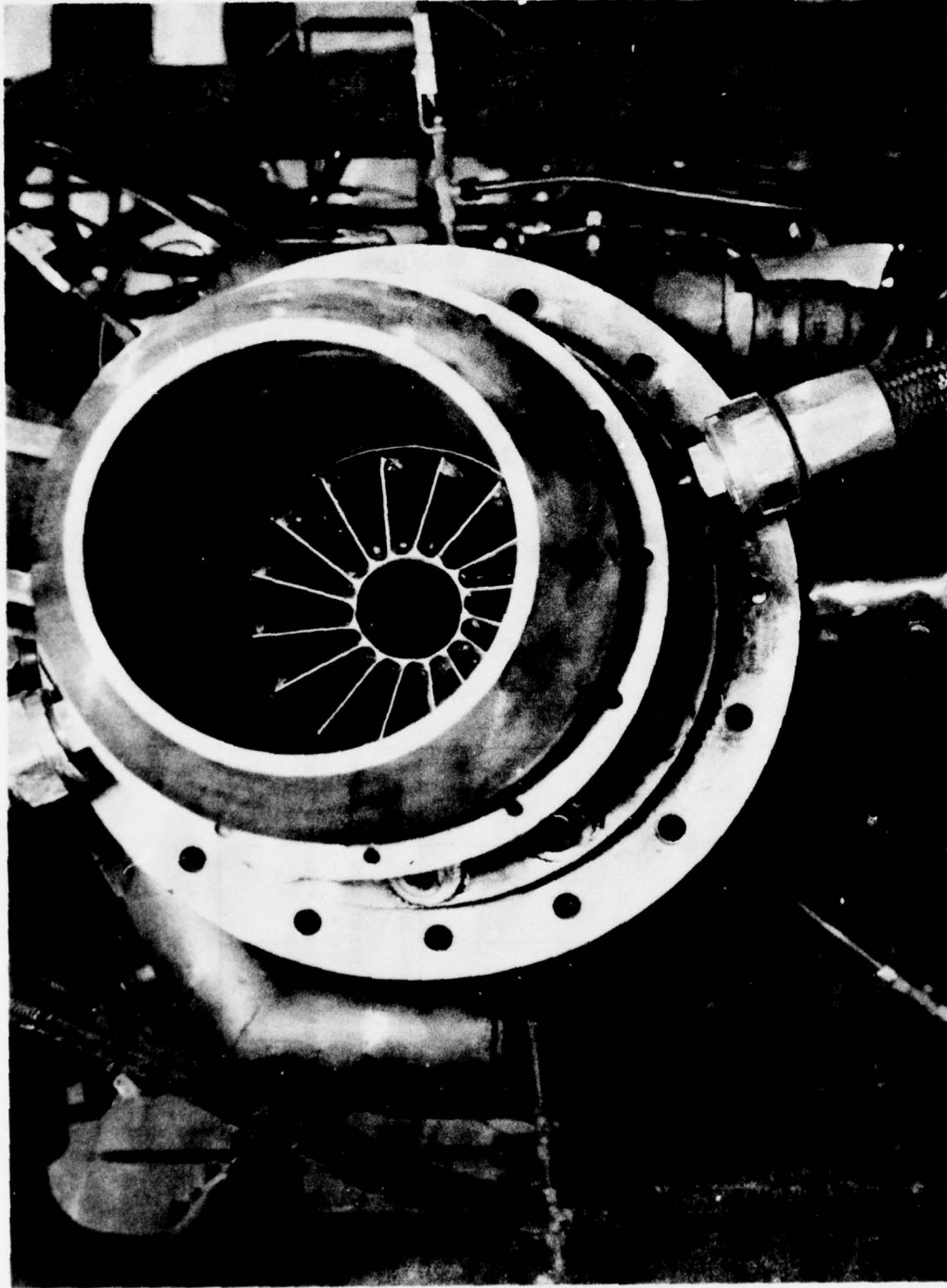


Figure 32. Photograph of Jet Swirl Test Rig.

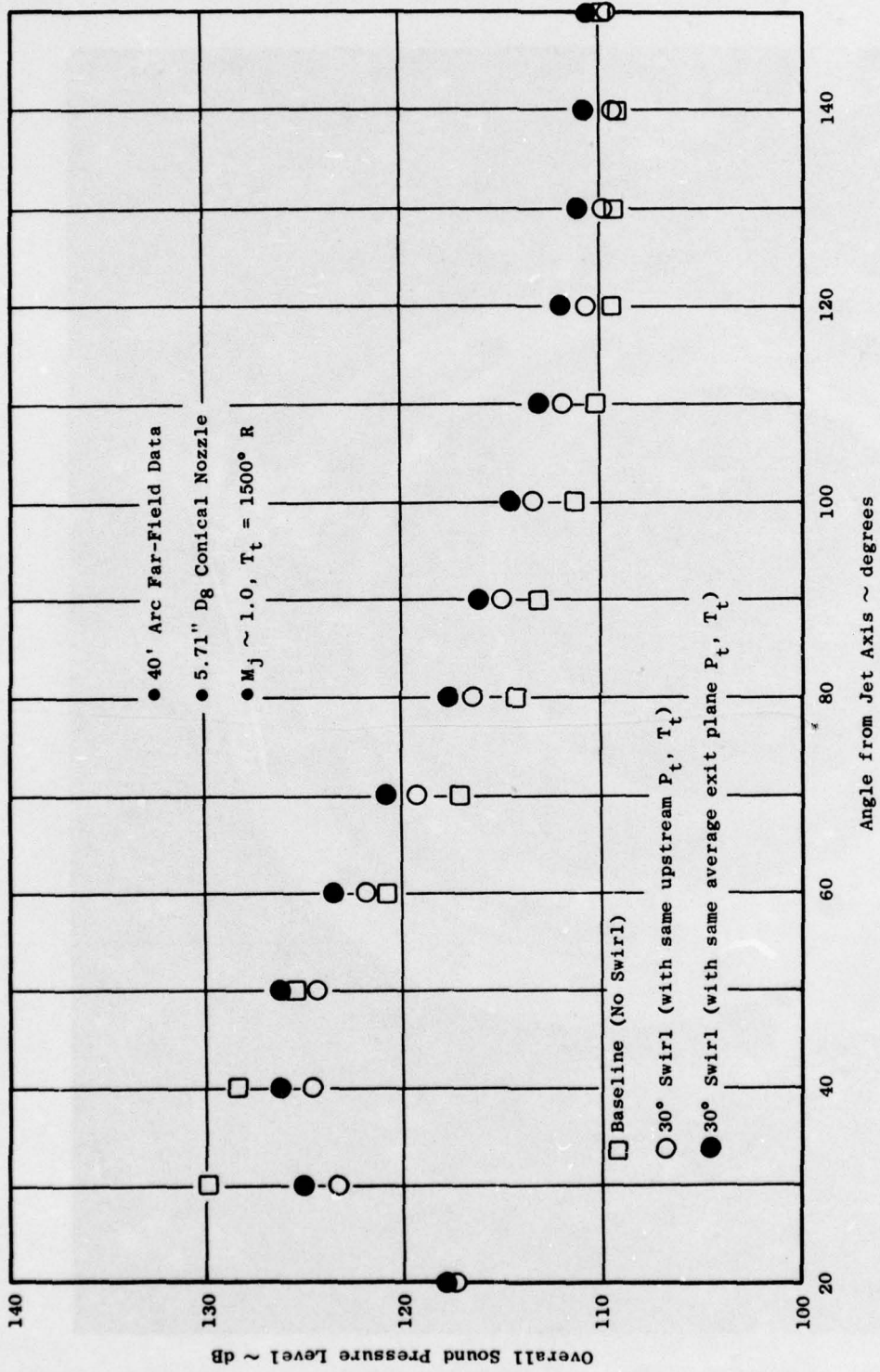


Figure 33. The Influence of Jet Swirl on OASPL Directivity.

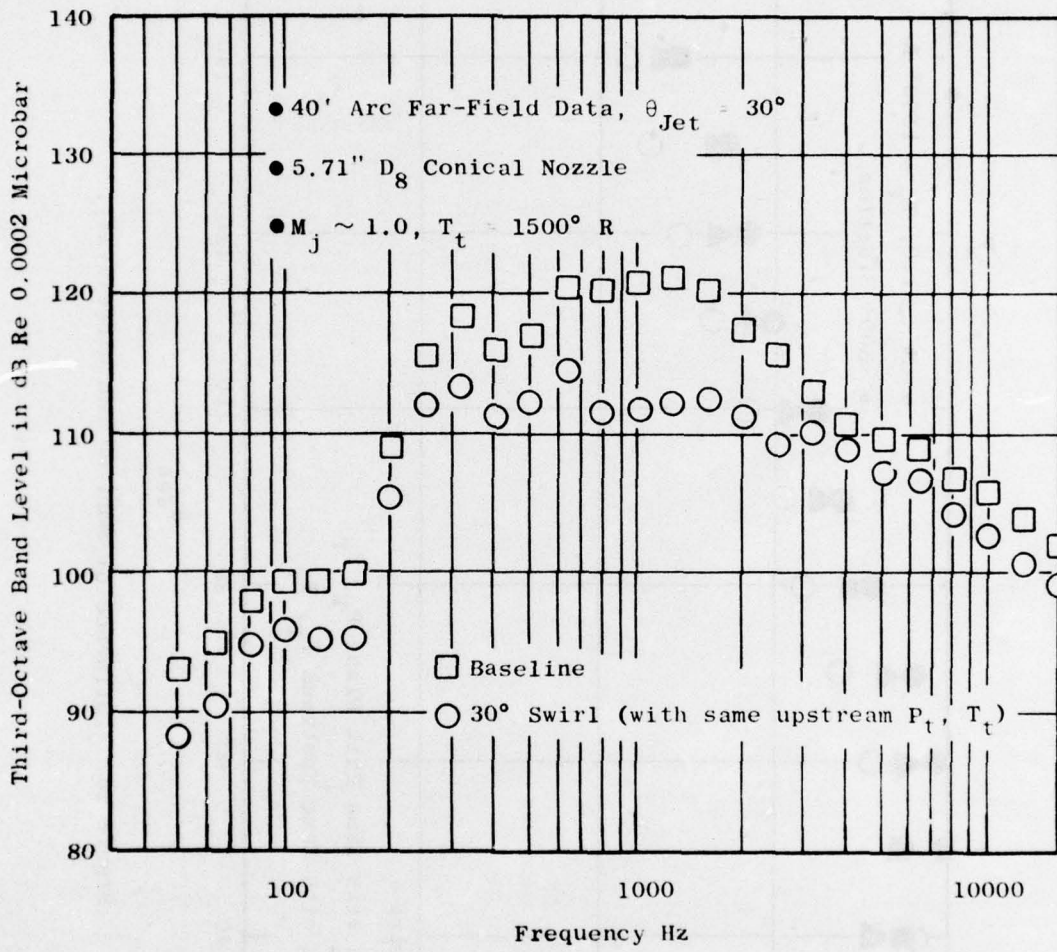


Figure 34. Influence of Jet Swirl on SPL Spectra.

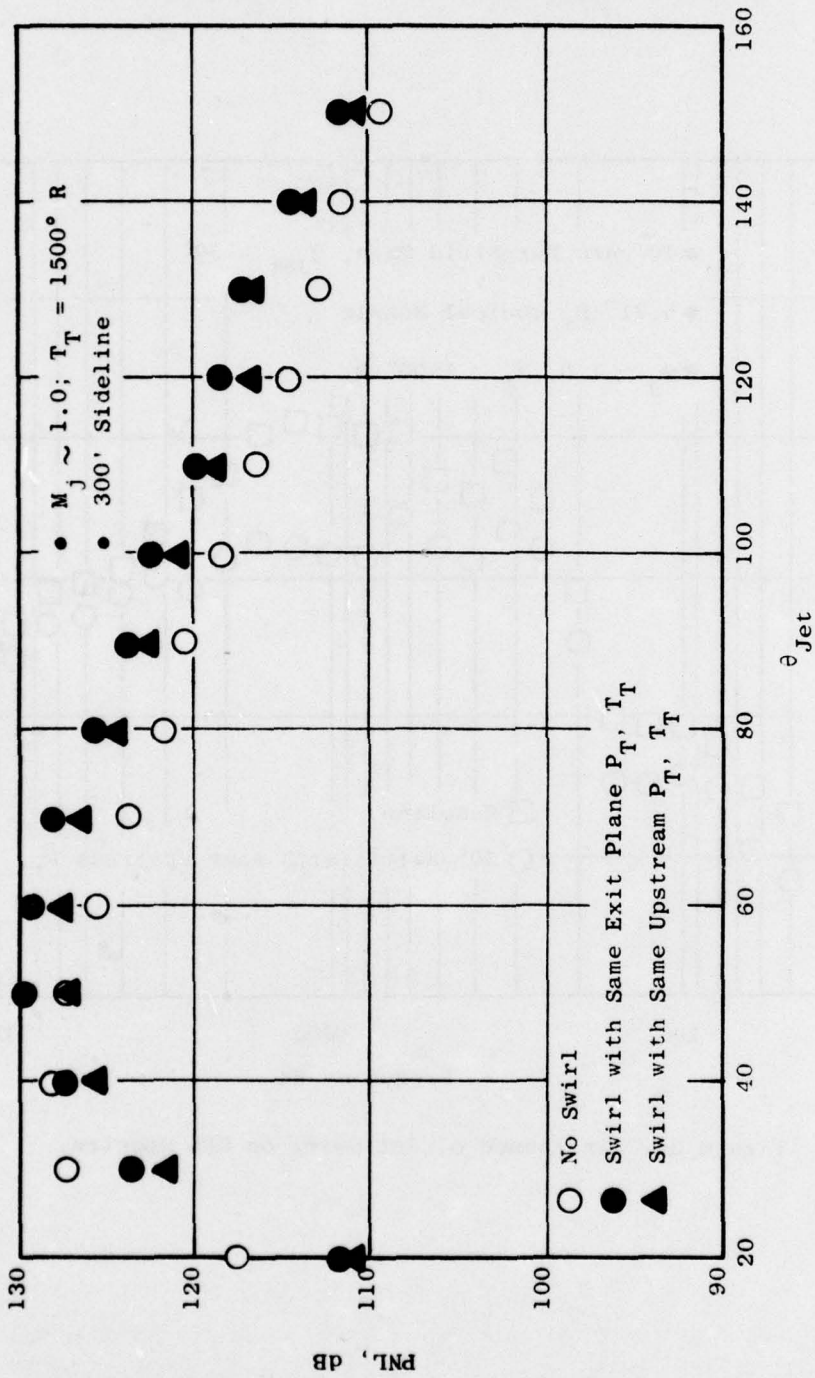


Figure 35. Influence of Swirl on PNL Directivity.

The results from this series of tests are certainly limited - and somewhat pessimistic. Recent engine tests at NASA-Ames⁽⁴³⁾ showed somewhat similar swirl jet characteristics except at the larger angles. The NASA-Ames results indicated that a noise reduction could be obtained even at the very large jet angles. The reasons for this discrepancy are not fully understood. However, the NASA-Ames tests were for engine scale, and the amount of swirl was somewhat less than the model scale test series discussed above.

One item which needs clarification is how much swirl is necessary to yield the on-set of swirl noise reduction. It is possible that, if the swirl is slight (so that the thrust loss is minimal) but suppression characteristics are similar to those given above, it would be feasible to enjoy a modest PNdB and EPNdB reduction with a modest thrust loss.

There are indications that such a swirl condition may be feasible and that further exploratory work may be warranted especially regarding its application toward small business jet suppression techniques. For the small business jet, only modest noise reductions are required. For high velocity jet noise reductions, where much larger reductions are desirable, it does not appear that jet swirl by itself would be of benefit. It is possible, however, that controlled swirl experiments, coupled with orderly structure concepts, may lead to some novel insights with regard to turbulent mixing noise and other suppression concepts.

5.2 SHOCK NOISE

In the second interim report for this contract, a series of shock noise tests was reported. At that time, it was concluded that shock noise would be influential only at large jet angles. Since then, new findings have emerged regarding shock noise and its impact on full-size engines.

Figures 36 and 37 illustrate what may be considered the influence of shock noise for full-size engines. Each figure compares a C/D shock-free jet with a corresponding shocked conic nozzle at the same flow conditions. The inner two curves on the polar plot represent the broadband SPL from a 10-Hz narrowband. The solid curve represents the shock screech fundamental. When the 10-hertz narrowband is converted to 1/3-O.B. SPL, the dashed-dot

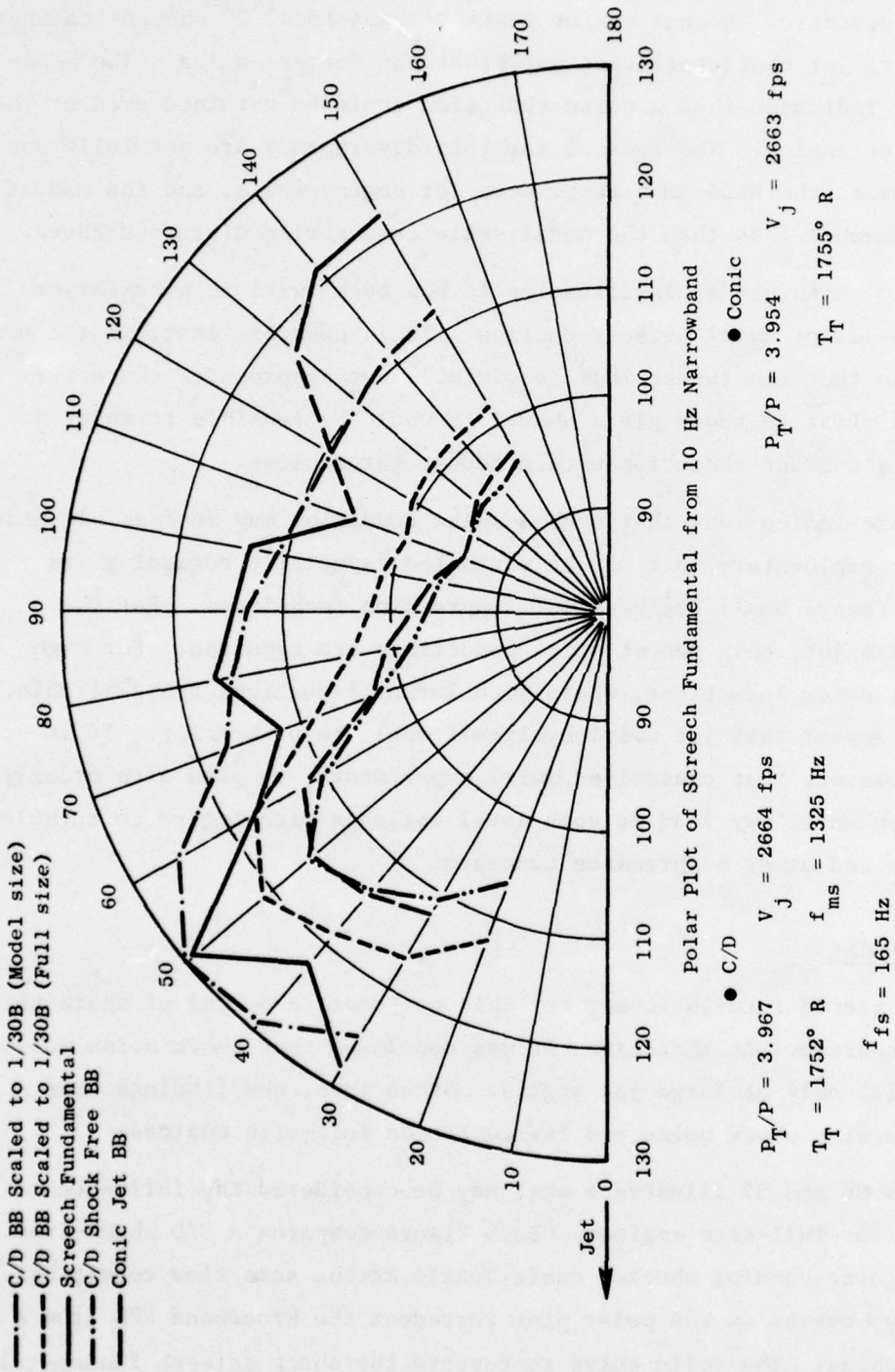


Figure 36. Estimated Influence of Shock Screech for Full-Size, Heated-Exhaust Jets.

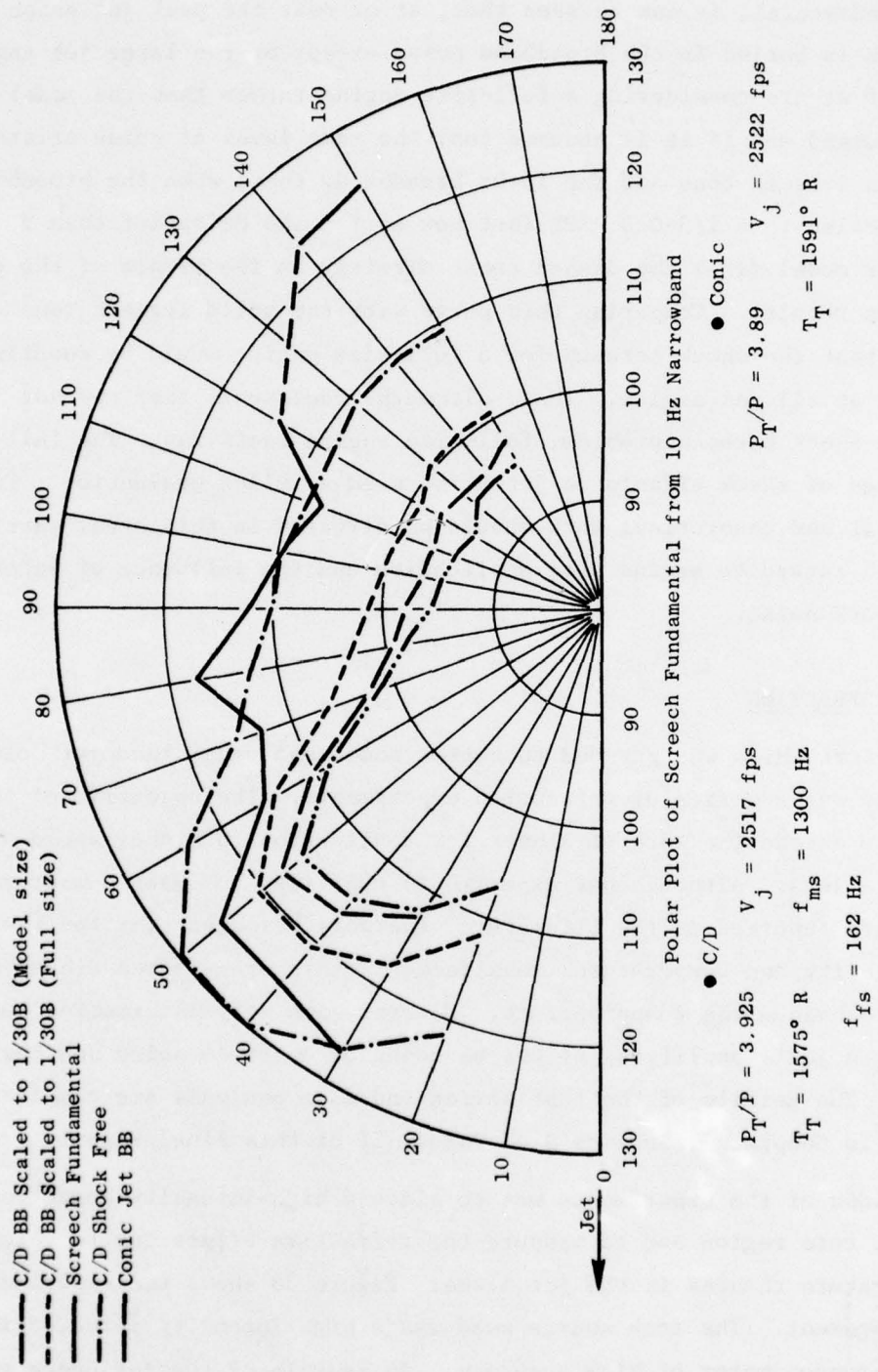


Figure 37. Estimated Influence of Shock Screech for Full-Size, Heated-Exhaust Jets.

curve (or the outermost curve) results. When this curve is compared to the screech fundamental, it can be seen that, at or near the peak jet noise angles, the screech is buried in the broadband noise except at the large jet angles. However, if we are considering a full-size engine rather than the model scale tests discussed and if it is assumed that the same level of noise exists between the screech tone and the 10-Hz broadband, then, when the broadband noise is scaled to a 1/3-O.B. SPL (but now at $f \sim 160$ Hz rather than $f \sim 1300$ Hz for model size) the dashed curve directly in the middle of the other four curves results. Comparing this curve with the solid screech tone curve indicates that the shock screech for a full-size engine would be readily observable at all jet angles. Thus, although model scale test may not indicate a shock screech problem, full-size engine tests may. The full consequences of shock effects on jet noise need a fuller evaluation. Further experimental and theoretical work should be directed in this area, particularly with regard to engine size application and the influence of external flow on shock noise.

5.3 JET REFRACTION

An effort which was pursued to better model and understand jet noise directivity was a series of refraction experiments. The objective of the work was to extend the work of Ribner for application to higher speed and temperature jets. Although our experiments confirmed low Mach number refraction results reported in the literature, the work revealed that for the higher velocity and temperatures considered in this program the Ribner refraction technique was inappropriate. However some very interesting results concerning a jet's amplifying effect on tones or upstream noise sources were revealed. The details of the test series and data analysis are completely discussed in Chapter 3, Section 2 of Volume II of this Final Report.

The idea of the experiments was to place a high-intensity sound source in the jet core region and to measure the refractive effect due to velocity and temperature changes in the jet plume. Figure 38 shows the experimental test arrangement. The tone source used was a high-intensity siren, driven by a synchronous motor of high accuracy. An example of the influence of jet



Figure 38. Refraction Experimental Setup.

flow on the tone directivity for a $M_j = .5$ ambient jet is shown in Figure 39. The relative levels between the tone SPL and the jet-alone SPL at 783 Hz is quite large.

Figure 40 shows SPL reduction of the tone due to jet flow for ambient subsonic jets. The results are in agreement with MacGregor, Ribner, and Lam's results. At higher velocities and for heated jets the picture of the simple refractive dip no longer appeared. At the smaller jet angles, an amplifying effect was observed as the velocity increased. Figures 41 and 42 illustrate these results.

To study these effects closer predictions of the directivity patterns were carried out using mini-directional point singularities in a slug flow. A question which was sought was what type of source is most appropriate for performing predictions (displacement source, velocity source, pressure source). To account for the observed amplifying effects, a model was designed (after Crow) to reflect the notion that the tone can excite columnar, travelling instability waves. This was obtained by applying a $(1 - M_c \cos \theta)^{-3}$ factor to the previous solutions. Figure 39 shows this modification using a displacement source, while Figure 40 uses a velocity source. The conclusions drawn from the study were that:

- At Mach numbers less than about 0.7, the injected sound sources in jets yield straightforward refraction patterns in good agreement with classical acoustics. It was found that, for Mach numbers of 0.5 and 0.7, the displacement source worked best.
- Above Mach numbers of 0.9, the suggestion by Crow that jets can act as amplifiers of injected or internally generated low frequency tones appears to be true. The mechanism appears to be the development of columnar-travelling instability waves whose strength and frequency are determined by the source strength and frequency, but whose speed of convection is some fraction of the jet velocity.
- No evidence was found that such tones can have any major impact on the externally generated turbulence jet noise. In all of the work performed, there was no evidence of the broadband jet-noise itself being modified by the tone.
- Although the technique used was successful for obtaining refraction information of low-Mach-number jets, at the higher Mach numbers

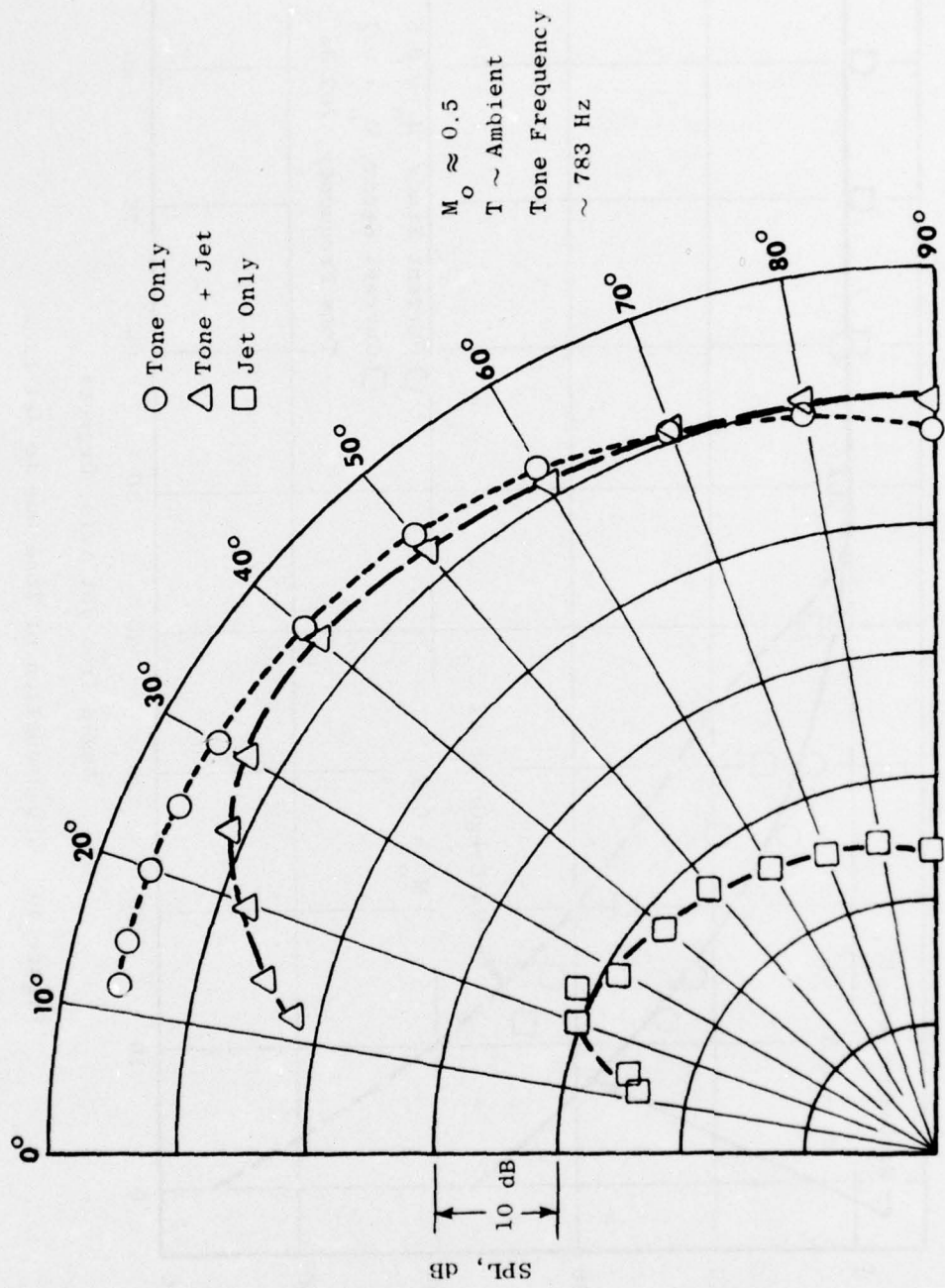


Figure 39. Influence of Refraction on Jet and Siren Tone.

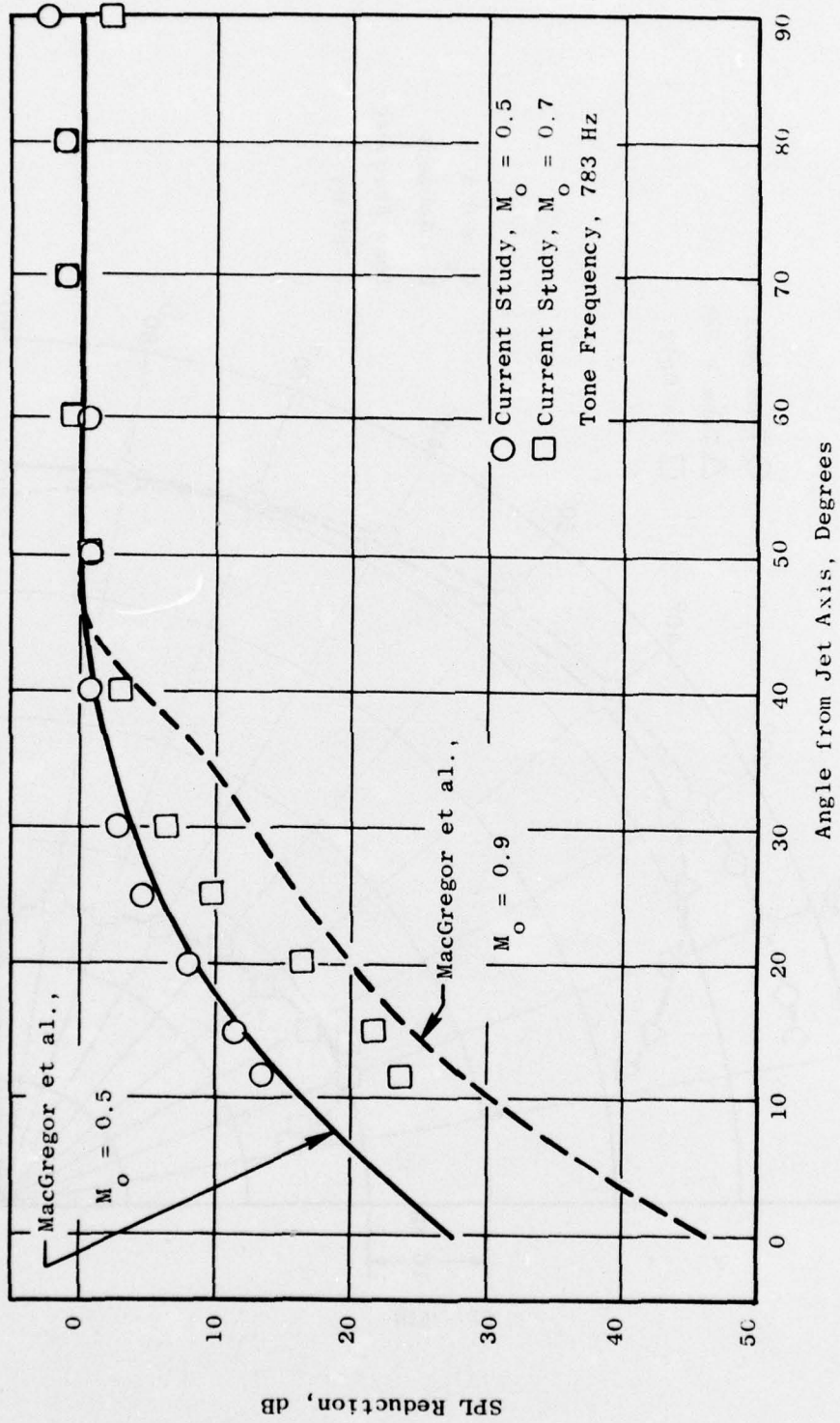


Figure 40. SPL Reduction of Tone Due to Jet Flow.

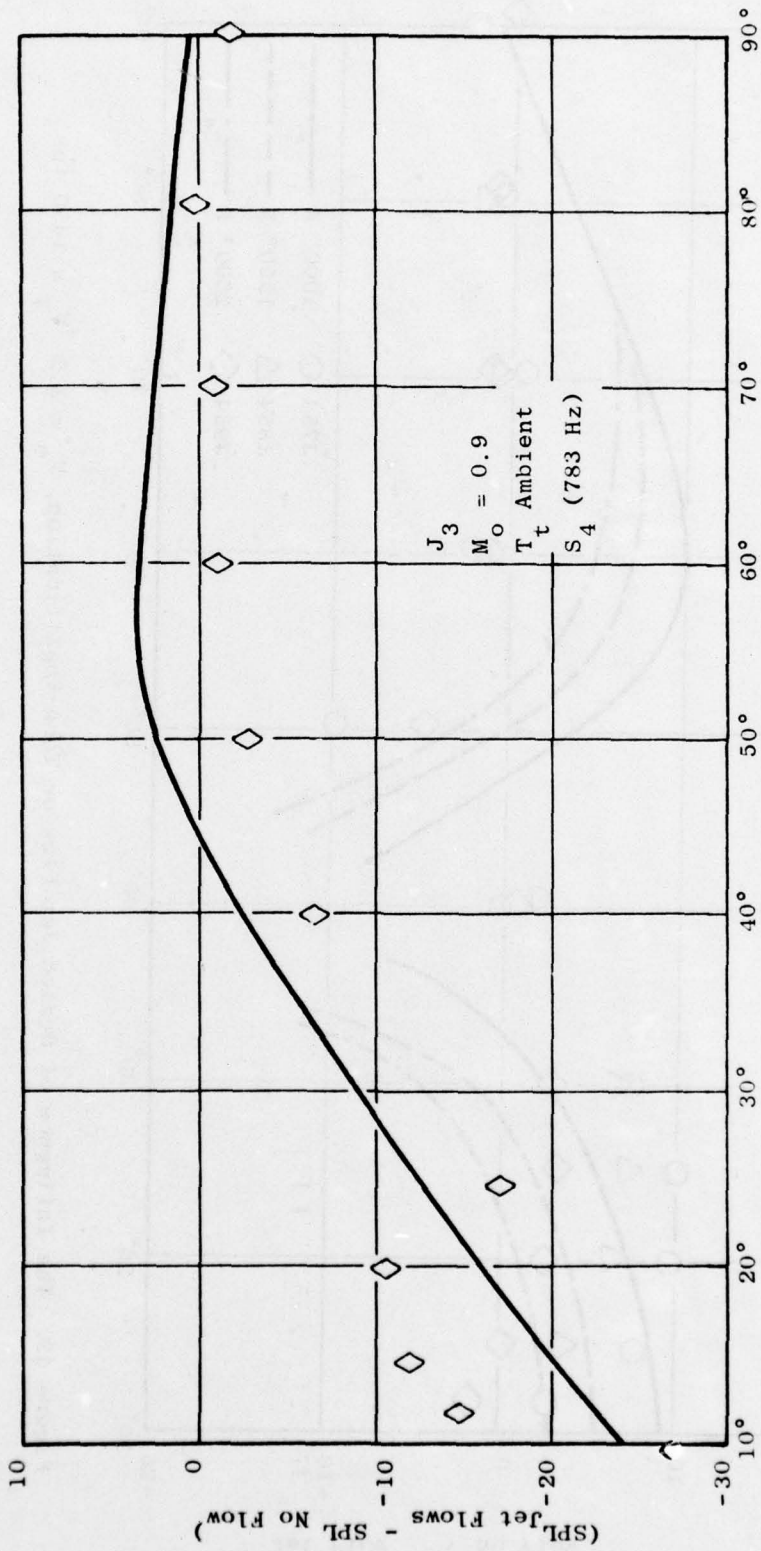


Figure 41. The Influence of Jet Flow on Tone.

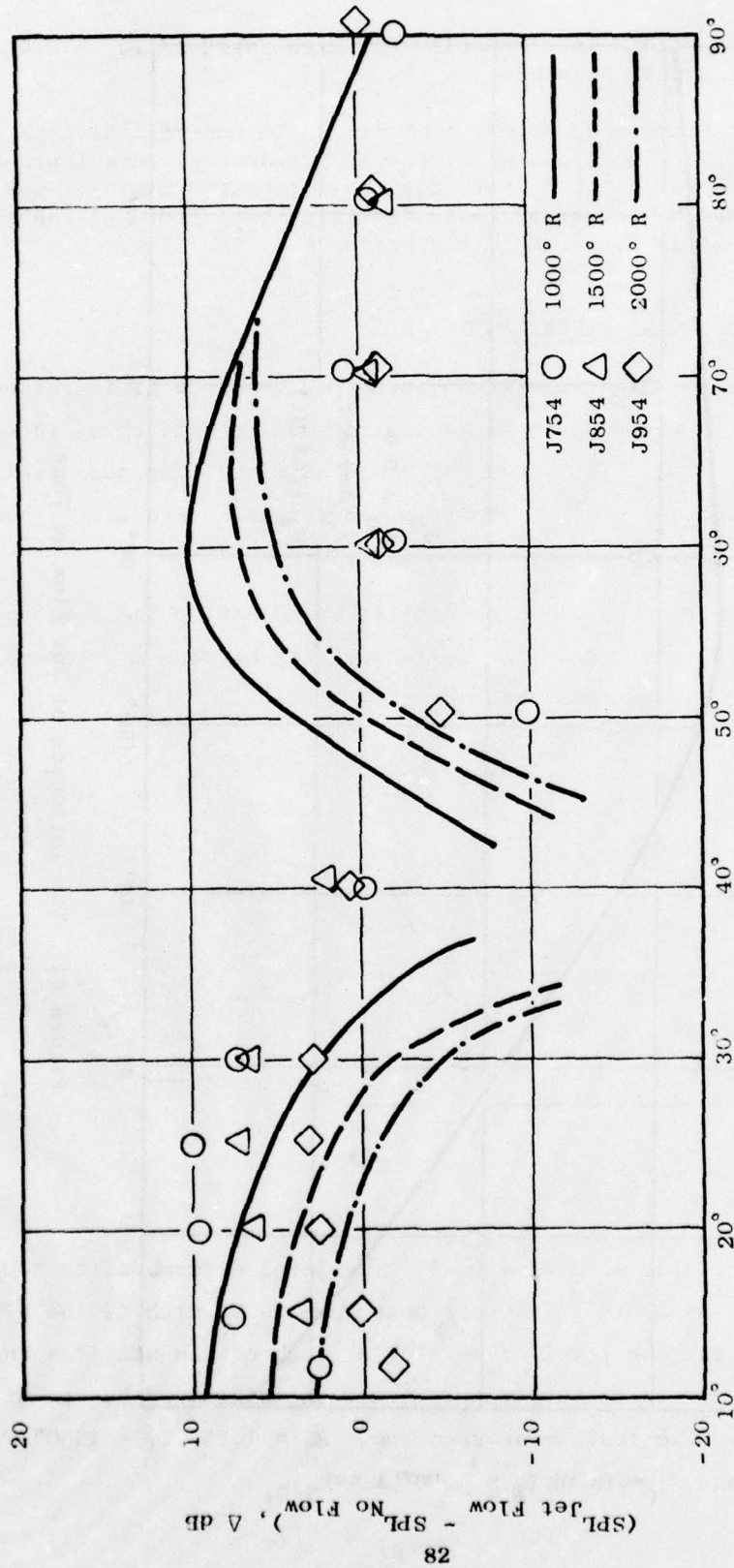


Figure 42. The Influence of Heated Jet Flow on Tone Amplification, $M_0 = 1.3$ $V_j = 1450$ fps.

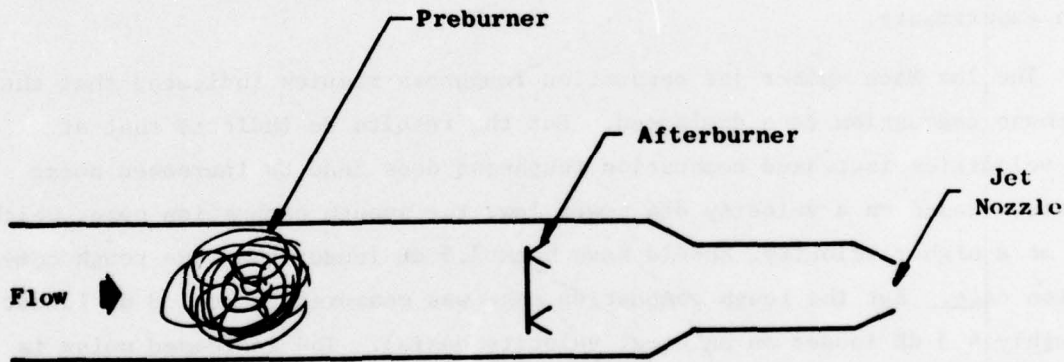
Greens Function experimentally for high speed ($V_j/a_0 > 0.9$) jets does not appear possible.

- Such experiments do appear relevant as to the role of jets as amplifiers of upstream-generated low frequency tones (such as combustion noise). It is very desirable to perform closer in-jet measurements of the source to determine the nature of the source and how it is modified by the presence of the flow.

5.4 COMBUSTION ROUGHNESS EXPERIMENTS

A small series of experiments was performed to study if increased combustion roughness would cause increased turbulence and, thus, increased turbulence mixing noise. The study was aimed at simulating more realistic engine burning processes, and to see if an additional noise level, because of these processes, would be encountered.

The combustion roughness was controlled by adjusting the level of total temperature for the model scale jet noise facility between a preburner (PB) and an afterburner system (see sketch).



Each system was operated with JP-4 fuel. The level of combustion roughness was monitored with pressure transducer measurements at each of the burner stations. By varying the level of burning at each of the stations in different combinations, the total temperature could be maintained but at different levels of burning. Two test cases were run, $M_j = 1.55$, $T_T = 1500^\circ \text{ F}$ (shock-free C/D nozzle) and $M_j = 0.3$, $T_T = 1650^\circ \text{ R}$.

Table 1 summarizes the overall test results. For the supersonic case, three conditions were run. Preburner alone, preburner with low afterburner, and an even split between the preburner and afterburner charging stations. For the subsonic tests, there was a case where combustion resonance existed in the preburner section, a second case was run just off-resonance (listed as rough burning), and a smooth burning case. (For details see Chapter 3, Section 1 of Volume II of this final report). Table 1 shows that, for the three levels of combustion roughness (also see Figure 43 for a comparison of combustion roughness vs. acoustic efficiency for these tests) for the shock-free supersonic jet case, there was essentially no difference in OAPWL and OASPL levels. The turbulence level at the exit plane could only be raised from 2% to 4.5%. Figure 44 shows a comparison of the measured OASPL directivities for these cases. The item which may be of significance is the low frequency data; for the afterburner with low preburner (the rougher combustion roughness case), the noise was somewhat increased (3-5 dB at 40° and 90° microphone locations - (see Figure 45). This is noted since this noise may be jet-flow-amplified combustion noise as was pointed out in the refraction experiments.

The low Mach number jet combustion roughness results indicated that the resonant combustion case dominated. But the results do indicate that at low velocities increased combustion roughness does lead to increased noise levels. Based on a velocity 8th power law, the smooth combustion case, which was at a higher velocity, should have been 2.5 dB louder than the rough combustion case. But the rough combustion case was measured to be 1.8 dB louder (roughly 4.3 dB louder on an equal velocity basis). The increased noise is likely due to an increase in turbulence throughout the jet plume. Unfortunately LV measurements were not possible for these cases. The operation at high temperatures and rough combustion at the low velocities did not permit any extended test time without possible facility damage.

Table 1. Summary of Results for the Combustion Roughness Experiments.

M _j	Configuration for Burning	OAPWL, dB	OASPL, dB	SPL(f) @ 40°/90°	LU (at Exit Plane), % Turbulence
1.55	Preburner	171.3	No Difference	---	2
	AB/Low Preburner	171.3	No Difference	There exists low frequency (combustion) noise	4.5
	PB/AB	171.0	No Difference	---	4.5

M _j	Configuration	V _j Ideal, ft/sec	OAPWL
0.3	Resonance (100 Hz)	522	138.6
	Rough	545	133.4
	Smooth	586	131.6

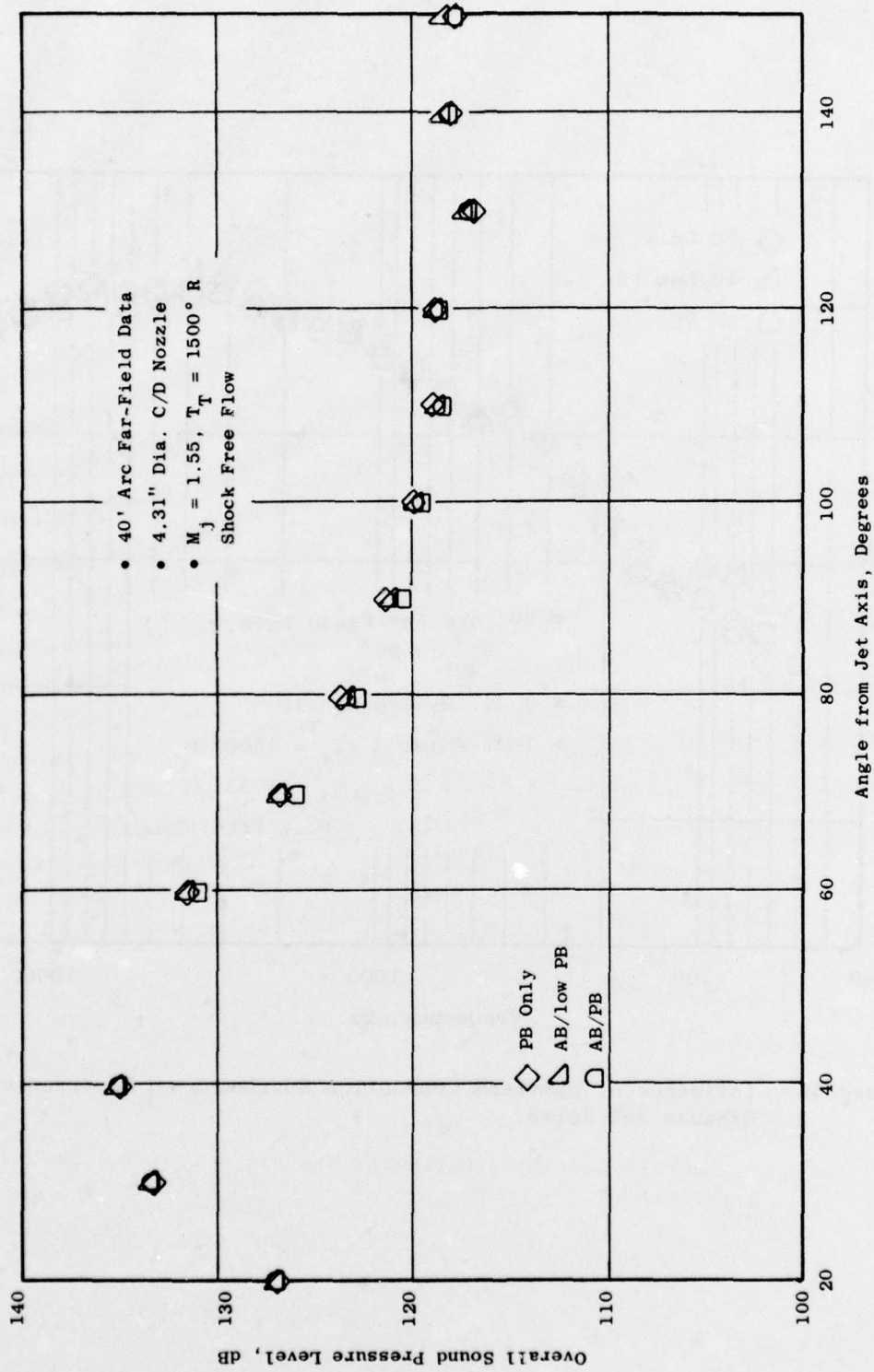


Figure 44. Influence of Upstream Combustion Roughness on Supersonic Exhaust Jet Noise.

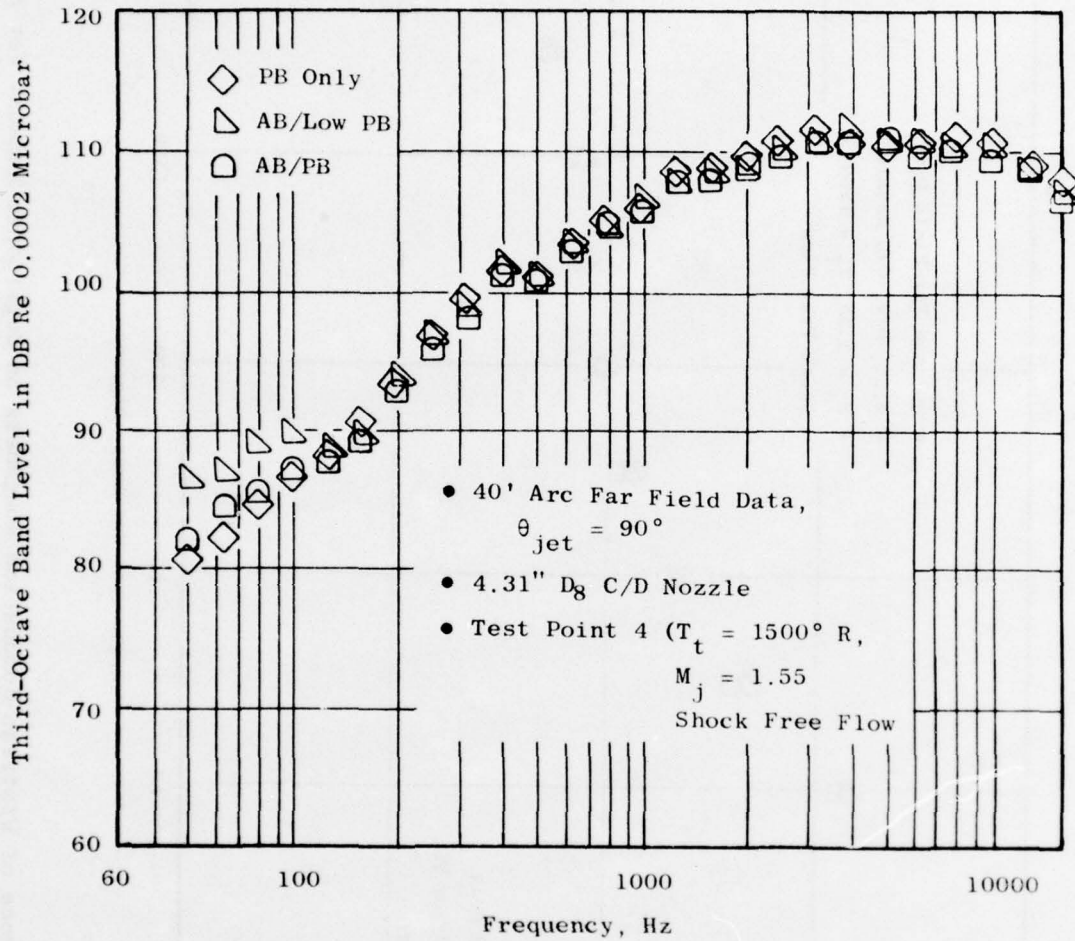


Figure 45. Influence of Upstream Combustion Roughness on Supersonic Exhaust Jet Noise.

SECTION 6.0

RECOMMENDATIONS FOR FUTURE WORK

Based on the studies conducted during the contract effort, the following items warrant future investigation:

1. Application of fluid shrouding theoretical modeling techniques toward formulation of aeroacoustic model equations for application in noise source location techniques. Currently all key analyses for noise source location depend on the Lighthill/Proudman formulations. These formulations do not incorporate fluid shrouding effects. New analyses should be performed to examine how the aerodynamic source terms are influenced by fluid shrouding and should assess the results toward determining the more exact type of measurement which must be performed for noise-source location.
2. Additional LV development work should be performed. More work is necessary in developing the random data techniques for performing second derivatives of cross-correlation products. More efficient techniques should be developed for utilizing the LV output signal in performing cross correlation between in-jet to far-field microphone measurements. Analytical/experimental feasibility studies should be performed to demonstrate the LV for two-point space-time correlations. Determination of error analysis for setting statistical criterion for performing accurate turbulent spectra, in-jet to far-field cross correlations, and in-jet/in-jet correlations should also be performed. Noise source assessment techniques should be evaluated for static and relative flow (simulated flight) environments.
3. Further experimental work is warranted to better understand the aeroacoustic nature of swirling flows. The areas of concentration should be toward parametric studies for very moderate amounts of swirl. Analytical/experimental investigations studying the possible link of swirling flow with helical modes of noise generation or reduction also should be considered. Consideration should be given toward the application of swirling jets to dual-flow systems and annular plug nozzles.
4. Further work is necessary to assess the influences of shock-generated noise on full-scale engines. Model-scale and full-scale assessments should be performed. The model-scale assessments should include wind-on (simulated in-flight) evaluation. Additionally, more efforts should be directed toward developing analytical methods for understanding and estimating the broadband content of shock-related noise.

5. Analytical/experimental investigations should be directed toward understanding the fluid amplifying effects on low frequency noise. The areas of concern deal with better understanding as to how the sources can be modeled, over what velocity and temperature range does tone amplification occur, and better assessment of flow/tone interaction as related to practical core engine noise technology.

ACKNOWLEDGEMENTS

The summary of results presented above was an attempt to give an overview of what were some of the key findings obtained during the course of this investigation. The results reported were taken freely from the many detailed accounts of individual investigations reported in Volumes II, III, IV, and the interim technical report. It is hoped that the reader will be stimulated to go to the referenced work. The key contributors during the contract effort were Drs. Mani, Merkle, Ribner, Bilwakesh, Chen and Messrs. Mossey, Scott, Algheren, Smith, and Brausch. Additionally, acknowledgement is given to Mr. P. Gliebe of the General Electric Company who performed the aeroacoustic data comparisons given in Section 3.0. Finally, acknowledgement goes to Mr. Paul Shahady and Dr. Gordon Banerian who supported these efforts.

REFERENCES

VOLUME I

1. Benzakein, M.J., and Knott, P.R.; "Supersonic Jet Exhaust Noise," AFAPL-TR-82-52 (August 1972).
2. Knott, P.R., et al.; "Supersonic Jet Exhaust Noise Investigation," AFAPL-TR-74-25 (June 1974).
3. Rotta, J.; "Statistical Theory of Non-Homogeneous Turbulence," Part II, NASA TTF-11 696, June 1968.
4. Clushko, G.S.; "Turbulent Boundary Layer on a Flat Plate in an Incompressible Fluid," NASA TTF-10, 030, 1965.
5. Spalding, D.B., and Patankar, S.V.; Heat and Mass Transfer in Boundary Layers, Morgan-Grampian: London, 1967.
6. Heck, P.H., and Ferguson, D.R.; "Analytical Solution for Free Turbulent Mixing in Compressible Flows," AIAA Paper 71-4, 1971.
7. Heck, P.A., and Merkle, C.L.; Analytical Flow Field Analysis for Compressible Turbulent Jets. Chap. 1 of "Supersonic Jet Exhaust Noise." Benzakein, M.J., Knott, P.R.; AFAPL-TR-72-52 (August 1972).
8. Merkle, C.L.; Theoretical Developments of the Aerodynamics of Supersonic Jets. Chap. 1 of "Supersonic Jet Exhaust Noise." Knott, P.R., et al.; AFAPL-TR-74-25 (June 1974).
9. Merkle, C.L., Keith, J.S., Knott, P.R.; "Prediction of the Flow Field of Turbulent Jets," Proceedings of Heat Transfer and Fluid Mechanics (1974).
10. Knott, P.R., and Benzakein, M.J.; Analytical and Experimental Supersonic Jet Exhaust Noise Research," AIAA 73-188 (1973).
11. Ribner, H.S.; The Generation of Sound by Turbulent Jets. Advances in Applied Mechanics. New York, London: Academic Press. Volume VIII, pp. 103-182 (1964).
12. Ribner, H.S.; Canadian Aeronautical and Space Journal 14, 281-298. Turnbull Lecture. Jets and Noise (1968).
13. Grande, E.; University of Toronto Institute for Aerospace Studies TN 110 (NASA CR-840 (1967)). Refraction of Sound by Jet Flow and Temperature.
14. Mac Gregor, G.R.; Ribner, H.S., Lam, H.; Journal of Sound and Vibration 27 (4) 437-454. "Basic Jet Noise Patterns."

15. Atvars, J., Schubert, L.K., Grande E., and Ribner, H.S.; University of Toronto, Institute for Aerospace Studies. TN 109 (NASA CR-494) Refraction of Sound by Jet Flow or Temperature.
16. Ribner, H.S.; "Reflection, Transmission and Amplification of Sound by a Moving Medium," J.A.S.A. 29, p. 435 (1957).
17. Ribner, H.S.; The Question of Convection and Refraction Coupling in Jet Noise Turbulent Mixing Theories, Chap. 2, Section 3, Supersonic Jet Exhaust Noise Investigation, Knott, P.R., ed., AFAPL-TR-74-25.
18. Lush, P.A.; "Measurements of Supersonic Jet Exhaust Noise and Comparisons with Theory," Journal of Fluid Mechanics, 46, pp. 477-500 (1971).
19. Hoch, R.G., et al., "Studies of the Influence of Density on Jet Noise, presented at the First International Symposium on Air Breathing Engines, Marseille, France, June 19-23, 1972.
20. Mani, R.; "Moving Source Models for Jet Noise," Chap. II, Section 1., Supersonic Jet Exhaust Noise Investigation, Knott, P.R., ed., AFAPL-TR-74-25.
21. Phillips, O.M.; "On the Generation of Sound by Supersonic Turbulent Shear Layers," J. Fluid Mech., 9, pp. 1-28 (1960).
22. Ffowcs -Williams, J.E.; Phil. Trans. Roy. Soc. A., 255, 469.
23. Ribner, H.S.; Energy Flux from an Acoustic Source Contained in a Moving Fluid Element and its Relation to Jet Noise, J.A.S.A., 32 (9), 1159.
24. Ribner, H.S.; Aerodynamic Sound from Fluid Dilatations: A Theory of the Sound from Jets and Other Flows. JTIAS No. 86.
25. Powell, A.; "Concerning the Noise of Turbulent Jets," J.A.S.A., 32, 1609.
26. Csanady, G.T.; "The Effect of Mean Velocity Variations on Jet Noise," Journal of Fluid Mechanics, 26, pp. 183-187 (1960).
27. Davies, P.A.O.L., et al.; "The Characteristics of the Turbulence in the Mixing Region of a Round Jet," J. Fluid Mechanics, 15, 337. (1969).
28. Lilley, G.M.; AFAPL-TR-72-53, Vol. IV (1972).
29. Goldstein, M.E., Howes, W.L.; "New Aspects of Subsonic Aerodynamic Noise Theory," NASA TN-D-7158.
30. Jones, I.S.F.; "Aerodynamic Noise Dependent on Mean Shear," J. Fluid Mechanics, 33, (1), 65.
31. Gottlieb, P.; J.A.S.A., 32 (3), 117.

32. Mollo-Christenson, E., Narasimha, R.J.; "Sound Emission from Jets at High Subsonic Velocities," J. Fluid Mechanics 8, (1), 49.
33. Berman, C.H.; Noise from Turbulent Flows, AIAA 74-2.
34. Ribner, H.S.; "Quadrupole Correlations Governing the Pattern of Jet Noise," J. of Fluid Mechanics, 38, 1969.
35. Ahuja, K.K., and Bushell, K.W.; "An Experimental Study of Subsonic Jet Noise and Comparison with Theory," J. Sound and Vibration, 30 (3), 317.
36. Nagamatsa, H.T., Sheer, R.E.; Advanced Fluid Probe Developments, Chap. VI, Supersonic Jet Exhaust Noise Investigation, Benzakein, M.J., Knott, P.R., eds., AFAPL-TR-72-52 (August 1972).
37. Mossey, P.W., Asher, J.A., Knott, P.R.; Differential Laser Velocimeter Investigation, Chap V, Supersonic Jet Exhaust Noise Investigations, Benzakein, M.J., Knott, P.R., eds., AFAPL-TR-72-52 (August 1972).
38. Knott, P.R., Mossey, P.W.; Laser Velocimeter Measurements in High Speed High Temperature Jet Exhausts, Proceedings of the 1974 Purdue Laser Velocimeter Workshop, March 1974.
39. Scott, P.F.; Theory and Implementation of the Laser Velocimeter Turbulence Spectrum Measurements, Proceedings of the 1974 Purdue Laser Velocimeter Workshop, March 1974.
40. Scott, P., Mossey, P.A., Knott, P.R.; Laser Velocimeter Developments, Supersonic Jet Exhaust Noise Investigation, Knott, P.R., ed., Chap. IV of AFAPL-TR-74-25.
41. Lee, H.K., Ribner, H.S.; "Direct Correlation of Noise and Flow of a Jet," J.A.S.A. 52, 1280-1290 (1972).
42. Siddon, T.E.; "Proceedings of Inter-Noise 1972 Conference, October 4-6, 1972, Washington, D.C., pp. 452-457.
43. Schwartz, I.R., "Jet Noise Suppression by Swirling the Jet Flow," AIAA 73-1003, October 1973.

VOLUME II

44. Lighthill, M.J.; 1952 Proceedings of the Royal Society A211, 564-587. "On Sound Generated Aerodynamically. I. General Theory."
45. Lighthill, M.J.; 1954 Proceedings of the Royal Society A222, 1-32. "On Sound Generated Aerodynamically. II. Turbulence as a Source of Sound."

46. Lighthill, M.J.; 1962 Proceedings of the Royal Society A267, No. 1329. 147-182. The Bakerian Lecture 1961. "Sound Generated Aerodynamically."
47. Ahuja, K.K. and Bushell, K.W.; "An Experimental Study of Subsonic Jet Noise and Comparison with Theory," J. Sound and Vibration, 30 (3), 317.
48. Hoch, R.G., et al.; "Studies of the Influence of Density on Jet Noise," J. Sound and Vibration, 28 (4), 649.
49. Eldred, K.M., et al.; "Suppression of Jet Noise with Emphasis on the Near Field," ASD-TDR-62-578.
50. Tester, B.J., and Burrin, R.H.; "On Sound Radiation from Sources in Parallel Sheared Jet Flows," AIAA Paper 74-57.
51. Berman, C.H.; "Noise from Variation from Turbulent Flows," AIAA 74-2.
52. Ribner, H.S.; "Energy Flux from an Acoustic Source Contained in a Moving Fluid Element and its Relation to Jet Noise," (1960), J.A.S.A., 32 (9), 1159.
53. Ribner, H.S.; "Aerodynamic Sound from Fluid Dilatation. A Theory of the Sound from Jet and Other Flows," (1962), UTIAS Report No. 86.
54. Mani, R.; "The Jet Density Exponent Issued for the Noise of Heated Subsonic Jets," J. Fluid Mechanics, 64 (3), 611.
55. Lee, H.K., and Ribner, H.S.; "Direct Correlation of Noise and Flow of a Jet," J.A.S.A., 52 (5), Part I, 1280.
56. Lighthill, M.J., Introduction to Fourier Analysis and Generalized Functions, Cambridge (1959).
57. Bushell, K.W.; "A Survey of Low Velocity and Coaxial Jet Noise with Application to Prediction," J. Sound and Vibration, 17, 271.
58. Tanna, H.K., et al.; "Effect of Temperature on Supersonic Jet Noise," AIAA 73-991.
59. Hoch, R.G., et al.; J. Sound and Vibration, 28 (b), 649.
60. Hoch, R.G.; (1974), Private Communication.
61. Lighthill, J.M.; 1963 American Institute of Aeronautics and Astronautics Journal. I. 1507-1517. Wright Brothers Lecture. Jet Noise.
62. Schubert, L.K.; 1972 Journal of the Acoustical Society of America 51, 447-463. "Numerical Study of Sound Refraction by a Jet Flow. II. Wave Acoustics."

63. Lilley, G.M., Morris, P.J., and Tester, B.J.; 1973 AIAA Paper No. 73-987. "On the Theory of Jet Noise and its Application."
64. Mani, R.; 1972 Journal of Sound and Vibration 25, 337-347. "A Moving Source Problem Relevant to Jet Noise."
65. Mani, R.; 1974, The Influence of the Flow on Jet Noise. Part I: The Noise of Unheated Jets. Part II. The Noise of Heated Jets. Sec I VIII, pp. 103-182.
66. Pao, S.P., and Lawson, M.V.; 1969 Wyle Laboratories - Research Staff, Report WR 68-21, prepared for NASA. "Spectral Techniques in Jet Noise Theory."
67. Goldstein, M.E., and Rosenbaum, B.M.; 1972 NASA TN D-6939. "Emission of Sound from Axisymmetric Turbulence Convected by a Mean Flow with Application to Jet Noise."
68. Morris, P.J.; 1972 Institute for Aerospace Studies, University of Toronto (unpublished). "Hot Wire-Microphone Cross-Correlation Based on Ribner's Source Terms, to Indicate Separately the Shear-Noise and Self-Noise Contributions to Jet Noise."
69. Seiner, J.M., and Reethof, G.; 1974 AIAA Paper No. 74-4. "On the Distribution of Source Coherency in Subsonic Jets."
70. Mollo-Christensen, E., Kolpin, M.A., Martucelli, J.R.; (1963) Mass. Inst. of Tech., Aeroelastic and Struct. Res. Lab., ASRL-TR-1007. "Experiments on Jet Flows and Jet Noise Farfield Spectra and Directivity Patterns."
71. Ahuja, K.K.; 1972 M. Phil. Thesis, University of London. "An Experimental Study of Subsonic Jet Noise with Particular Reference to the Effect of Upstream Disturbances."
72. Chu, W.T.; (1974) Dept. of Aerospace Engineering, University of Southern California. (Unpublished narrow band measurements of jet noise, carried out in U.S.C. anechoic jet facility.)
73. Proudman, I.; 1952 Proceedings of the Royal Society A214, 119-132. "The Generation of Noise by Isotropic Turbulence."
74. McCartney, J.R.; (1974) J. Sound and Vibration. "Ratio of Peak Frequencies of Jet Self and Shear Noise Spectra."
75. Powell, Alan.; 1960 Program, 59th Meeting of the Acoustical Society of America, Providence, Rhode Island, June 9-11, Paper 05 (Abstract). "Fundamental Notions Concerning Convection of Aerodynamic Noise Generators."
76. Ribner, H.S.; 1960 Journal of the Acoustical Society of America 32, 1159-1160. "Energy Flux from an Acoustic Source Contained in a Moving Fluid Element and its Relation to Jet Noise."

77. Benzakein, M.J., Chen, C.Y., and Knott, P.R.; 1971 AIAA Paper No. 71-583. "A Computational Technique for Jet Aerodynamic Noise."
78. Knott, P.R., Chen, C.Y.; 1972 Ch. II. Analytical Acoustic Model Developments for Supersonic Farfield Jet Noise in Supersonic Jet Exhaust Noise, Benzakein, M.J., and Knott, P.R., Ed., General Electric Co., Aircraft Engine Group, sponsored by Air Force Aero Propulsion Lab. Report, AFAPL-TR-72-52, pp. 118-179.
79. Chen, C.Y., 1973 Ph. D. Thesis, Dept. of Mechanical Engineering, Univ. of Cincinnati. "Investigation of Far Field and Near Field Jet Noise."
80. Tam, C.K.W.; 1972, "On the Noise of a Nearly Ideally Expanded Stability in Edgetone Generation," AIAA J., Vol. 12, p. 1457.
81. Betchov, R., and Crimanale, W.O., Jr.; 1967, Stability of Parallel Flows, Academic Press, New York.
82. Crow, S.C., and Champagne, F.H.; 1971, "Orderly Structure in Jet Turbulence," JFM, Vol. 48, p. 547.
83. Berman, C.H., Ffowcs-Williams, J.E.; "Instability of a Two Dimensional Compressible Jet," JFM, 42 (1), p. 151.
84. Hussain, A.K.M.F., and Reynolds, W.C.; 1970, "The Mechanics of an Organized Wave in Turbulent Shear Flow," JFM, Vol. 41, p. 241.
85. Reynolds, W.C., and Hussain, A.K.M.F., 1972, "The Mechanics of an Organized Wave in Turbulent Shear Flow. Part 3. Theoretical Models and Comparisons with Experiment," JFM, Vol. 54, p. 263.
86. Liu, J.T.C.; 1974, "Developing Large-Scale Wavelike Eddies and the Near Jet Noise Field," JFM, Vol. 62, p. 437.
87. Ko, D.R.S., Kubota, T., and Lees, L.; 1970, "Finite Disturbance Effect in the Stability of a Laminar Incompressible Wake behind a Flat Plate," JFM, Vol. 40, p. 315.
88. Ko, D.R.S., 1971, "Integral Theory for the Instability of Laminar Compressible Wakes behind Slender Bodies," AIAA J., Vol. 9, p. 1777.
89. Lin, C.C., 1955, Theory of Hydrodynamic Stability, Cambridge University Press.
90. Morris, P.J.; 1974, "A Model for the Orderly Structure of Turbulence as a Source of Noise," AIAA Paper 74-1.
91. Liu, J.T.C.; 1971, "On Eddy-Mach Wave Radiation Source Mechanism in the Jet Noise Problem," AIAA Paper 71-150.

92. Woolley, J.P., and Karamcheti, K.; "Role of Jet Stability in Edgetone Generation," AIAA Journal, Vol. 12, No. 11, 1974, pp. 1457-1458.
93. Bishop, K.A., Ffowcs-Williams, J.F., and Smith, W.; 1971, "On the Noise of the Unsuppressed High-Speed Jet," JFM, Vol. 50, p. 21.
94. Michalke, A., "The Production of Sound by Amplified Disturbances in Free Shear Layers," Royal Aircraft Establishment LT-1517, 1970.
95. Chan, Y.Y.; 1974, "Spatial Waves in Turbulent Jets," Phys. of Fl., Vol. 17, No. 1, p. 46.
96. McLaughlin, D.K., and McColgan, C.J.; 1974, "Hot-Wire Measurements in a Supersonic Jet at Low Reynolds Numbers," AIAA J., Vol. 12, p. 1279.
97. Fuchs, H.V.; 1972, "Space Correlations of the Fluctuating Pressure in Subsonic Turbulent Jets," J. Sound and Vibration, Vol. 23, p. 77.
98. Scharton, T.D., and White, P.H.; 1972, "Simple Pressure Source Model of Jet Noise," J. Acoust. Soc. Am., Vol. 52, No. 1.
99. No, N.W.M., and Davies, P.O.A.L.; 1971, "The Near Field within the Potential Cone of Subsonic Cold Jets," JFM, Vol. 50, p. 49.
100. Lilley, G.M., Morris, P.J., and Tester, B.J.; 1973, "On the Theory of Jet Noise and its Applications," AIAA Paper 73-987.
101. Rose, W.G.; "A Swirling Round Turbulent Jet," Journal of Applied Mechanics, Vol. 29, December 1962, pp. 616-625.
102. Chigier, N.A., and Beér, J.M.; "Velocity and Static Pressure Distributions in Swirling Air Jets Issuing from Annular and Divergent Nozzles," Journal of Basic Engineering, Vol. 86, December 1964, pp. 788-798.
103. Kerr, N.M., and Fraser, D.; "Swirl, Part I: Effect on Axisymmetrical Turbulent Jets," Journal of the Institute of Fuel, Vol. 38, December 1965, pp. 519-526.
104. Chigier, N.A., and Chervinsky, A.; "Experimental Investigation of Swirling Vortex Motion in Jets," Journal of Applied Mechanics, Vol. 34, June 1967, pp. 443-451.
105. Pratte, B.D., and Keffer, J.F.; "The Swirling Turbulent Jet," Journal of Basic Engineering, Vol. 94, December 1972, pp. 739-748.
106. Chigier, N.A., and Chervinsky, A.; "Aerodynamic Study of Turbulent Burning Free Jets with Swirl," Eleventh International Symposium on Combustion. The Combustion Institute, Pittsburgh, Pa., 1967, pp. 489-499.

107. Chervinsky, A.; "Turbulent Swirling Jet Diffusion Flames," AIAA Journal, Vol. 7, October 1969, pp. 1877-1883.
108. Schwartz, I.R.; "Effects of Rotating Flows on Combustion and Jet Noise," AIAA Paper 72-645, June 1972 (or, see "A Preliminary Investigation of Combustion with Rotating Flow in an Annular Combustion Chamber," NACA RM L51E25a, 1951).
109. Schwartz, I.R.; "Jet Noise Suppression by Swirling the Jet Flow," AIAA Paper 73-1003, October 1973.
110. Norton, D.J., Farquhar, B.W., and Hoffman, J.D.; "An Analytical and Experimental Investigation of Swirling Flow in Nozzles," AIAA Journal, Vol. 7, October 1969, pp. 1992-2000.
111. Baker, V.D., Johnson, R.A., Brasket, R.G., and Lamb, O.P.; "Experimental Results with Lift Engine Exhaust Nozzles," AIAA Paper 65-574, June 1965.
112. Boussinesq, J.; "Théorie de l'écoulement Tourbillant," Mém prés Acad Sci, Vol. 23, 1877, p. 46.
113. Prandtl, L.; "Bericht Über Untersuchungen zur ausgebildeten Turbulenz," ZAMM, Vol. 5, 1925, pp. 136-139.
114. Prandtl, L.; "Über ein neues Formelsystem der ausgebildeten Turbulenz," Nachr. Akad. Wiss. Göttingen, 1945, pp. 6-19.
115. Kolmogorov, A.N.; "Equations of the Turbulent Motion of an Incompressible Turbulent Fluid," Izv. Akad. Nauk. SSSR, Ser. Phys. VI, 1942, pp. 56-58.
116. Launder, B.E., and Spalding, D.B.; Mathematical Models of Turbulence, Academic Press, 1972.
117. Birch, S.G., Rudy, D.H., and Bushnell, D.M., (Eds.), "Free Turbulent Shear Flows, Volume I - Conference Proceedings," NASA SP-321, 1973.
118. Spalding, D.B., et al.; "Turbulent Mixing in Combustion Chambers," Northern Research and Engineering Corporation, Report No. 1118-1, October 1966.
119. Benzakein, M.J., Chen, C.Y., and Knott, P.R.; "A Computational Technique for Jet Aerodynamic Noise," AIAA Paper 71-583, June 1971.
120. Rubel, A.; "Swirling Jet Turbulent Mixing and Combustion Computations," NASA CR-2231, March 1973.
121. Koosinlin, M.L., Launder, B.E., and Sharma, B.I.; "Prediction of Momentum Heat and Mass Transfer in Swirling Turbulent Boundary Layers," AIAA Paper 74-703 (also ASME Paper 74-HT-23), July 1974.

122. Lilley, D.G.; "Prediction of Inert Turbulent Swirl Flows," AIAA Journal, Vol. 11, July 1973, pp. 955-960.
123. Koosinlin, M.L., and Lockwood, F.C.; "The Prediction of Axisymmetric Turbulent Swirling Boundary Layers," AIAA Journal, Vol. 12, April 1974, pp. 547-554.
124. Lilley, D.G., and Chigier, N.A.; "Nonisotropic Turbulent Shear Stress Distribution in Swirling Flows from Mean Value Distributions," International Journal of Heat and Mass Transfer, Vol. 14, 1971, pp. 573-585.
125. Kazin, S.B., and Matta, R.K., (Eds); "Core Engine Noise Control Program, Volume II - Identification of Noise Generation and Suppression Methods," Federal Aviation Administration FAA-RD-74-125, II, December 1974.
126. Ortwerth, P.J.; "Mechanism of Mixing of Two Nonreacting Gases," Air Force Aero Propulsion Laboratory AFAPL-TR-71-18, October 1971.
127. Ortwerth, P.J.; "Mechanism of Mixing of Two Nonreacting Gases," AIAA Paper 71-725, June 1971.
128. Kushida, R., and Rupe, J.; "Effect on Supersonic Jet Noise of Nozzle Plenum Pressure Fluctuations," AIAA Journal, Vol. 10, July 1972, pp. 946-948.
129. Platt, E.G., and Summerfield, M.; "Jet Engine Exhaust Noise Due to Rough Combustion and Nonsteady Aerodynamic Sources," Journal of the Acoustical Society of America, Vol. 56, August 1974, pp. 516-522.
130. Schubert, L.K.; "Numerical Study of Sound Refraction by a Jet Flow, I. Ray Acoustics," Journal of the Acoustic Society of America, 51, 1972, pp. 439-446.
131. Schubert, L.K.; "Numerical Study of Sound Refraction by a Jet Flow, II. Wave Acoustics," Journal of Acoustic Society of America, 51, 1972, pp. 447-463.
132. Bilwakesh, K.R., Kazin, S.B., Matta, R.K., et al.; "Core Engine Noise Control Program, Vol. II - Identification of Noise Generation and Suppression Mechanisms," General Electric Company, DOT/FAA Report No. FAA-RD-74-125, III.
133. Hayden, Richard E.; "Noise from Interaction of Flow with Rigid Surfaces: A Review of Current Status of Prediction Techniques," Bolt, Beranek and Newman Report No. 2276.
134. Sharland, I.J.; "Sources of Noise in Axial Flow Fans," Journal Sound Vibration, 1 (3), 1964, pp. 302-322.

135. Gordon, Colin G.; (a) "Spoiler-Generated Flow Noise. I. The Experiment," Journal Acoustic Society, America, 43 (5), May 1968.
136. Paterson, R.W., Vogt, P.G., Fink, M.R., and Munch, C.L.; "Vortex Noise of Isolated Airfoils," Paper 72-656, AIAA 5th Fluid and Plasma Dynamics Conference, Boston, 1972.
137. Crow, S.C.; "Acoustic Grain of a Turbulent Jet," American Physical Society, T.G. 25th Annual Meeting of the Division of Fluid Dynamics, November 20-22, 1972.
138. Benzakein, M.S., Knott, P.R., "Supersonic Jet Noise," AFAPL-TR-72-52 (August 1972).
139. Knott, P.R., et al.; "Supersonic Jet Exhaust Noise Investigation," AFAPL-TR-74-25 (June 1974).
140. Wooldridge, C.E., Wooyen, D.C., Amaro, A.S., "The Structure of Jet Turbulence Producing Jet Noise," Stanford Research Institute Annual Report, June 1971.
141. Knott, P.R., Mossey, P.W.; "Laser Velocimeter Measurements in High Speed High Temperature Jet Exhausts," Proceedings of the 1974 Purdue Laser Velocimetry Workshop, March 1974.
142. Scott, P.F.; "Theory and Implementation of Laser Velocimeter Turbulence Spectrum Measurements," Proceedings of the 1974 Purdue Laser Velocimeter Workshop, March 1974.
143. Meecham, W.C.; "On the Sample - Source Theory of Sound from Statistical Turbulence," Journal of Statistical Physics, Vol. 8, No. 2, 1973.
144. Siddon, T.E.; "Fluctuating Pressure Probe/Design and Calibration," Bolt, Beranek and Newman Report, July 1971.
145. Hurdle, P.M., Meecham, W.C.; "Investigation of the Aerodynamic Noise Generating Region of a Jet Engine by Means of the Simple Source/Fluid Dilatation Model," JASA, March 1974.
146. Papoulis, A.; Probability, Randoni Variables and Stochastic Processes, McGraw-Hill, 1965.
147. Papoulis, A.; Fourier Transform and its Application, McGraw-Hill, 1962.

VOLUME III

148. Townsend, A.A.; The Structure of Turbulent Shear Flow, Cambridge Press, 1956.
149. Hinze, J.O.; Turbulence, McGraw-Hill Book Company, 1959.

150. Corrisin, S.; "Local Isotropy in Turbulent Shear Flow," NACA RM58B11, May 1958.
151. Bradshaw, P., Ferriss, D.H., and Atwell, N.P.; "Calculation of Boundary Layer Development Using the Turbulent Energy Equation," Journal of Fluid Mechanics, Vol. 28, Pt. 3, 1967, p. 593.
152. Mellor, G.L., and Herring, H.J.; "Two Methods of Calculating Turbulent Boundary Layer Behavior Based on Numerical Solutions of the Equations of Motion," Proceedings - Conference on Computation of Turbulent Boundary Layer Prediction, Stanford University, 1968.
153. Harsha, P.T.; "Free Turbulent Mixing: A Critical Evaluation of Theory and Experiment," in AGARD-CP-93, January 1972.
154. Kelly, J.T.; "Multiple Underexpanded Plume Computational Technique Including Turbulent Mixing and Non-Equilibrium Chemistry," AIAA Paper 73-695, 1973.
155. Edelman, R.B., and Wellerstein, G.; "A Solution of the Inviscid-Viscous Equations with Applications to Bounded and Unbounded Multi-Component Reacting Flows," AIAA Paper 69-83, 1969.
156. Chen, C.Y.; "Estimation of Jet Noise," General Electric Co., R72AEG341, December 1972.

APPENDIX 1

157. Bradshaw, P., and Ferriss, D.H.; "Calculation of Boundary-Layer Development Using the Turbulent Energy Equation. II - Compressible Flow on Adiabatic Walls," NPL Aero Report 1217, 1966.
158. Mellor, G.L., and Herring, H.J.; "A Method of Calculating Compressible Turbulence Boundary Layers," NASA CR-1144, September 1968.
159. Ollerhead, J.B.; "On the Prediction of Nearfield Noise of Supersonic Jets," NASA CR-857, August 1967.
160. Spalding, D.B., and Patankar, S.V.; Heat and Mass Transfer in Boundary Layers, Morgan-Grampian, London, 1967.
161. Laurence, J.C.; "Intensity, Scale and Spectra of Turbulence in Mixing Region of a Free Subsonic Jet," NACA Report 1292, 1956.

APPENDIX 2

162. Averenkova, G.I., Ashratov, E.A., and Volkonskaia, T.G.; "Investigation of the Parameters of Axisymmetric Underexpanded Ideal Gas Jets," Vychislitelnye Metody: Programmirovaniye, No. 15, Moscow Univ. Press, pp. 92-101, 1970.

163. MacCormack, R.W., and Paullay, A.J.; "Computational Efficiency Achieved by Time Splitting of Finite Difference Operators," AIAA Paper 72-154, 1972.
164. Richtmyer, R.D., and Morton, K.W.; Difference Methods for Initial Value Problems, 2d. ed., Interscience, New York, 1967.
165. Moretti, G.; "The Importance of Boundary Conditions in the Numerical Treatment of Hyperbolic Equations," PIBAL Rept. 68-34, Polytechnic Institute of Brooklyn, Nov. 1968.
166. Abbett, M.J.; "Boundary Condition Calculation Procedures for Inviscid Supersonic Flow Fields," Proceedings, AIAA Computational Fluid Dynamics Conference, AIAA, New York, 1973.
167. Presley, L.L., and Kutler, P.; "Comparison of a Discrete-Shock, Finite-Difference Technique and the Method of Characteristics for Calculating Internal Supersonic Flows," Proceedings, AIAA Computational Fluid Dynamics Conference, AIAA, New York, 1973.
168. Love, E.S., Grigsby, C.E., Lee, L.P., Woodling, M.J.; "Experimental and Theoretical Studies of Axisymmetric Free Jets," NASA TR-R-6, 1959.
169. Oswatitsch, K., Gas Dynamics, Academic Press, New York, 1956.
170. Abbett, M., "The Mach Disc in Underexpanded Exhaust Plumes," AIAA Paper 70-231, 1970.
171. Fox, J.H.; "On the Structure of Jet Plumes," AIAA Journal, Vol. 12, p. 105, January, 1974.
172. Ribner, H.S.; "Connection of a Pattern of Vorticity Through a Shock Wave," NACA TN 1164, 1954.
173. Ribner, H.S.; "Shock Turbulence Interaction and the Generation of Noise," NACA TN 1233, 1955.
174. Ribner, H.S.; "Acoustic Energy Flux from a Shock-Turbulence Interaction," Journal of Fluid Mechanics, Vol. 35, p. 299, 1969.

APPENDIX 3

175. Ribner, H., et al.; "Refraction of Sound by Jet Flow or Jet Temperature," UTIAS TN 109; NACA CR 494 (1966).
176. Schubert, L.K.; "Computer Study of Refraction of Sound by Jet Flow and Jet Temperature," UTIAS Rept. 144.
177. Mani, R.; "A Moving Source Problem Relevant to Jet Noise," GE Class I Report (May 1972).

178. Paterson, A.R.; NATO AGARD Rept. 460 (1963).
179. Crow, S.C.; Lawrence Radiation Lab., UCRL 70189 (1966).
180. Obermeier, F.; 1967 *Acustica*, 18, 4, 38 (1967).
181. Pao, S.P.; "Development of a Generalized Theory of Jet Noise," *AIAA J.* Vol. 10, No. 5, pp. 596 (May 1972).
182. Liepmann, H.W.; "On the Acoustic Radiation from Boundary Layers and Jets," Guggenheim Aeronautical Laboratory, CIT, August 1952.
183. Laufer, M.T., Ffowcs-Williams, J.E., and Childress, S.; *AGARDograph*, 90 (1964).
184. Landau, L.; "Stability of Tangential Discontinuities in a Compressible Fluid," *C.R. Acad. Sci., U.S.S.R.* 44, pp. 139-141 (1944).
185. Sedelnikov, T. Kh.; "The Frequency Spectrum of a Supersonic Jet," *NASA TT F-538*, pp. 71 (1969).
186. Tam, C.K.W.; 1973, "Supersonic Jet Noise Generated by Large-Scale Disturbances," *AIAA Paper* 73-882.
187. Lilley, G.M.; "On the Noise from Air Jets," *ARC* 20, 376 (1958).
188. Maestrello, L., McDaid, E.; "Acoustic Characteristics of a High Subsonic Jet," *AIAA* 9, No. 6, 1058-1066 (1971).
189. Pao, S.P.; "Aerodynamic Noise Emission from Turbulent Shear Layer," *JFM* (1973).
190. Howes, Walton, L., Callaghan, Edmund E., Coles, Williard D., and Mull, Harold R.; "Near Noise Field of a Jet-Engine Exhaust," *NACA Rept.* 1338, 1957 (Supersedes *NACA TN's* 3763 and 3764).
191. Wolfe, M.O.W.; "Near Field Jet Noise," Report 113, NATO AGARD, April-May 1957.
192. Hermes, P.H., and Smith, D.L.; "Measurement and Analyses of the J57-P21 Noise Field," *AFFDL-TDR-66-147*, 1967.
193. Morgan, L.C., Sutherland, and K.J. Young; "The Use of Acoustic Scale Models for Investigating Nearfield Noise of Jet and Rocket Engines," *WADD-TR-61-178*, April, 1961.
194. Franken, Peter, A., and Kerwin, E.M., Jr.; "Methods of Flight Vehicle Noise Predictions," *WADC-TR-58-343*, November, 1958.

195. Plumblee, H.E., Ballentine, J.R., and Passinas, B.; "Near Field Noise Analyses of Aircraft Propulsion Systems with Emphasis on Prediction Techniques for Jets," WADC-TR-58-343, August, 1967.
196. Franz, G.J.; "The Near-Sound Field of Turbulence," David Taylor Model Basin, Rept. 986, AD 630684, October, 1959.
197. Chen, C.Y.; "Analytical Models for Nearfield Jet Noise Calculations," General Electric Co., AEG TM 72-349 (1972).